

Solar Live Steam Generation and Solar Bagasse Drying for South African Sugar Mills

by
Willem Krog

Thesis presented in partial fulfilment of the requirements for the degree of Master of Engineering (Mechanical) in the Faculty of Engineering at Stellenbosch University



UNIVERSITEIT
iYUNIVESITHI
STELLENBOSCH
UNIVERSITY

100
1918 · 2018

Supervisor: Dr J.E. Hoffmann
Co-supervisor: Dr S. Hess

March 2018

Declaration

By submitting this thesis electronically, I declare that the entirety of the work contained therein is my own, original work, that I am the sole author thereof (save to the extent explicitly otherwise stated), that reproduction and publication thereof by Stellenbosch University will not infringe any third party rights and that I have not previously in its entirety or in part submitted it for obtaining any qualification.

Date:March 2018.....

Copyright © 2018 Stellenbosch University

All rights reserved

Abstract

Two solar thermal integration concepts have been identified as promising options for implementation in South African sugar mills as a result of work within the Sugarcane Technology Enabling Programme for Bio-Energy. The two integration options are the drying of bagasse using solar heated air and the generation of live steam using concentrating solar thermal collectors. This study further develops and evaluates the two integration options.

Solar integration into the bagasse drying concept will help to save exhaust steam, which can be used to dry bagasse. An evacuated tube air collector field was simulated to assess the impact it could make on the bagasse drying system. It was calculated that 3 140 ton of bagasse or 1020 ton coal can be saved through solar thermal integration. If only exhaust steam is used in the bagasse drying system, bagasse usage can be reduced with 5 %, but if the solar system is integrated it can be decreased with 7.05 %.

The System Advisor Model was used to simulate two parabolic trough fields for the live steam generation integration point, one for a normal sugar mill and one for a mill with a back-end refinery. The simulations showed that the solar systems have low capacity factors, ranging from 13 - 14.9 % depending on the mill and time of operation. This was due to the low amount of direct normal irradiance received in Durban, which severely hampers the performance of the solar system.

Three different solar live steam configurations were evaluated for the two mills, each of which can save bagasse or coal and/or generate extra electricity. By using the simulation results, it was determined that Configuration 1 can save 2 459.7 ton coal for a normal mill and 3 248 ton coal for a mill with a refinery. Configuration 2 can save 2 241 ton of coal and increase electricity exports with 257 % for a normal mill. For a mill with a refinery 3 072 ton coal can be saved and electricity exports can be increased by 102 %. Configuration 3 can generate the most extra electricity and would enable the mill to increase its electricity exports with 297 % for the normal mill and 111 % for the mill with the refinery.

The simulation results were also used in an economic assessment for both of the integration options. The assessment determined that none of the integration options are financially feasible under current conditions. As none of the integration points could achieve a levelised cost of heat lower than that of coal (4.03 Euro-ct/kWh) or an internal rate of return higher than 10 %.

There is, however, a possibility that the integration points can become more financially rewarding in the future, as the cost of solar thermal technology is set to reduce significantly over the next 10 years. Furthermore, the possible carbon tax which is to be implemented in South Africa will increase the cost of using coal, making solar energy the cheaper option to supply thermal power.

Opsomming

Twee son termiese integrasi konsepte is as belowende opsies vir implementering in Suid-Afrikaanse suikermeulens deur 'n vorige studie van die Suikerriet Tengologie Instaatstellings Program vir Bio-Energie geïdentifiseer. Die twee integrasie konsepte is die uitdroog van bagasse deur son verhitte lug en die opwekking van hoë drukstoom deur gebruik te maak van gekonsintreerde sonkrag. Hierdie studie ontwikkel die integrasie opsies verder en evalueer die impak wat dit kan maak op 'n suikermeule.

Son termiese energie kan die gebruik van uitlaatstoom in die verdrogings sisteem verminder. 'n Veld van vakuumbuis sonkollektors is gesimuleer om die potensiële energie opbrengs wat dit kan bied te bepaal, asook die impak wat dit kan maak op die verdrogingsstelsel. Dit was bereken dat 3 140.62 ton bagasse of 1020.38 ton steenkool gespaar kan word deur die sonkragstelsel. As net uitlaatstoom gebruik sou word vir die verdrogings proses dan sal die gebruik van bagasse met 5 % kan afneem, maar as son termiese energie ook gebruik word dan kan dit met 7.05 % verminder.

Die *System Advisor Model* is gebruikom twee parabolise trog sisteme te simuleer vir die hoë druk stoom opwekking stelsel, een sisteem vir 'n gewone suiker meule en een vir 'n meule met 'n suikerraffinadery. Die simulاسies wys dat die sonkragstelsel lae jaarlikse kapasiteitsfaktore het wat wissel tussen 13 – 14.9 %. Die lae kapasiteitsfaktore in die simulاسies is veroorsaak deur die lae jaarlikse direkte normale sonsbestraling in Durban, wat die sonkragstelsel se prestasies ernstig benadeel.

Drie verskillende konfigurasies vir die hoë druk stoom opwekking stelsel is evalueer, die konfigurasies kan bagasse of steenkool bespaar en/of ekstra elektrisiteit opwek. Die simulاسie resultate was gebruik om te bereken dat Konfigurasie 1, 2 459.7 ton steenkool kan spaar vir die gewone suikermeule en 3 248.5 ton steenkool vir die meule met die raffinadery. Konfigurasie 2 kan 2 241 ton steenkool spaar en die elektrisiteits uitvoere met 257 % vermeerder vir die gewone meule, terwyl dit 3072 ton steenkool kan spaar en die elektrisiteits uitvoere met 102 % kan vermeerder vir 'n meule met 'n raffinadery. Konfigurasie 3 kan die meeste ekstra elektrisiteit opwek, dit kan lei tot 'n 297 % toename in elektrisiteit uitvoere vir 'n normale meule en 'n toename van 111 % vir 'n meule met 'n raffinadery.

Die ekonomiese evaluering toon dat nie een van die integrasiekonsepte finansieel lonend sal wees onder huidige ekondisies nie. Dit is as gevolg van die feit dat nie een van die twee 'n laer gebalanseerde koste van hitte kan bied as steenkool nie, wat staan op 4.03 Euro-ct/kWh. Die integrasiekonsepte kan ook nie 'n interne oprenskoeers hoër as 10 % behaal nie.

Daar is egter hoop dat die integrasiekonsepte meer finansieel lonend sal wees in die toekoms as gevolg van die potensiële koste vermindering van sonkragsisteme in die volgende 10 jaar. Suid-Afrika beplan ook om 'n koolstofbelasting in te stel, wat die gebruik van steenkool beboet en sodoende son termiese energie die goedkoper opsie kan maak.

Acknowledgements

I would like to express my gratitude to my supervisor, Dr Jaap Hoffmann, and co-supervisor, Dr Stefan Hess, for their support and guidance throughout this project. Thank you for the opportunity to learn from you and all your help. I would also like to thank Dr Katherine Foxon (SMRI) and Dr RynoLaubscher (Stellenbosch University) for all their help and input regarding information and knowledge of South African sugar mills.

I am grateful to the Centre of Renewable and Sustainable Energy Studies (CRSES) and the Sugarcane Technology Enabling Programme for Bio-Energy (STEP-Bio), which is co-funded by the Department of Science and Technology (DST) and the South African sugar industry under the DST's Sector Innovation Fund for their financial support throughout this project.

To the team at the Solar Thermal Energy Research Group (STERG) – Thank you for your friendship and informative talks over the last two years. I feel fortunate to have been surrounded by people with a shared enthusiasm for renewable and sustainable energy.

Lastly, I would like to thank my family and friends for their support and kindness which carried me throughout this project. I would like to say a special thank you to Maria for her endless love and emotional support.

Table of Contents

Declaration	i
Abstract.....	ii
Opsomming.....	iii
Acknowledgements	v
Table of Contents	vi
List of Figures.....	viii
List of Tables	xi
Nomenclature	xii
1 Introduction.....	1
1.1 Background.....	1
1.2 Motivation.....	2
1.3 Objectives	2
1.4 Methodology.....	3
1.5 Research Limitations	4
2 Project Background.....	5
2.1 Sugar Milling Industry in South Africa	5
2.2 Generic Sugar Milling Process	6
2.3 Possible Solar Thermal Integration Points	9
2.3.1 Live steam generation	9
2.3.2 Exhaust steam generation.....	9
2.3.3 Pre-heating of boiler feed water	10
2.3.4 Drying of bagasse.....	10
2.3.5 Drying of raw sugar.....	11
2.3.6 Heating of clear juices.....	11
2.3.7 Integration points selected for further investigation	11
3 Literature Study.....	13
3.1 Solar Energy	13
3.1.1 Solar technology review.....	13
3.1.2 Solar resource review	20
3.2 Bagasse Drying	24
3.2.1 Advantages of bagasse drying.....	24
3.2.2 Potential problems and disadvantages of bagasse drying	25
3.2.3 Drying process.....	28
3.2.4 Dryer types	30
3.3 Cogeneration and Hybridisation with CSP.....	33
4 Solar Bagasse Drying.....	38

4.1	Integration Point	38
4.2	Drying Model.....	40
4.2.1	Simprosys	40
4.2.2	Drying simulation setup with Simprosys	42
4.2.3	Simulation results	43
4.3	Solar Field Modelling and Simulation.....	44
4.3.1	Modelling of an evacuated tube air collector	44
4.3.2	Matlab simulation results	48
4.3.3	System planning using Aircow	50
4.3.4	Aircow results	53
4.4	Solar Field Simulation	56
4.4.1	Simulation setup with Solgain.....	56
4.4.2	Simulation results	59
4.5	Effect on Sugar Mill	61
5	Solar Live Steam Generation.....	63
5.1	Integration Point	63
5.2	Increasing Electricity Production	65
5.3	System Advisor Model Simulation Setup.....	67
5.4	System Advisor Model Simulation Results.....	69
5.5	Effect on Sugar Mill	72
6	Economic Assessment.....	75
6.1	Investment Costs.....	75
6.1.1	Specific investment costs of the bagasse drying solar field	75
6.1.2	Specific investment costs of the live steam generation solar field	76
6.2	Levelised Cost of Heat.....	76
6.3	Internal Rate of Return	79
7	Conclusion	81
7.1	Summary of Findings	81
7.2	Concluding Remarks	82
7.3	Recommendations for Further Work	83
	Appendix A: Airwasol Brochure	84
	Appendix B: Matlab Model Calculations	87
	Appendix C: Matlab Model Comparison	91
	Appendix D: Aircow Optimisation.....	93
	Appendix E: Comparison of Tracking Systems.....	97
	References.....	98

List of Figures

Figure 1: Modelling and simulating the solar bagasse drying integration option. ...	3
Figure 2: Locations of Sugar Mills in South Africa (Beukes et al., 2015)	5
Figure 3: Simplified sugar milling processes (Hess et al. 2016)	6
Figure 4: BRTEM sugar mill steam network adapted from Hess et al. (2016)	7
Figure 5: Schematic of a flat plate collector (Solar Advice, 2016).	14
Figure 6: Energy input and losses for an evacuated tube.	15
Figure 7: (a) Schematic of a parabolic trough collector (Cabrera et al., 2013). (b) Actual parabolic trough from Sunray Energy facility in Daggett (Sun & Wind Energy, 2017).	16
Figure 8: (a) Reflection of sunrays onto absorber in linear Fresnel collector (Electromagnetic Foundations of Solar Radiation Collection, 2017). (b) Linear Fresnel collector at Kimberlina, U.S.A. (CSP World Organisation, 2015)	18
Figure 9: Central receiver system at Crescent Dunes (Solar Reserve, 2017).	20
Figure 10: (a) Direct normal irradiance. (b) Global tilted irradiance. (Meyer, 2016)	21
Figure 11: KwaZulu Natal Solar Resource (GeoSUN, 2012).	22
Figure 12: DNI comparison of Upington and Durban (Meyer, 2016).....	23
Figure 13: (a) Annual GHI for Durban from 1994 - 2016. (b) Monthly average GHI for Durban (Solargis, 2017)	23
Figure 14: (a) Bagasse to steam ratio as a function of the bagasse moisture content. (b) Boiler fan power as a function of the bagasse moisture content (Magasiner, 1987).	25
Figure 15: Simulation of different bagasse moisture contents for a boiler, similar to the one assumed for the BRTEM model (Laubscher, 2017)	26
Figure 16: Drying rate under constant drying conditions (Tawfik et al., 2003)....	28
Figure 17: The heating of bagasse under an oxygen atmosphere from Sosa- Arnoa and Nebra, 2009).....	29
Figure 18: Co-current rotary dryer system	31
Figure 19: Pneumatic dryer system	32

Figure 20: Layout of the Borges Termosolar hybrid power plant (Biomass Knowledge Portal, 2015).	33
Figure 21: Electricity output of the hybrid concept designed by (Peterseim et al, 2014)	34
Figure 22: Simplified layout of CSP integration into a Brazilian sugar mill (Burin, et al., 2016)	35
Figure 23: LCOE and additional electricity produced for different solar multiples (Burin, et al., 2016)	36
Figure 24: Basic schematic of solar bagasse drying integration point.	39
Figure 25: Simprosys model layout.	42
Figure 26: (a) Airwasol air collector. (b) One of the evacuated tubes in the Airwasol air collector (Siems, 2017).	44
Figure 27: Schematic of heat transfer resistances in an evacuated tube.	45
Figure 28: Matlab simulation results for the evacuated tube	48
Figure 29: Extract of Paradis et al. (2015) experimental results. (a) Ambient air temperature, simulation output temperature and experimental output temperature as a function of time. (b) Tilted irradiance, horizontal irradiance and reflected irradiance. (c) Wind speed during testing. (d) Volume flow rate through evacuated tube.	49
Figure 30: (a) Flow in a manifold's lateral from Bajura& Jones (1976). (b) Airwasol collectors connected in a row, with headers on the far left and far right and supports in between (Siems, 2017).....	52
Figure 31: Solgain system layout (Ilchmann et al., 2016).....	58
Figure 32: Comparison of available solar radiation and thermal energy delivered to process.....	60
Figure 33: Simulated solar thermal energy delivered to the drying system.	61
Figure 34: Solar live steam integration into a generic sugar mill, adapted from Hess et al. (2017).	64
Figure 35: Schematic of Configuration 2	65
Figure 36: Schematic of Configuration 3	66
Figure 37: Simulated annual solar field output.....	70
Figure 38: Simulated annual solar field output for an east-west tracking axis system	71
Figure 39: Possible electricity exports.....	74

Figure 40: The transmissivity of Borofloat 33 over various wavelengths (Schott, 2017).....88

Figure 41: Change in collector outlet temperature as flow rate changes as predicted by model of Paradis et al. (2015)91

Figure 42: Change in collector outlet temperature as flow rate changes as predicted by model used in thesis.91

Figure 43: Change in collector efficiency as flow rate changes as predicted by model of Paradis et al. (2015)92

Figure 44: Change in collector efficiency as flow rate changes as predicted by model used in thesis.92

Figure 45: Aircow’s Global system considered for mass flow optimisation as shown in the Aircow manual (Fraunhofer ISE, 2017).93

Figure 46: Comparison of different number of collectors in a row with optimised flow as shown in the Aircow manual (Fraunhofer ISE, 2017).96

Figure 47: Comparison of the performance of the two tracking systems on 21 June.97

Figure 48: Comparison of the performance of the two tracking systems on 20 December.97

List of Tables

Table 1: Sugar milling parameters used for this study.	9
Table 2: Typical design and performance values for rotary dryers (Bruce & Sinclair, 1996).....	31
Table 3: Typical design and performance values for a pneumatic dryer (Bruce & Sinclair, 1996).....	32
Table 4: Input values for Simprosys simulation.	43
Table 5: Simprosys outputs.....	43
Table 6: Airwasol evacuated tube characteristics	45
Table 7: Data points for Aircow input	53
Table 8: Evacuated tube quadratic model coefficients as determined by Aircow.....	54
Table 9: Converted coefficients for liquid collector simulation.	56
Table 10: Inputs for Solgain	59
Table 11: Simulation characteristics as calculated by Solgain	60
Table 12: Solar field parameters for the two SAM simulations.	69
Table 13: SAM simulation results	69
Table 14: SAM simulation results for an east-west tracking system.....	71
Table 15: Impact of solar live steam generation.....	72
Table 16: Values used to determine electricity generation.....	73
Table 17: LCOH of the solar thermal integration options.....	78
Table 18: IRR for the integration options.....	79

Nomenclature

Symbol	Description	Unit
A	Cross sectional area	m^2
A_a	Outside area of the absorber	m^2
c_{ad}	Specific heat capacity of dry air	J/(kg K)
c_{am}	Specific heat capacity of the moisture in air	J/(kg K)
c_{bd}	Specific heat capacity of dry bagasse	J/(kg K)
c_{bm}	Specific heat capacity of the moisture in bagasse	J/(kg K)
c_{eff}	Effective collector heat capacity	$kJ/(m^2 K)$
$c_{p,HTF}$	Specific heat capacity of the heat transfer fluid	J/(kg K)
$c_{p,c}$	Specific heat capacity air in collector	J/(kg K)
C_1	Linear heat loss coefficient	$W/(m^2 K)$
C_2	Quadratic heat loss coefficient	$W/(m^2 K^2)$
C_m	Mass flow dependant heat loss coefficient	h/kg
C_n	Capital investment costs	Euro
d	Nominal discount rate	%
D_g	Glass tube outer diameter	m
E_b	Energy emitted for specific wave length	W
f	Friction factor	-
F	Solar fraction	-
G	Global horizontal irradiance	W
G_b	Direct horizontal irradiance	W
G_d	Diffuse horizontal irradiance	W
G_{bn}	Direct normal irradiance	W
G_{bt}	Direct irradiance on tilted collector	W
G_{rt}	Reflected irradiance on tilted collector	W
G_{st}	Diffuse irradiance on tilted collector	W
G_t	Solar irradiance on tilted collector	W
h_{cond}	Enthalpy of condensate	kJ/kg
h_{exhs}	Enthalpy of exhaust steam	kJ/kg
h_{ls}	Enthalpy of live steam	kJ/kg

h_{BFW}	Enthalpy of boiler feed water	kJ/kg
h_{rad}	Heat transfer coefficient between glass and sky	W/(m ² K)
Δh_A	Latent heat of vaporisation	kJ/kg
Δh_B	Heat of sorption	kJ/kg
I_A	Enthalpy of drying air	kJ/kg
I_B	Enthalpy of bagasse	kJ/kg
I_s	Irradiance through glass tube	W
k	Thermal conductivity	W/(m K)
K_b	Direct irradiance incidence angle modifier	-
K_d	Diffuse irradiance incidence angle modifier	-
\dot{m}	Air mass flow in collector	kg/s
\dot{m}_a	Air mass flow in dryer	kg/h
\dot{m}_b	Bagasse mass flow in dryer	kg/h
\dot{m}_{bag}	Bagasse mass flow into boiler	ton/h
\dot{m}_{exhs}	Exhaust steam flow rate	ton/h
\dot{m}_{ls}	Live steam flow rate	ton/h
\dot{m}_{BFW}	Boiler feed water flow rate	ton/h
\dot{m}_{HTF}	Mass flow in parabolic trough loop	kg/s
M_{ev}	Moisture evaporated	kg/h
n	Year	-
N	Project financial life span	years
N_L	Number of loops	-
p	Pressure	Pa
Δp_{coll}	Pressure drop in collector	Pa
Δp_{sys}	System pressure drop	Pa
P_{fan}	Fan power	W
Q_{ag}	Radiation heat transfer between absorber and glass	W
Q_c	Indirect supplied heat to dryer	kW
Q_{coll}	Thermal energy delivered by the solar field	kW
Q_{gain}	Collector energy gain	W
Q_l	Heat losses in dryer	kW
Q_m	Mechanical input into dryer	kW

Q_n	Annual yield of the parabolic trough system	kWh
Q_{need}	Thermal energy needed by the process	kW
Q_p	Thermal energy delivered to the process	kW
Q_{PT}	Thermal power of parabolic trough field	kW
Q_{rad}	Radiation onto absorber	W
$Q_{rad,a}$	Radiation absorbed by glass	W
Q_{sun}	Sun's energy delivered to solar field	kW
Q_t	Heat carried into dryer by transport device	kW
$Q_{th,dry}$	Thermal energy for dryer	kW
r_a	Outer radius of absorber	m
r_g	Inner radius of glass tube	m
R_1	Linear pressure drop coefficient	Pa/(kg/h)
R_2	Quadratic pressure drop coefficient	Pa/(kg ² /h ²)
R_{ag}	Resistance to heat transfer from absorber to glass	K/W
R_{air}	Resistance to heat transfer from absorber to air	K/W
R_{gsky}	Resistance to heat transfer from glass to sky	K/W
$R_{g\infty}$	Resistance to heat transfer from glass to ambient air	K/W
R_{sys}	System flow resistance	Pa/(m ³ /h) ²
T	Temperature	K
T_a	Absorber temperature	K
T_{air}	Air temperature in collector	K
T_b	Bulk temperature	K
T_f	Mean collector temperature	K
T_g	Glass temperature	K
T_{sky}	Sky temperature	K
T_∞	Ambient temperature	K
v	Air velocity in collector tube	m/s
v_g	Gas velocity	m/s
X	Moisture content of bagasse	%
Y	Moisture content of air	%

Greek Symbol	Description	Unit
α	Absorptance	-
β	Volume expansivity	1/K
β_c	Collector tilt	-
ε_a	Emissivity of absorber	-
ε_g	Emissivity of glass	-
η_{NCV}	Boiler efficiency based on net calorific value of fuel	%
η	Collector efficiency	%
η_0	Conversion factor	%
η_s	Annual system efficiency	%
η_u	Degree of utilisation	%
θ	Incidence angle	°
θ_s	Zenith angle of the sun	°
λ	Wavelength	μm
ν	Kinematic viscosity	m^2/s
ρ	Reflectivity	-
ρ_{grad}	Ground reflectivity	-
τ	Transmissivity	-

Dimensionless Numbers

Nu	Nusselt number
Pr	Prandtl number
Ra	Raleigh number
Re	Reynolds number

Abbreviations

AE	Additional Electricity
BPST	Back pressure steam turbine
CSP	Concentrated solar power
CEST	Condensing extract steam turbine
DNI	Direct normal irradiance

ECO	Economiser
EfB	Energy from Boiler
EfW	Energy from Waste
EVAP	Evaporation
GCV	Gross calorific value
GHI	Global Horizontal irradiance
GTI	Global tilted irradiance
IPP	Independent power producer
IPPPP	Independent power producer procurement plan
IRR	Internal rate of return
LCOE	Levelised cost of electricity
LCOH	Levelised cost of heat
NCV	Net calorific value
REIPPPP	Renewable Energy Independent Power Producer Procurement Program
SAM	System advisor model
SH	Super Heater
SMRI	Sugar Milling Research Institute
STEP-Bio	Sugarcane Technology Enabling Programme for Bio-Energy
ST	Solar Thermal
TMY	Typical meteorological year

1 Introduction

1.1 Background

The South African sugar industry wants to be more cost competitive and energy efficient. To support this endeavour, the South African Department of Science and Technology fund the Sugarcane Technology Enabling Programme for Bio-Energy (STEP-Bio) with the Sugar Milling Research Institute (SMRI) coordinating the research within the program. The overall aim is to increase the revenue per unit sugarcane processed by developing fully integrated sugarcane bio-refineries. This will also allow the sugar milling industry to diversify their income, which can help with economic growth and lessen the impact of low sugar production due to droughts, as in 2016 and 2017.

The aim of the research reported in this study is to assess to what extent solar thermal energy can be used to reduce the running costs of South African sugar mills and to open up additional income streams. This can ensure sustainability and will make the industry less susceptible to South Africa's increasing energy prices. In initial studies on the topic by Beukes et al. (2015) and Hess et al. (2016), along with feedback from the STEP-Bio steering committee, two solar integration concepts have been identified as plausible options for implementation in the near future. These are: the generation of live steam using concentrated solar power (CSP) collector technology and the drying of bagasse using solar heated air.

Renewable energy has received a lot of focus the past few decades and the 2015 Paris Climate Conference put great emphasis on countries incorporating renewable and sustainable technology into their energy sectors. There are various renewable energy resources which can be used instead of fossil fuels, the challenge, however, lies in creating economically viable solutions in an ever growing and competitive environment. Various sources believe that renewable energy will be able to meet most of the growing demand in energy, and this at equal or lower prices than conventional energy sources (Kalogirou, 2009), painting a bright future for renewable energy technologies.

The solar generation of live steam aims to increase electricity production in order to sell it to the grid. This will allow the mills to expand their income stream. The drying of bagasse will increase the calorific value of the bagasse, which can lead to bagasse or coal savings and higher boiler efficiencies.

This project builds on the work of Beukes et al. (2015) and Hess et al. (2016) and will focus on the above-mentioned solar thermal integration points and their effect on the sugar milling process. This study worked closely with the SMRI regarding the integration of the solar thermal technology, to ensure that the solar integration options can provide realistic solutions and that it suits the sugar mills' operating conditions.

1.2 Motivation

The Department of Energy created a programme for independent power producers (IPP) to help increase South Africa's electricity capacity. The programme, called the Independent Power Producer Procurement Programme (IPPPP), requests bids for cogeneration projects. The programme caters for a maximum of 800 MW_{el} in the first bidding round and this was later increased to 1800 MW_{el}. Approximately 25% of this capacity is allocated for combined heat and power projects. Priority is given to projects where the energy output can be increased by upgrading existing equipment and improving operating efficiencies. The STEP-Bio programme seems to fit all the criteria of this program. This would enable sugar mills to export electricity to the grid and open up a new income stream.

Large scale Solar Process Heat (SPH) integration within South Africa's industrial sector is still in a developmental phase, with no recorded high temperature processes using solar energy. This project can help the country realise its potential in terms of SPH integration. It can put the sugar milling industry in the spotlight as an innovative and green industrial sector and serve as a demonstration of how solar energy can be utilised for process heat.

1.3 Objectives

This study focuses on solar bagasse drying and solar live steam generation in order to give a sugar factory a feasible solution for increasing their revenue per unit sugarcane processed. The objectives of this study are to:

- Further develop specifically adapted solar thermal system concepts for the two most promising integration points.
- Create detailed simulation results for the annual heat production of the solar thermal systems in the integration concepts.
- Determine the impact the solar process heat technologies can have on the sugar mill.
- Determine the financial feasibility of the two integration points.

The above objectives will allow this study to paint a clear picture of how solar thermal energy can be incorporated in South African sugar mills, the impact it can have and if it is financially viable.

1.4 Methodology

The first step of this study was to review the work of Beukes et al. (2015) and Hess et al. (2016) to better understand the potential of solar thermal integration options for South African sugar mills. A brief study on the South African sugar industry was done to be able to understand and work with the generic sugar mill model of Starzak and Zizhou (2015). In order to further develop the two chosen solar thermal integration points a good understanding of solar energy, bagasse drying and cogeneration with CSP was needed, and therefore researched.

To further develop the solar bagasse drying integration point a drying model of the bagasse dryer is created in Simprosys (Simprotek, 2006). By simulating this model the needed thermal energy and air flow to dry the bagasse can be determined. Figure 1, shows how this was used along with other models to setup a simulation in Solgain (Ilchmann et al., 2016).

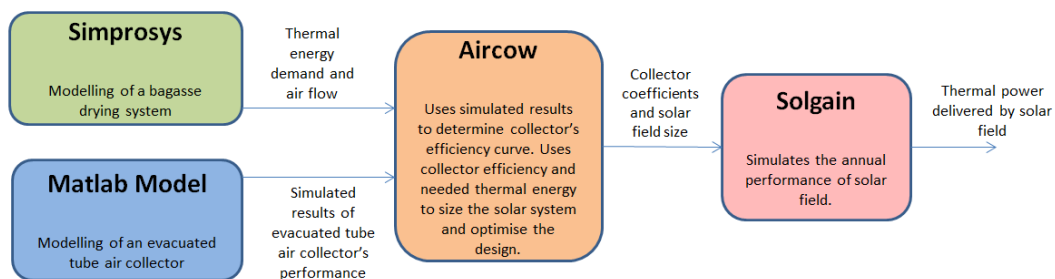


Figure 1: Modelling and simulating the solar bagasse drying integration option.

The thermal power delivered by the solar field is used to determine how much energy the integration point can save for the bagasse drying system. Furthermore, the amount of bagasse and coal that can be saved by the drying system is calculated.

To further develop the solar live steam generation integration point two new turbine configurations and their possible impact on the sugar mill are discussed. System Advisor Model (SAM) (National Renewable Energy Laboratory, 2017) is used to simulate the suggested solar field. The simulation gives the thermal power generated by the solar system as one of its outputs, and this is used to determine the effect the integration point can have on the sugar mill.

The simulation results of the two integration points are then used to determine the financial feasibility of the two integration points. Literature sources and solar project databases are assessed in order to try and get an as accurate as possible estimate of the investment costs. An economic assessment is done by determining

the levelised cost of heat (LCOH) and internal rate of return (IRR) for both options.

Finally, conclusions are drawn regarding the technical and financial feasibility of solar thermal integration into South African sugar mills.

1.5 Research Limitations

This study is based on a generic South African sugar mill as described by Starzak and Zizhou (2015), specifications regarding this generic mill will be discussed in section 2.1. In reality no two sugar mills are alike, varying in size and technology. This is why a mill which represents the average industry practices was chosen.

Therefore, the integration options specified in this study will have to be adapted for a specific mill, if it is considered implementing the proposed solar thermal technology. This will mean having to re-evaluate certain assumptions and the solar thermal technology's suitability for the mill. Furthermore, the solar resource at the mill's location will have to be evaluated and the simulations and economic assessment will have to be done again, incorporating all the new factors.

2 Project Background

This section will give more information regarding the sugar milling industry, the various processes in the sugar mills and the work that Beukes et al. (2015) and Hess et al. (2016) did for the STEP-Bio project.

2.1 Sugar Milling Industry in South Africa

The agriculture and agro-processing of sugarcane in South Africa are very important, employing almost 80 000 people and making important contributions to the national economy and especially the provincial economies of KwaZulu Natal and Mpumalanga (Smith et al., 2016). South Africa has 14 sugar mills scattered across the two above mentioned provinces, as can be seen in Figure 2.



Figure 2: Locations of Sugar Mills in South Africa (Beukes et al., 2015)

In 2016 a total of 14.86 million tons of sugarcane were processed by these mills, producing 1.64 million raw and refined sugar as well as a wide range of sugar by-products (Smith et al., 2016). However, 2016 and 2017 were both below average years in terms of sugar production, due to the severe drought in the area during these two years (Singels et al., 2017). The industry actually has the capacity to process 22 million tons of sugarcane per crushing season and prospects for future production looks good due to the end of the drought (Madho et al., 2017).

Each mill's capacity differs, ranging from 90 to 550 tons of cane processed per hour (Smithers, 2014). In the 2016 season the average sugar mill ran for 233 days

and had an overall time efficiency (OTE) of 80.83 % (Smith et al., 2016). The crushing season, during which the sugarcane is harvested and processed by the mills, stretch between March and December and during this time the sugar mills run day and night. Most South African cane producers use manual harvesting techniques to get the sugarcane; this usually requires burning the sugar cane field before hand, making it easier for the workers to harvest. The cane is then cut, bundled and transported to the mills. There are, however, producers which use motorised harvesters and harvests the cane while it is still green.

2.2 Generic Sugar Milling Process

As mentioned in Section 1.4, Starzak and Zizhou (2015) created a model which represents a theoretical South African diffuser sugar mill as part of their study called the Biorefinery Techno-Economic Modelling Project (BRTEM). The process parameters used for this study are all results from the BRTEM model, unless stated otherwise. It is important to note that the BRTEM model under predicts the energy consumption of a real factory, as the modelled sugar milling processes are more energy efficient than what they are in reality (Foxon, 2017). The BRTEM model was designed and validated for describing the process flow characteristics of a generic sugar mill, with less emphasis on validating the energy consumption of the mill. Figure 3 shows the sugar milling processes for the generic South African mill.

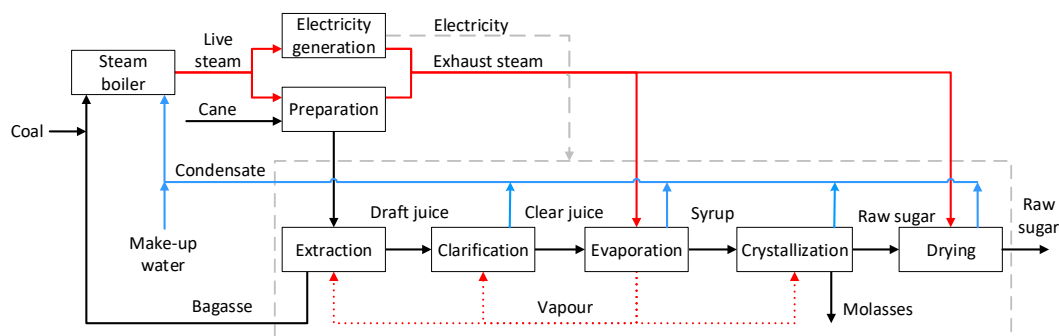


Figure 3: Simplified sugar milling processes (Hess et al. 2016)

During the cane preparation process dirt and rocks are removed from the harvested cane, where after it is shredded in order to ease extraction. Sucrose is leached from the shredded cane through the addition of imbibition water to form the draft juice during the extraction process. After extraction the shredded cane passes through roller mills to press out remaining sucrose and to reduce the cane's moisture content. The shredded cane, now called bagasse, and sucrose are then split up, with the bagasse heading to the boiler house where it is used as fuel. The draft juice goes on to be clarified in order to remove impurities. The clear juice then enters an evaporation process where it forms a syrup. The syrup is then

crystallized by boiling it under a vacuum, forming raw sugar and molasses (Rein, 2007). The raw sugar is separated from the molasses and the surface moisture dried off.

There are two types of mills in use worldwide, namely: milling tandem systems and diffuser systems. These systems differ in the way the sugars are extracted from the sugarcane. The milling tandem system uses a series of mills which mechanically squeezes the juice out of the sugarcane. The diffuser relies on the diffusion and leaching of sugars to the imbibition water it soaked in (Oliverio et al., 2014). Figure 3 represents a generic South African diffuser mill, because the *Extraction* process relies on diffusion, the processes thereafter is to create raw sugar from the imbibition water and sugarcane juice mixture.

It is important to distinguish between the two types of mills, because it has a major influence on the mill's energy and steam consumption. The milling tandem sugar mills rely on live steam to drive the mechanical mills, while diffuser mills uses lower temperature steam for heating the imbibition water (Foxon, 2017).

Figure 4 shows a schematic of the steam network of the generic South African mill as specified in the BRTEM model. A sugar mill's main energy source is bagasse, the fibrous residue left of the sugarcane after the sugar extraction process. Some of the mills export their bagasse, it can be sold to produce fertiliser, animal feed, or paper, alternatively the mill can use it to create bio-ethanol. The mills that do export their bagasse need extra fuel and in South Africa the sugar mills use coal as an auxiliary fuel, because of its abundance and low price in the country.

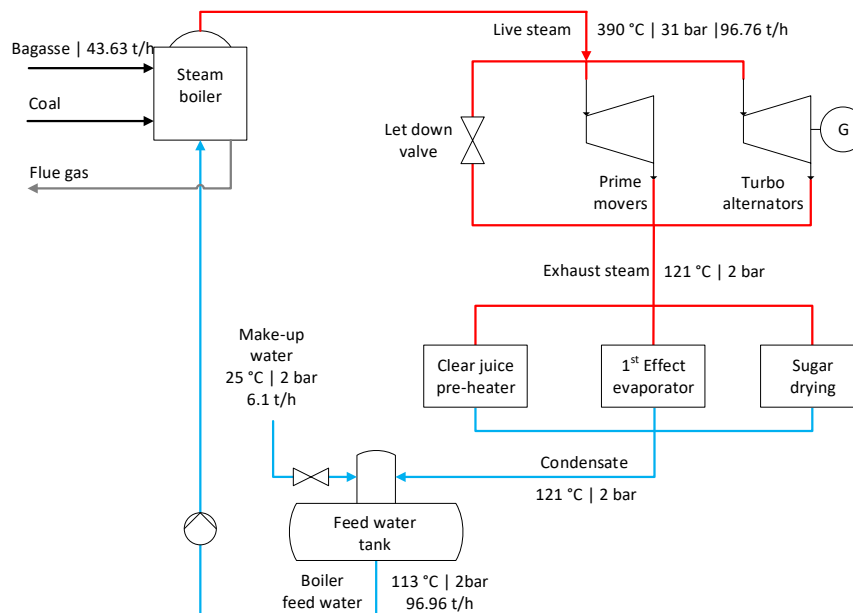


Figure 4: BRTEM sugar mill steam network adapted from Hess et al. (2016)

Live steam is used to drive three prime movers (cane knives, cane shredder and dewatering mill) and a back pressure steam turbine (BPST). The three prime movers prepare the sugarcane for sugar extraction while the turbine is connected to an electric generator which supplies electricity to the mill. The exhaust steam from the prime movers and turbine is used to supply thermal energy to the sugar extraction and production processes via various heat exchangers. If the sugar extraction processes need more exhaust steam than can be delivered by the prime movers and turbine, live steam passes through a let-down station where it is turned into exhaust steam.

The BRTEM model assumes that there is no need for let-down steam; however, in reality most sugar mills are designed so that all the turbines do not supply more than the lowest exhaust steam demand under relatively normal conditions. This relates to 75 % - 95 % of the normal exhaust steam demand, therefore, the live steam let-down valve is used to supply the remaining 5 % - 25 % of the necessary exhaust steam (Rein, 2007; Foxon, 2017). For this study it is assumed that the let-down valve needs to supply 10 % of the exhaust steam on average for the generic sugar mill.

The system described above and by the BRTEM model is for a generic South African sugar mill, however, four of the mills have back-end sugar refineries, where the raw sugar produced by the mill is refined to white sugar. These sugar mills tend to use a lot of extra coal, since they also operate outside of the crushing season, when there is very little bagasse available. Refineries need exhaust steam to provide thermal energy for the sugar refining process, as well as some electricity. This means that sugar mills with back-end refineries need to produce more steam and electricity during the crushing season, as can be seen in Table 1. Outside of the crushing season the steam and electricity production is significantly lower, since only the refinery is in operation as it processes the raw sugar produced by other mills which do not have back-end refineries.

Table 1 shows the difference in energy needs between the normal mill and the mill with a refinery. The values for the normal mill come from the BRTEM model simulation results, while the refinery values were calculated for this study as described below.

Rein (2007) gives the mass flow ratio between exhaust steam used in a refinery and raw sugar refined as 1:1. The BRTEM model's simulation results show that the mill produces 29.08 ton/h raw sugar. Assuming that the refinery only has the capacity to process the 29.08 ton/h raw sugar coming from the mill, its steam consumption will be 29.08 ton/h. It is important to note that the sugar mill does not operate outside of the crushing season, only the refinery does, as it refines the raw sugar from other factories without back end refineries.

Table 1: Sugar milling parameters used for this study.

System	Live Steam Heat Demand		Steam Usage		Cane Crushed + Raw Sugar Refined	
	Crushing Season [MW]	Outside Crushing Season [MW]	Crushing Season [ton/h]	Outside Crushing Season [ton/h]	Crushing Season [ton/h]	Outside Crushing season [ton/h]
Sugar Mill	73	0	95	0	244.18	0
Sugar Mill with Refinery	95	22	125	29.08	244.18 + 29.08	0 + 29.08

2.3 Possible Solar Thermal Integration Points

As mentioned before, Beukes et al. (2015) and Hess et al. (2016) looked at various options for solar thermal integration for South African sugar mills. They came up with six different integration options, they are: live steam generation, exhaust steam generation, pre-heating of boiler feed water, drying of bagasse, drying of raw sugar and the heating of clear juices. This section will very shortly explain each of the integration options as they developed it.

2.3.1 Live steam generation

For this integration point a concentrating solar system will heat up thermal oil (used as heat transfer fluid) which will be used to produce steam in a kettle type heat exchanger. The steam will have to be of a high enough pressure to pass through the pressure valve and enter the conventional steam system.

By providing extra live steam through the solar thermal system, the boiler's load can be reduced. This will allow the mill to save either bagasse or coal. The mill could produce extra electricity as well, if there was a process which could use the extra exhaust steam from the BPST or if an alternative turbine configuration can be installed, this will be discussed further in Section 4.

2.3.2 Exhaust steam generation

In this possible solar integration point stationary concentrating collectors or stationary non-concentrating collectors can be used to supply the necessary thermal energy. These technologies are considerably less complicated than what is needed for the live steam generation point, because of the relatively low temperature of the exhaust steam. The lower temperature and pressure of exhaust steam allows for direct steam generation technology to be used, eliminating the need for a kettle type heat exchanger and expensive heat transfer fluids.

This integration option is similar to the previous one, in the sense that it lessens the boiler's load, however, for this integration option it is to a lesser extent and the solar thermal energy is provided as exhaust steam. By producing exhaust steam, the mill can reduce the amount of live steam that needs to be let down and therefore the amount of live steam that needs to be generated. The solar system can provide the extra exhaust steam needed by the sugar extraction processes, which the prime movers and turbine cannot provide. This will allow the mill to save bagasse or coal.

The exhaust steam integration option could allow the mill to produce extra electricity if there was an alternative turbine configuration which exhausted the live steam in the turbine to below atmospheric conditions. This will then allow the solar system to provide the necessary exhaust steam to the mill which the turbine usually provided.

2.3.3 Pre-heating of boiler feed water

For this integration point concentrated solar collectors can be used to heat the boiler feed water to 200 °C. This can be done by using pressurised water or thermal oil as heat transfer fluid. The heat transfer fluid heats up the feed water through a cost-effective plate heat exchanger, which has to be located downstream from the feed water pump in order to avoid steam forming in the heat exchanger.

In the sugar milling industry the role of feed water pre-heating is usually fulfilled by economisers, which recovers heat from the boiler's flue gas to heat up the feed water. As mentioned before, the BRTEM model does not take energy efficiency measures like this into account, which opens the door for solar thermal integration. However, it is good practice to implement energy efficiency measures before solar thermal integration is considered.

2.3.4 Drying of bagasse

Bagasse moistures typically vary between 46 % and 52 % as they leave the dewatering mills for the boiler. In the 2015/2016 crushing season the average moisture content of the bagasse from all the mills was 51 % (Smith et al., 2016). Bagasse can be dried to a technical lower limit of 30 % moisture content (Rein, 2007), but for the South African sugar milling industry the limit is set to 40 %. This is the bottom range for which the boilers were designed and they might struggle to perform properly using bagasse with lower moisture contents (Foxon, 2017). Bagasse drying is also not included in the BRTEM model, this is due to the fact that it is not common practice in South Africa.

Bagasse drying has numerous advantages; it can improve boiler efficiency, reduce fuel consumption, create higher flame temperatures and reduce excess air requirements. By drying bagasse from 51 % to 40 % the bagasse gross calorific value can increase by 24 % (Beukes et al., 2015). For the drying system a

stationary solar air collector can be used to heat air which would then pass through a rotary dryer where the bagasse is dried.

2.3.5 Drying of raw sugar

Sugar drying is a very common in South African sugar mills and is therefore included in the BRTEM model. Exhaust steam is used to heat air which then enters a rotary dryer where the sugar is dried. Stationary solar air collectors can be used to pre-heat the air, which would reduce exhaust steam consumption for the sugar drying process. This integration option can work out very cheap for the sugar mills due to the fact that dryers and exhaust steam air heaters are already installed. Only a small solar field would be required for this integration point, because of sugar dryings low thermal requirements.

2.3.6 Heating of clear juices

For his integration concept stationary solar collectors can be used to pre-heat the clear juices to 110 °C. A heat transfer fluid, like pressurised water can be heated up and pass through a heat exchanger to heat up the clear juices. This will happen between the clarification stage and the evaporation stage. This will allow the mill to save exhaust steam, as less thermal energy will be required to boil the heated clear juices.

For this integration point it is important that the heat exchanger is bypassed during times when the solar field cannot deliver the needed 110 °C. This would avoid a heat flux from the process to the collector loop.

2.3.7 Integration points selected for further investigation

The STEP-Bio steering committee was very interested in the solar live steam generation and solar bagasse drying integration points (Hess, 2016). They felt that it warranted further investigation based on the results of the above mentioned studies.

From Hess et al.'s (2016) economic assessment, the live steam generation option fared relatively well considering the return on investment. However, it was still a more expensive option to provide thermal energy compared to coal and requires the highest capital investment. What interests the STEP-Bio steering committee is the option of using solar live steam generation in a setup which will allow for more electricity to be generated. This option was discussed in Hess et al. (2016) and will be explained in detail in Section 4.

Bagasse drying fared very well in the economic assessment mentioned above. It finished as second cheapest option and with the second highest return on investment. Only the sugar drying option did better. Both sugar and bagasse

drying were considered for further development as they would make excellent demonstration plants to showcase solar thermal technology's benefits. In the end the steering committee decided on the bagasse drying option as it offers multiple new benefits for the sugar mills.

3 Literature Study

This section looks at information found in books, journal articles, reports and conference papers regarding solar energy, bagasse drying and co-generation and hybridisation with CSP.

3.1 Solar Energy

This subsection will contain information about various solar thermal technologies commercially available and briefly explain how each technology works. The solar resource available in South Africa will also be discussed, specifically looking at KwaZulu Natal where most of the sugar mills are situated. It will explain the difference between the types of irradiance measured and what is used by the different technologies.

3.1.1 Solar technology review

Solar thermal systems convert sunlight into a heat source which can be used to drive various thermal processes. Non-concentrating collectors like flat plate and evacuated tube collectors are usually associated with low-medium temperature applications and is mostly utilised for domestic uses and process heat applications. Concentrating collectors like parabolic troughs, central receivers and linear Fresnel systems are usually associated with high temperatures and are mostly utilised for power generation. Beukes et al. (2015) and Hess et al. (2016) suggested that stationary, non-tracking collectors be used for the bagasse drying integration point and concentrating, tracking collectors be used for the solar live steam generation. This section will give a brief overview of the above mentioned collector technologies.

Flat Plate Collector:

A flat plate collector is arguably the simplest collector available. It basically consists of a transparent cover, a dark absorber plate, flow tubes and insulation as can be seen in Figure 5. It is due to this simplicity that it is one of the most common collectors and is used mostly for domestic hot water systems for single family homes (Joubert et al., 2016).

The transparent cover lets solar radiation pass through, allowing it to fall on the absorber. The absorber heats up due to its high radiation absorptivity, a heat transfer fluid passes through the flow tubes to transport the heat/thermal energy to where it is needed. Unfortunately, not all the energy can be transferred to the heat transfer fluid, there are various thermal and optical losses in the collector. Some of the radiation is reflected and absorbed by the transparent cover and there are convection, conduction and radiation losses from the absorber. The cover helps to reduce convection losses by keeping air stagnant in the collector, it also reduces

radiation losses by being transparent to the short waves received from the sun, but being nearly opaque to the long wave radiation emitted from the absorber (Kalogirou, 2009). The insulation on the sides and bottom of the absorber helps to decrease conduction losses.

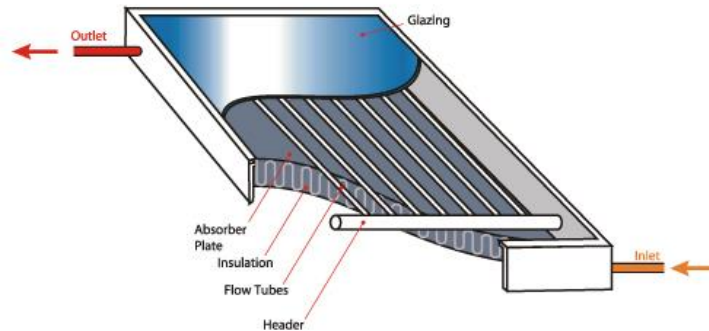


Figure 5: Schematic of a flat plate collector (Solar Advice, 2016).

Most collectors have glass covers with low iron content (which have a higher radiation transmittance than high iron content glass) however, there are low temperature collectors which use plastic covers as well. To allow the absorber to absorb as much of the solar radiation as possible and emit as little radiation as possible, it has a selective coating. The selective coating along with the limited radiation losses through the cover allows the collector to reach temperatures up to 100 °C (Duffie and Beckman, 2006). This makes it suitable for various low temperature applications, like cleaning, cooling and drying (Weiss and Rommel, 2008).

One of the main advantages of the flat plate collector is that it is inexpensive. It can use water, water-glycol mixtures or air as heat transfer fluid, all of which are very cheap. They are fixed collectors, so no expensive tracking systems are required and they do not require much maintenance (Kalogirou, 2009).

Evacuated Tube Collector:

Evacuated tube collectors are a non-tracking technology, like flat plate collectors, but can reach considerably higher temperatures (up to 200 °C) due to better heat loss prevention measures. A drawback of flat plate collectors are that they perform poorly in cold, windy and cloudy conditions due to high heat losses (Kalogirou, 2009). Evacuated tubes can perform better in these adverse conditions, due to the fact that the absorber is enclosed in a glass tube under vacuum, minimizing convection heat losses. The glass tube allows the sun's rays to pass through it and heat up the absorber and also reduces radiation losses as the transparent cover does for the flat plate collector. Figure 6 shows the energy input and losses of the

evacuated tube. The absorber also has a selective coating with low emissivity, which further reduces radiation losses.

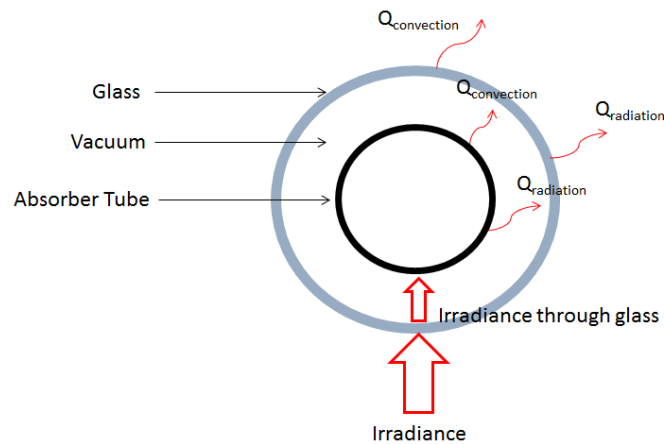


Figure 6: Energy input and losses for an evacuated tube.

Evacuated tubes collectors have similar advantages as the flat plate collectors; they are also relatively inexpensive and do not require much maintenance (Sabiha et al., 2015). If one of the tubes in the collector breaks or need to be replaced, then only that tube can be replaced, there is no need to replace the whole collector. The glass is quite fragile though and can break due to hail or poor handling (Sabiha et al., 2015).

Various heat transfer fluids can also be used for evacuated tube collectors, like water and water-glycol mixtures, for higher temperature applications above 100 °C, air and pressurised water can be used (Joubert et al., 2016). Sabiha et al. (2015) suggests that evacuated tube collectors should be used for processes with a continuous and ample load which will ensure that the heat transfer fluid does not become too hot. For lower temperature applications where water or a water-glycol mixture is used it is essential to keep the temperature below 100 °C to prevent over boiling. Boiling in the collector can expose weaknesses in the material and damage the collector and vacuum.

Evacuated tube collectors can be used for the same applications as flat plate collectors. They are especially useful if higher temperatures are needed or smaller solar fields are required, because of their higher operational temperature (Weiss and Rommel, 2008).

Parabolic Trough Collector:

Parabolic trough collectors are the most mature CSP technology in use today. In 2015, just more than 80 % of the installed and planned CSP capacity was in the

form of parabolic trough collectors (Liu, et al., 2016). Projects like the SEGS plants, Nevada Solar One and Andasol helped to prove that parabolic troughs using thermal oils are trustworthy technology for power generation. Parabolic troughs are also used for medium and high temperature solar process heat applications, with the database for applications of solar heat integration in industrial processes (AEE Intec, 2017) listing 45 parabolic trough plants.

Parabolic troughs are classified as a line focusing technology, consisting out of a parabolic mirror, receiver tube, support structure, tracking axis and supports as can be seen in Figure 7 a and b. The parabolic mirrors or reflective coating reflects sunlight onto a receiver tube to heat it up to temperature slightly above the needed heat transfer fluid temperature. Temperatures above 500 °C can be reached, with coatings which do not degrade at such high temperatures being commercially available. However, it is the heat transfer fluid's maximum temperature which is the limiting factor for high temperature operations (Munoz-Anton et al., 2014). The hot receiver heats up the heat transfer fluid which flows through it and transports the thermal energy to where it is needed. In most cases superheated steam is created in steam generators, usually for power generation and sometimes for process heat.

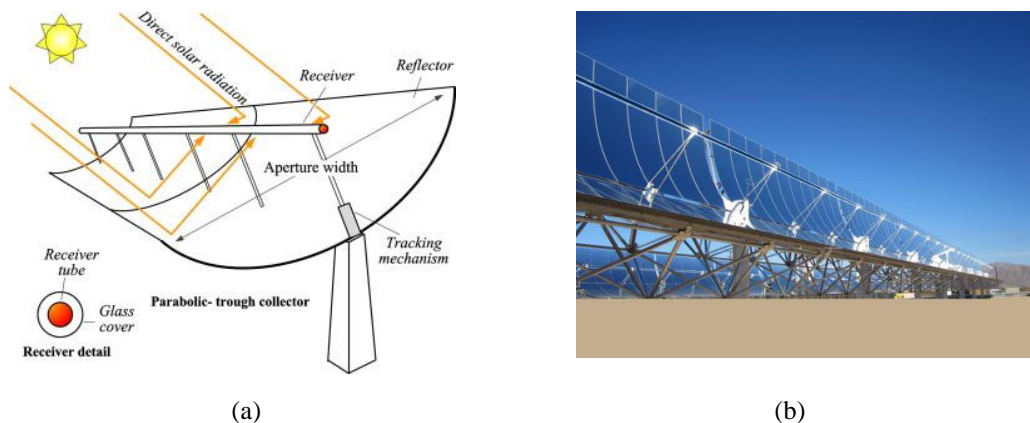


Figure 7: (a) Schematic of a parabolic trough collector (Cabrera et al., 2013). (b) Actual parabolic trough from Sunray Energy facility in Daggett (Sun & Wind Energy, 2017).

High temperature parabolic troughs have single axis tracking systems, which follows the sun during the day, allowing the parabolic mirrors to reflect the DNI onto the receiver tube. The tracking system can either be orientated on a north-south axis or an east-west axis. The north-south tracking axis is used to track the sun along the day, while the east-west axis can be used for seasonal tracking. A north-south orientation allows for more energy to be collected during the summer, while the east-west orientation has an even spread over summer and winter (Baharoon et al., 2015). The solar live steam generation integration option may benefit from the east-west tracking axis system, as most sugar mills only function during the crushing season and with the winter months coinciding with most of the crushing season.

The receiver tube onto which the DNI is reflected and through which the heat transfer fluid flows is usually put inside an evacuated glass tube for high temperature applications, similar to the evacuated tube collector. This minimises convection and radiation losses as mentioned before. For parabolic trough collectors expansion bellows are fitted at the end of the receiver tube to accommodate for differences in thermal expansion between the metal receiver and glass tube (Fernandez-Garcia et al., 2010).

Synthetic oils are by far the most common heat transfer fluid used in parabolic troughs (Gunther et al., 2013). This is mainly due to its low freezing temperature (12 °C), relatively high specific heat capacity and the fact that it can be obtained in large quantities making it easy to operate in parabolic troughs. For locations with sustained low temperatures through the winter months, trace heating might be necessary to ensure the oil does not become too thick and reach the minimum temperature of 12 °C. However, for subtropical climates such as where the sugar mills are located, trace heating should not be necessary, as temperatures rarely drop so low, and usually not for very long (Solargis, 2017).

Synthetic oil can only operate up to 400 °C, with almost all operations limiting the temperature to 393 °C as not to take any risks and damage the oil. Other disadvantages of synthetic oil are that it degrades over time, it is quite expensive, it is not environmentally friendly and it presents a fire risk since it is flammable (Heller, 2013).

In order to increase the solar field's outlet temperature, the use of molten salt as heat transfer fluid has been researched. Molten salts can operate at temperatures of up to 600 °C and holds a lot of advantages for solar thermal power generation. The main advantage of higher temperatures is a higher Rankine cycle efficiency (Giostrì, et al., 2012), which would allow for more power to be generated. However, there are few process heat applications that can benefit from these high temperatures.

Molten salt is widely considered to be the best sensible heat storage medium, with 80 % of CSP plants under construction having molten salt storage systems (Liu, et al., 2016). If it can be used in the solar field as well as the storage system, direct storage can be implemented. Previously a heat exchanger was needed between the synthetic oil of the solar field and the molten salt of the storage tanks. Another advantage of the higher temperature is that it will result in smaller storage systems (Gunther et al., 2013). Other advantages of using molten salt are that it is less expensive than synthetic oils, it is more environmentally friendly and not flammable.

The biggest worry when working with molten salts is its high freezing temperature, which can be between 120-220 °C, depending on what salt is used. This is especially problematic for line focussing systems like parabolic troughs where there are long pipe lines, increasing the risk of solidification during times

of low solar irradiance and low temperatures. There are solutions like trace heating or the circulation of stored hot salts, but this would result in higher costs, higher auxiliary electricity consumption by the plant and higher heat losses (Heller, 2013).

Direct steam generation in parabolic troughs have also been a topic of study for some while now. Direct steam generation differs from the previously mentioned heat transfer fluids, because no heat exchanger or steam generator is necessary to transfer the thermal energy to the power block. Direct steam generation allows for higher temperatures and no expensive heat transfer fluid is needed (Giotri, et al., 2012).

Operating a direct steam generation parabolic trough field is a lot more complex than operating the heat transfer fluids mentioned above, due to the two-phase flow that exists in parts of the solar field. This requires a sophisticated control system, furthermore, the mass flow of the water/steam must be high to avoid stratified flow. Another drawback is that for power generation the solar field has to operate at the same pressure as the turbine inlet, placing a lot of stress on the solar loop (Giglio et al., 2017).

Linear Fresnel Collector:

Linear Fresnel collectors are classified as a line focussing technology, like the parabolic troughs, but uses multiple long, flat mirrors to reflect the sun onto an absorber above them as in Figure 8 and b. Another difference is that the absorber is stationary, in a parabolic trough setup the absorber moves with the trough as it tracks the sun; while for the linear Fresnel collector the absorber is stationary and only the mirrors move as they track the sun (Liu, et al., 2016). Most high temperature collectors have a secondary reflector around the absorber which ensures that all of the radiation reflected upwards from the mirrors eventually hit the absorber. The absorber is then also encased with a glass cover in front and insulation at the back.

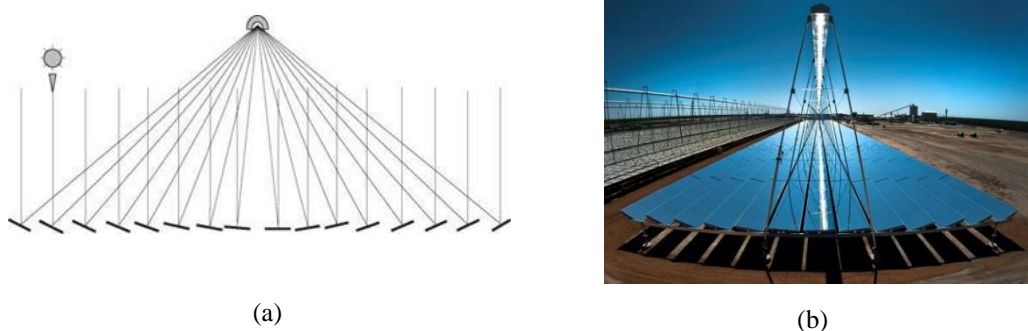


Figure 8: (a) Reflection of sunrays onto absorber in linear Fresnel collector (Electromagnetic Foundations of Solar Radiation Collection, 2017). (b) Linear Fresnel collector at Kimberlina, U.S.A. (CSP World Organisation, 2015)

Linear Fresnel systems are quite new in terms of commercial deployment, the National Renewable Energy Laboratory (2017) lists only 15 Linear Fresnel power projects of which 7 are still under construction. The database for applications of solar heat integration in industrial processes (AEE Intec, 2017) only lists 2 linear Fresnel systems used for process heat. Blackdot Energy (2017) also lists a linear Fresnel system which is used in an absorption cooling system in Johannesburg, South Africa.

Linear Fresnel systems are seen by many as a technology which can significantly reduce the price of CSP. The collectors cost less to produce because the mirrors are cheaper than that of parabolic troughs, the structure is lighter and it is less affected by high wind speeds (Abbas et al., 2016). Direct steam generation can further reduce prices by eliminating the need for expensive heat transfer fluids.

However, the collector efficiency of linear Fresnel collectors is lower than for parabolic trough collectors. This is due to lower optical efficiencies of the mirrors and because of blocking and shading of mirrors. Parabolic troughs also have higher thermal efficiencies due to the absorber being enclosed in a vacuum. Abbas et al. (2016) report that linear Fresnel collectors are 37 % less efficient than parabolic troughs, but that they can generate 21 % more energy per square meter of land used due to its more efficient use of space. Although linear Fresnel systems are not the most efficient and technical CSP option, it does offer various economic benefits and can become the best commercial choice in the right conditions (Peterseim et al., 2014).

Central Receiver Systems:

The first commercial central receiver power plants were only built in 2007, near Seville in Spain. Making it a relatively new commercial CSP option, although the first test facilities have already been built in 1978, near Albuquerque, in the U.S.A. (Ho, 2017). Central receiver systems or power towers, as they are often called, consists of an elevated receiver onto which an array of mirrors (called heliostats) reflects and focusses the sun on, as can be seen in Figure 9. The heliostats follow the sun on a two axis tracking system in order to focus it on the central receiver, making it a point focussing system (Stine and Geyer, 2001).

Central receiver systems have the potential to reach much higher temperatures (above 1000 °C) than parabolic trough and linear Fresnel collectors (Liu, et al., 2016). This is due to the much higher concentration ratio that can be reached through the heliostat field. As mentioned before, there are various advantages related to higher temperatures in solar power plants. This is why 60 % of the planned CSP power plants at the end of 2016 were central receiver systems (Ho, 2017). At the moment central receivers are mainly being used for power generation, since this application can utilise the high maximum temperatures.



Figure 9: Central receiver system at Crescent Dunes (Solar Reserve, 2017).

There are various heat transfer fluids and mediums which can be used in central receivers like air, gas, ceramic particles and liquid sodium which can handle the high temperatures; but most installed systems still use water/steam and molten salts as heat transfer fluids, operating at temperatures below 600 °C (Ho, 2017). The design of receiver itself depends what heat transfer fluid is being used, to ensure efficient heat transfer and minimal radiation heat losses. For the very high temperature systems it is very important that the receiver does not experience extremely high radiative losses due to the high temperatures, as this would defeat the purpose of trying to create a more efficient plant.

The high temperatures suit power generation perfectly, but process heat applications cannot really benefit from it. This might be the reason why there are no recorded central receiver systems which are used for solar process heat, according to the database for applications of solar heat integration in industrial processes (AEE Intec, 2017).

One drawback of using a central receiver system in a subtropical climate is that the high humidity associated with these areas would negatively impact the solar field efficiency. This is because the radiation reflected from the heliostats are absorbed and scattered by the moisture in the air as it travels to the receiver (Cardemil et al., 2013). The solar attenuation due to humidity and aerosol can reduce the annual plant yield up to several percentile points, depending on the size of the solar field, location and the plant's operation strategy (Hanrieder et al., 2017).

3.1.2 Solar resource review

Solar thermal technologies utilises the radiation within the ultraviolet, visible and infrared spectrums from the sun to supply thermal energy (Kalogirou, 2009). The sun emits radiation at an intensity of $6.33 \times 10^7 \text{ W/m}^2$ from its surface (Stine and Geyer, 2001), the intensity of the radiation decreases with distance from the

sun. The radiation falling on Earth's outer atmosphere varies between 1330 W/m^2 and 1400 W/m^2 , depending how far the Earth is from the sun during its elliptic orbit (Stine and Geyer, 2001).

The solar radiation reaching the earth's surface is usually lower than the radiation which reached the outside of the atmosphere. This is due to gas, dust and water particles in the sky which absorbs some of the radiation and also reflects and scatters it (Duffie and Beckman, 2006). Some of the reflected and scattered radiation leaves the earth's atmosphere, but most of the scattered irradiance eventually reaches the surface due to the entire sky vault, this is called diffuse radiation (Stine and Geyer, 2001). The solar radiation that directly reaches the earth's surface is called direct or beam radiation.

Concentrating collectors only use direct irradiance, as diffuse irradiance cannot be concentrated due to its nature of coming from various angles to the collector. Non-concentrating collectors can use both direct and diffuse irradiance. In order to measure how much irradiance is available to concentrating tracking collectors, the direct normal irradiance (DNI) is measured. As can be seen in Figure 10.a, this is the direct radiation that will reach the collector when the collector is directly facing the sun.

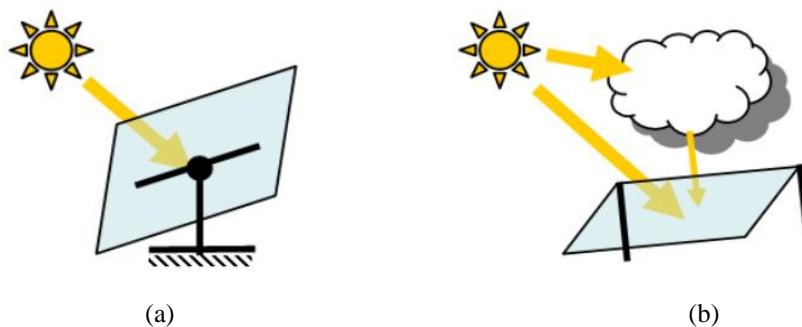


Figure 10: (a) Direct normal irradiance. (b) Global tilted irradiance. (Meyer, 2016)

To measure how much irradiance is available for the stationary, non-tracking collectors, the global tilt irradiation (GTI) is measured. As can be seen in Figure 10.b, this is the total radiation that reaches the tilted surface. The surface is tilted, as most collectors are installed at an angle to the horizontal, equal to the latitude of the location. This will enable the collectors to get a relatively equal distribution of power throughout the year. Using this tilt, the sun's angle at noontime will only vary by a maximum 23.5 degrees, above or below the normal, minimizing the cosine losses (Stine & Geyer, 2001). The most common way, however, to assess the solar resource at a location is to look at the global horizontal irradiance (GHI), it is very similar to the GTI, but the plane considered is horizontal.

Beukes (2015) and Hess (2016) assessed the solar resource at various sugar milling locations. They found that Durban would make a good reference location, as it has a similar solar resource compared to the other sugar milling locations. The GTI only varies 5 % between milling locations, while the DNI varies 10 %. Figure 11 shows a solar resource map of KwaZulu Natal, showing the annual DNI on the left and the annual GTI on the right. From these maps we can come to expect that the annual DNI at Durban should be about 1250 kWh/m² to 1400 kWh/m², while the GTI can be between 1700 kWh/m² and 1850 kWh/m².

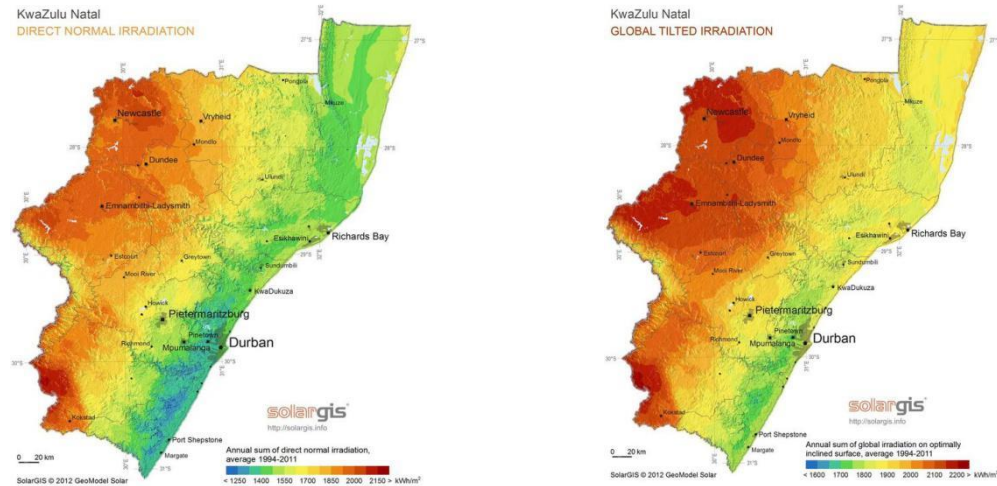


Figure 11: KwaZulu Natal Solar Resource (GeoSUN, 2012).

One of this study's objectives is to create detailed simulations of the solar thermal systems. In order to do this, accurate data will be needed, therefore solar data was purchased from Solar Resource Data Solargis[®]. The purchased data is hourly typical meteorological year (TMY) solar data. This set of data consists of 12 months selected from individual years to form a year of data which best represent the average solar radiation and weather conditions (Solargis, 2017).

The TMY data purchased for this study stretches over a time span of 22 years. The data gives the GHI, GTI and diffuse irradiance of Durban, by using this it was also possible to calculate the DNI with Equation 3.1 as recommended by Meyer (2016). Here h represents the sun's elevation angle.

$$DNI = \frac{GHI - Diffuse}{\sin(h)} \quad (3.1)$$

It was calculated that Durban's annual DNI is 1350 kWh/m², falling in the expected range, mentioned previously. The GHI is 1609 kWh/m² and the GTI is 1821 kWh/m², at the upper limit of what was expected. This data shows that Durban is better suited for collectors utilizing GTI, like the flat plate and

evacuated tube collectors which can be utilized for the bagasse drying system, as there will be a higher solar resource available to them.

Looking at Durban’s TMY DNI data, it can reach values above 1000 W/m² quite regularly. However, Durban’s tropical climate causes lots of clouds to form during the day and from September to November there tends to be lots of rain, which blocks off DNI. Figure 12 shows a comparison of the DNI of Durban and Upington for 21 days. From this figure, one can see that the total amount of DNI for Durban is significantly lower than for Upington, due to transient conditions. This is why the region around Upington is preferred for the development of CSP plants. It is thus expected that the solar live steam generation would not perform as well as a commercial CSP plant, but would still be able to make a significant impact due to the high maximum DNI which can be reached quite regularly.

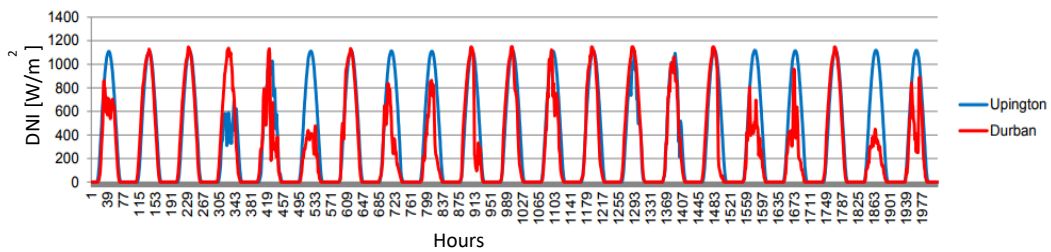


Figure 12: DNI comparison of Upington and Durban (Meyer, 2016)

As part of the purchasing agreement, Solargis[®] compiled a report of the solar resource in Durban. Figure 13.a shows how much the GHI varied for the 22 years the data was measured and highlights the importance of using averaged or TMY data rather than the data of a chosen year. Figure 13.b shows the monthly averages of GHI over these years.

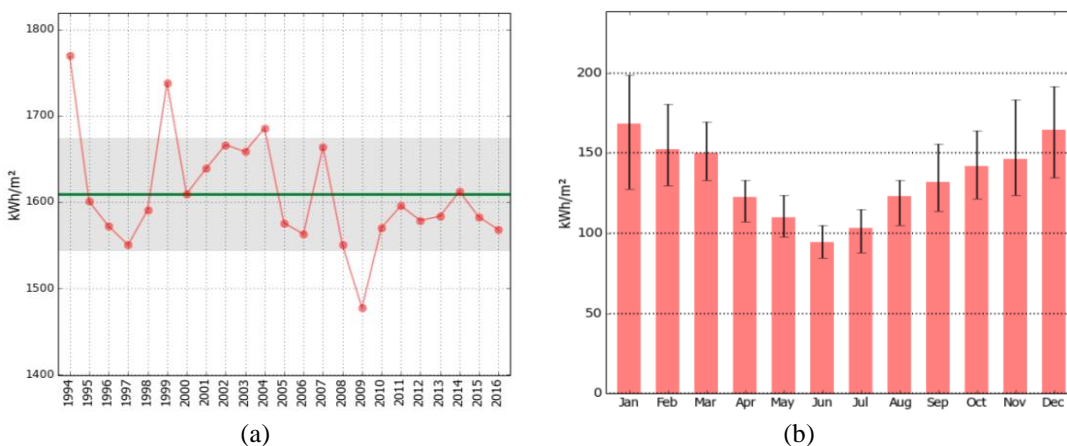


Figure 13: (a) Annual GHI for Durban from 1994 - 2016. (b) Monthly average GHI for Durban (Solargis, 2017)

3.2 Bagasse Drying

Literature on bagasse drying is analysed to highlight the importance of the process. Potential problems and drawbacks found in the literature are also discussed here. The drying process itself will be explained and the different types of bagasse dryers will be analysed.

3.2.1 Advantages of bagasse drying

When bagasse leaves the dewatering mills it is still rather wet, about half the weight of bagasse consists of water. The average moisture content of the bagasse fed into the boilers across the South African industry was 50.78 % (weight percentage) for the 2015/2016 milling season (Smith et al., 2016) and in the BRTEM Matlab model bagasse moisture was set to 51 % (Starzak and Davis, 2016). As mentioned before, one of the main advantages of bagasse drying is that it can significantly increase the calorific value of the bagasse. By increasing the calorific value, less bagasse has to be used to produce the same amount of heat.

The higher heating value, also known as the gross calorific value (GCV), represents the total energy that can potentially be released by bagasse when combusted (Wienese, 2001). If there is no moisture, ash or Brix content in the bagasse, this value is 19 605 kJ/kg (Don et al., 1977). The moisture, ash and Brix contents have a negative impact on the calorific value. Don et al. (1977) developed a formula for determining the GCV, shown as Equation 3.2. *M* represents moisture content, *B* the Brix content and *A* the ash, all expressed as weight percentages of the bagasse.

$$GCV = 19605 - 196.05 M - 31.14 B - 196.05 A \quad (3.2)$$

The lower heating value, also known as the net calorific value (NCV) represents the amount of energy that the combustion of bagasse can release minus the latent heat of the water formed during the combustion process. The NCV is a good indication of the heat that is theoretically available from the combustion of the fuel. It also gives a better indication of what is realistically possible (Hugot, 1972). Equation 3.3 from Wienese (2001) shows how to calculate the NCV:

$$NCV = 18260 - 207.01 M - 31.14 B - 182.60 A \quad (3.3)$$

From both Equations 3.2 and 3.3 it is clear that reducing the moisture content in the bagasse will lead to an increase in calorific value. A reduction of 5 % in the moisture content can lead to a 12 % increase in GCV (Vijayaraj et al., 2007). Sosa-Arnoa et al. (2006) mentions a study where bagasse was dried from 50% moisture content to 38% and this resulted in an a 16% increase in steam production. Figure 14.a shows how bagasse drying improves the fuel usage to steam production ratio.

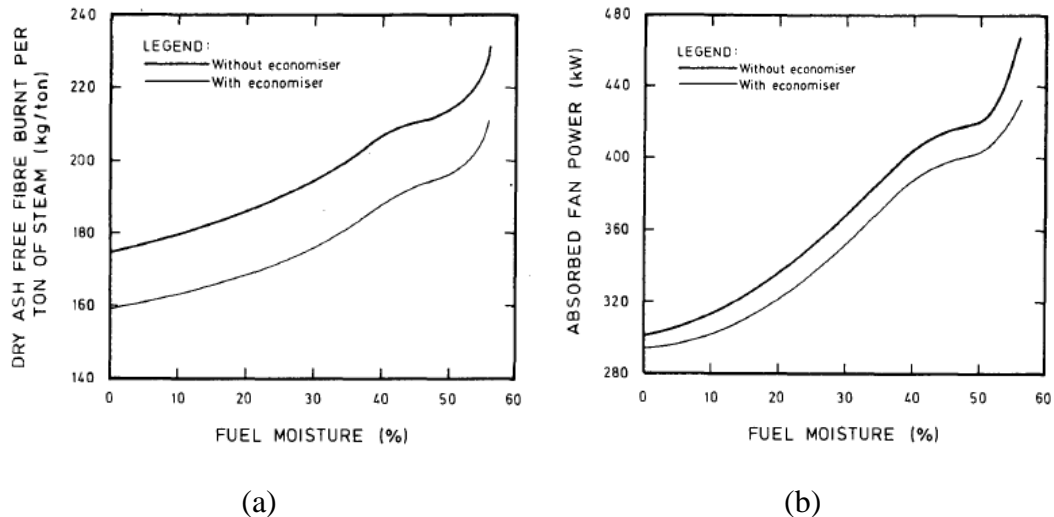


Figure 14: (a) Bagasse to steam ratio as a function of the bagasse moisture content. (b) Boiler fan power as a function of the bagasse moisture content (Magasiner, 1987).

Another advantage of bagasse drying is that the boiler efficiency increases; this is because by reducing the water vapour released by the bagasse during combustion the heat losses through the flue gas can be reduced. Furthermore, dried bagasse needs less excess air for effective combustion, this, along with the reduced amount of vapour will lessen the load of the induced draft fans (Sosa-Arnoa et al., 2006; Bruce & Sinclair, 1996). Figure 14.b shows the effect of bagasse moisture on absorbed fan power.

Older boilers with old types of grates like pin hole or steeply sloping fixed grates, sometimes struggle with handling wet fuel and could benefit greatly from a bagasse drying operation (Wienese, 2001). This is because the moisture content in bagasse has a significant effect on the combustion process itself. Drier fuel improves combustion since it burns faster and hotter. This in turn enables the boiler to be more responsive to changes in load (Bruce & Sinclair, 1996).

3.2.2 Potential problems and disadvantages of bagasse drying

Laubscher (2017) warns that a major reduction in combustion air, because of dryer bagasse, may lead to a smaller convection heat flux in the boiler, leading to lower steam temperatures and boiler efficiency. However, for the bagasse drying up to 35 % moisture content this will not be an issue as Figure 15 shows. Here we can see that the boiler's efficiency still increases as the bagasse moisture is reduced, however, the increase is slightly less for each 5 % moisture content interval.

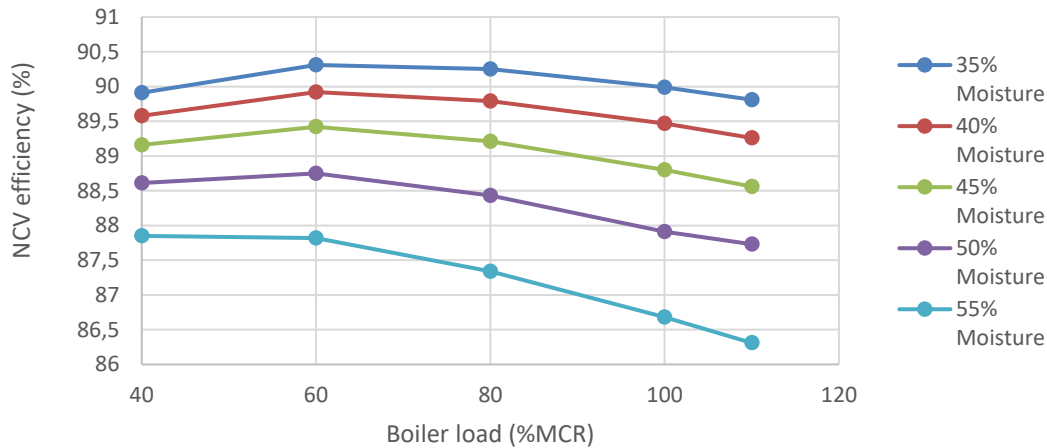


Figure 15: Simulation of different bagasse moisture contents for a boiler, similar to the one assumed for the BRTEM model (Laubscher, 2017)

The hotter and more vigorous combustion of dry biomass compared to wetter biomass increases the probability for ash fouling and slagging. Fouling occurs when volatile ash components (usually alkali metal oxides) condenses in the boiler and attaches itself to the heat transfer surfaces, where it is then later sintered due to the extreme heats (Magasiner et al., 2001). Fouling is more likely to occur with higher concentrations alkali metals in the fuel and there are various ways to try and determine if it will occur. A simple measure to see if there is a risk for fouling, is to look at the mass ratio of alkali metal oxides to silica, as shown in Equation 3.4.

$$(\text{Na}_2\text{O} + \text{K}_2\text{O}) : \text{SiO}_2 \quad (3.4)$$

Bruce & Sinclair (1996) gives an index that can be used as a rough guide to predict fouling using Equation 3.4. According to this index a ratio above 2 indicates a high fouling potential. Miles, et al., (1995) developed a more complex fouling indicator formula, as shown in Equation 3.5.

$$\frac{1 \times 10^6}{\text{GCV}_{\text{kg}}^{\text{kJ}}(\text{dry})} \times \text{Ash}\% \times \text{Alkali}\% \text{ in Ash} = \frac{\text{kgAlkali}}{\text{GJ}} \quad (3.5)$$

For a value higher than 0.17 kg/GJ the risk of fouling increases and for a value higher than 0.34 kg/GJ fouling is almost certain to occur. Magasiner et al. (2001) suggests that this should be used together with Equation 3.4 above, since Miles's indicator may sometimes overstate the potential problem. This happens when the ratio is moderate or high but the total amount of the offending materials is too small to have a significant effect. For Equation 3.4 bagasse is calculated to have a ratio of 0.06 and for Equation 3.5 the answer is 0.07 kg/GJ, both of the values are far below the predicted fouling points.

It is, however, important to keep in mind that these indexes are only indicators of potential problems. Fouling cannot be anticipated by looking at fuel properties alone. Although the tendency for this generally increases with higher alkali content in the fuel, the form of the alkali and other inorganic constituents along with boiler operating conditions and boiler design play an important role as well (Miles, et al., 1995).

Slagging can occur when the high temperatures in the furnace reaches a level where the ash begins to exhibit stickiness. This enables the ash to attach itself to colder surfaces and prohibit effective heat transfer in the boiler (Bruce & Sinclair, 1996). The potential of slagging occurring with a certain fuel can be determined by looking at the phase diagrams to see if the boiler's operation temperature would melt the ash or not (Magasiner et al., 2001).

The ash fusion temperature of bagasse is 1310 °C – 1380 °C according to Magasiner et al. (2001). This is the temperature where ash becomes soft and starts to melt. This temperature, however, can be lower when bagasse is used in multi-fuel firing. It is possible that ashes from the different fuels chemically interact to form a eutectic compound with a lower ash fusion temperature than that of the ashes of the initial fuels (Rayaprolu , 2009).

However, bagasse has been used successfully as a boiler fuel without any major concerns, even when used with coal. This could be attributed to the fact that both potassium and chlorine are substantially leached from the sugarcane in the process of sugar extraction (Miles, et al., 1995).

When dryer bagasse is used it is important to take the boiler design into consideration (Magasiner, 1987). If a boiler was designed for high moisture content bagasse, then the bagasse should not be dried too much, since this might create complications in boiler operations. For example boilers with a refractory band in the ignition zone can experience heavy fouling if bagasse moisture levels drop below 45 %. It would be best to remove the refractory band if the bagasse fed into the boiler is predominantly below 45 % in moisture content. It would be better to use refractory backed open pitched tubing in the ignition zone (Magasiner, 1987). The SMRI also feels that substantial changes may have to be made to current South African sugar milling boilers if it uses bagasse with a moisture content below 40 % (Foxon, 2017).

Another aspect that has to be kept in mind when drying bagasse is what will happen if bagasse with different moisture contents are fed into the boiler. In order to do this it is important to mix the bagasse so that there is an even spread of the wetter and dryer bagasse and a constant fuel density (Naude et al., 1993). This will prevent the formation of puffs in the boiler. Furthermore, it is important to control the fuel-air ratio to ensure efficient combustion (Naude et al., 1993).

Rein (2007) also notes that a bagasse drying system adds additional cost and complexity to a sugar mill. The extra technology needed to support a drying system, apart from the dryer itself, like fans and a conveyor system can add significant additional cost.

3.2.3 Drying process

During the drying process the liquid on a solid's surface will be heated to an equilibrium temperature by the hot air stream. At this temperature the rate of drying is constant due to the fact that the evaporation of moisture absorbs latent heat. This can be seen as the horizontal line between points B and C on Figure 16. During this constant drying rate period, the moisture movement inside the solid is rapid enough to maintain a saturated condition at the solid's surface. Eventually the moisture content has been so reduced that dry spots start to appear on the surface, this reduces the drying rate quite significantly as can be seen by the line between C and D in Figure 16. With further drying the drying rate starts to depend on the rate at which moisture can move through the solid, as a result of concentration gradients (Tawfik et al., 2003). This period is represented by the line between points D and E in Figure 16.

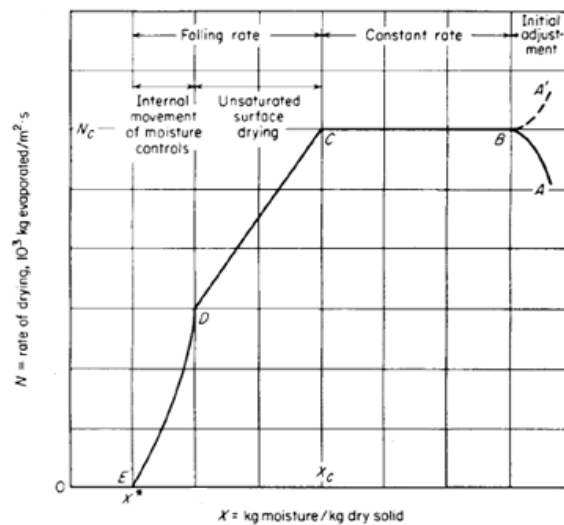


Figure 16: Drying rate under constant drying conditions (Tawfik et al., 2003)

However, some studies (Vijayaraj et al., 2007; Bakshi & Singh, 1980; Freire et al., 2001) have shown that bagasse does not quite follow this drying curve. Bagasse has no constant drying rate period, despite having relatively high moisture content. Freire et al. (2001) observed that the bagasse goes through a short heating period and from there on dries only according to the falling rate period, points C to E in Figure 16. Vijayaraj et al. (2007) mentions that bagasse's drying rate is mainly dependant on the moisture diffusion inside the bagasse.

When drying bagasse the moisture is released between 120 °C and 210 °C. When the bagasse is heated to more than 210 °C it starts to emit CO₂ and at 228 °C it starts to combust (Naude et al., 1993). This is clearly evident in Figure 17, which shows how the CO₂ emissions of bagasse increase when it reaches a temperature above 200 °C and also how it starts to lose weight a short while after that. Sosa-Arnoa and Nebra (2009) recommend that the hot air temperature should not exceed 200 °C by much. They used 215 °C for their experimental setup, which uses a pneumatic dryer. Fires do not occur often in drying systems, but most of those that have occurred started in the collector due to particle build-up, which creates favourable circumstances for fires (Cook, 1991).

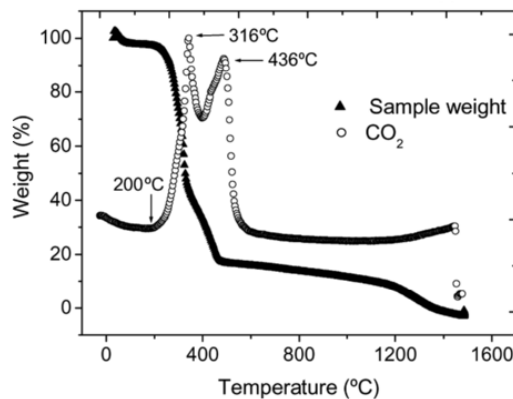


Figure 17: The heating of bagasse under an oxygen atmosphere from Sosa-Arnoa and Nebra, 2009)

High temperatures are beneficial for the drying system since it increases heat transfer and minimizes equipment size. However, it does create a fire hazard. The fire risk can be minimized by understanding the different drying phases (Amos, 1998). There are two points where the fire risk is quite high. One point is where dry spots start to form (point C in Figure 16). During this period there is no water vapour on the particle's surface which causes the particles' temperature to rise to dangerous levels. So bagasse might be under constant risk if we assume that it has no constant drying rate interval. However, the moisture which is still within the particle helps to control this risk since it moves to the surface, which in effect cools the particle again (Amos, 1998).

The second high fire risk arises when the particle is completely dry. The particle's temperature would rise until its combustion temperature, if the drying air is hot enough. This is luckily a very small risk since bagasse is never dried to this point; as mentioned before, bagasse has a technical lower limit for drying in the order of 30 % (Rein, 2007).

3.2.4 Dryer types

Sosa-Arnoa et al. (2006) did a review of bagasse drying and of the 32 drying systems that they listed, 20 was pneumatic dryers. The other 12 was mainly rotary dryers. This study will only look at these two dryer technologies, since they are the technologies that are most used in the specific industry. Pneumatic dryers are most often used for bagasse drying because they are relatively cheap and have small space requirements (De Oliveira, et al., 2011). Rotary dryers are more robust than pneumatic dryers and can handle the largest capacity of any type of dryer; it can also be used in cases where there are large particles or a variety of particle sizes (Amos, 1998; Bruce and Sinclair, 1996).

Rotary Dryers:

In a rotary dryer, the hot air comes in contact with the bagasse inside the rotating drum. Most of the drying takes place as flights inside the drum lifts the bagasse and lets it cascade through the hot air stream (Cook, 1991). This allows more of the bagasse particles to be in direct contact with the air and promotes mass and heat transfer.

The flow of hot air and bagasse can be co-current or counter current. For the latter case the driest solids are exposed to the highest temperatures with the lowest humidity. This can be seen as a possible fire risk and would not be advised for drying systems working at high temperatures (Amos, 1998). Counter current drying can be problematic when working with bagasse, because bagasse particles are light and have high drag coefficients and therefore a lot of the particles can be caught in the airstream, blowing it back to the inlet (Foxon et al, 2017).

Co-current rotary dryer systems are designed so that the wettest particles come in contact with the hottest air, minimizing the fire risk. Some systems are designed so that the exhaust stream passes through an air and fine particle separator like a cyclone, baghouse filter, scrubber or electrostatic precipitator to retrieve any particles still entrained in the air stream, as shown in Figure 18.

The residence time for very small particles can be as short as 30 seconds, but for most of the bigger particles in is in the order of 10 – 30 minutes. This long residence time allows the particles to dry out quite uniformly. Non-uniformity in particle moisture content can be a problem with certain dryers, especially if there is a large range of particles sizes present (Bruce & Sinclair, 1996). The bagasse should typically occupy 9 – 15 % of the drum shell to ensure effective drying (Cook, 1991) and the dryer is most efficient with length – diameter ratio between 4-10 (Mujumdar et al. 2006). One of the drawbacks of a rotary dryer system is that the moisture content of the particles are hard to control because the rather long residence time create a lag in the system (Fredrikson, 1984).

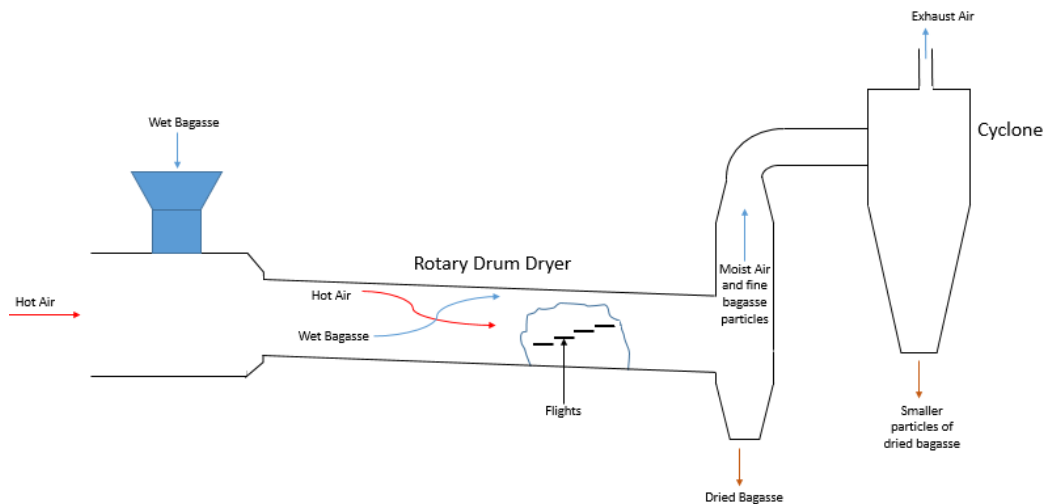


Figure 18: Co-current rotary dryer system

Table 2 shows some of the capabilities of a rotary dryer. The bagasse drying operations being considered for this study fall well within the feed moisture content and discharge moisture content performance parameters of the rotary dryer. However, the particle sizes of the bagasse do not quite match that of the rotary dryer's design. Bagasse has a wide variety of particle sizes, which can range from 1 mm to 150 mm. 30 % of the bagasse consist of very small particles, called pith, which forms part of the lower range of sizes, usually ranging from 1 – 5 mm (Foxon et al., 2017; Rein, 2007).

Table 2: Typical design and performance values for rotary dryers (Bruce & Sinclair, 1996)

Parameter	Unit	Value
Evaporation	t/h	3 – 23
Capacity	t/h	3 – 45
Feed moisture content	%	45 – 65
Discharge moisture content	%	10 – 45
Pressure drop	kPa	2.5 - 3.7
Particle size	mm	19 – 125
Thermal requirements	GJ/ t_{evap}	3 – 4

Pneumatic Dryers:

In pneumatic dryers, also called flash dryers, the hot air carries the solid particle up a flash tube, drying the material through direct contact, Figure 19 shows a typical pneumatic dryer setup. These type of dryers have short contact times between the hot air and wet material, usually between 0.5 – 10 s (Mujumdar et al., 2006). This is due to the large surface area of the material exposed to the air,

where heat and mass transfer can take place. The short contact time minimizes the fire hazard because the material temperature stays relatively low.

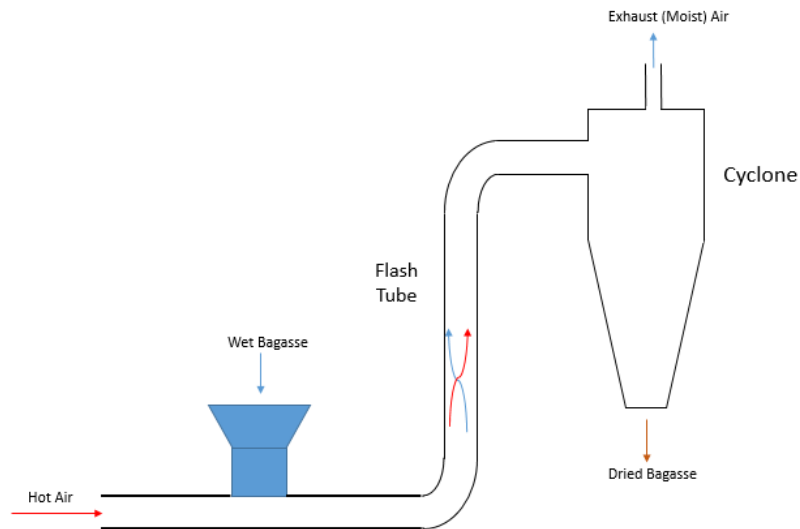


Figure 19: Pneumatic dryer system

In order for the hot air stream to transport the material the air velocity needs to be larger than the free fall velocity of the largest particle to be dried (Mujumdar et al., 2006). Strumillo and Kudra (1986) recommends that the air velocity should be 2.5 m/s above the largest particles' terminal velocity. Therefore, in a pneumatic drying system the ratio between the air velocity and particle velocity needs to be high. Table 3 shows some of the capabilities of a conventional pneumatic dryer. From these values it is possible to see that pneumatic dryers can dry of more moisture than rotary dryers and that they use less heat, however the typical discharge values are considerably lower than what is considered for this study. Pneumatic dryers, furthermore, are designed to dry a smaller range of particles sizes compared to rotary dryers.

Table 3: Typical design and performance values for a pneumatic dryer (Bruce & Sinclair, 1996)

Parameter	Unit	Value
Evaporation	t/h	4.8 – 17
Capacity	t/h	4.4 – 16
Feed moisture content	%	45 - 65
Discharge moisture content	%	10 - 15
Pressure drop	kPa	7.5
Particle size	mm	0.5 - 50
Thermal requirements	GJ/t _{evap}	2.7 – 2.8

Pneumatic dryers are simple to construct and have low capital cost. The maintenance cost is also quite low due to the small amount of moving parts. However, the operating cost of pneumatic dryers is high because of the blower system that needs to maintain a high air flow rate through the system (Amos, 1998).

3.3 Cogeneration and Hybridisation with CSP

By using biomass along with CSP, electricity can be generated using renewable energy at low CO₂ emission levels (Burin, et al., 2016). CSP-biomass hybrid power plants can be used as reliable base load providers, the only problem being that there are only a few areas with both adequate solar and biomass resources (Peterseim et al., 2013). Peterseim et al. (2013) mentions that possible locations should have an annual DNI higher than 1700 kWh/m² to be financially feasible.

One of the few suited areas is Les Borges Blanques in Spain, where the first commercial solar-biomass power plant, Borges Termosolar, has been in operation since December 2012. The hybrid power plant has a capacity of 22.5 MW and operates 24 hours a day (National Renewable Energy Laboratory, 2013). The plant generates 98 000 MWh annually, which is 89 % of the output of a 50 MW solar-only plant (Biomass Knowledge Portal, 2015).

The solar loop, parabolic troughs with a combined aperture area of 183 120 m², heats thermal oil to 393 °C which is used to create steam at 40 bar in the steam generator. From there on the steam is superheated to 520 °C by the dual biomass-natural gas boiler and enters the high pressure steam turbine as can be seen in Figure 20. The biomass and auxiliary natural gas boiler are tasked with heating the thermal oil during times of low solar irradiance. They hybridisation helps to save biomass and allows the steam turbine to operate without any interruptions, resulting in higher efficiencies.

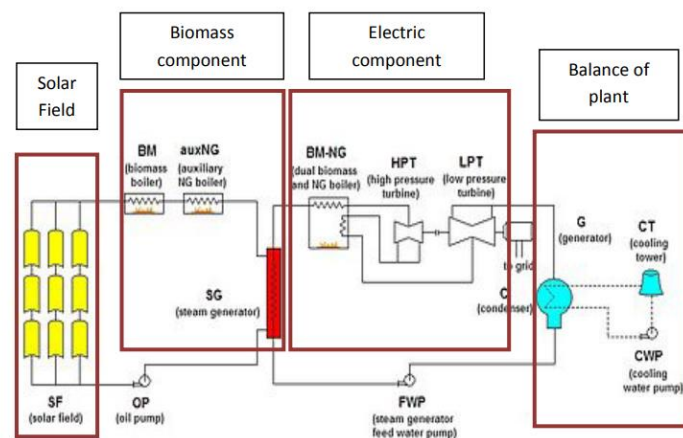


Figure 20: Layout of the Borges Termosolar hybrid power plant (Biomass Knowledge Portal, 2015).

The way a hybrid plant operates can differ from plant to plant, depending on what they want to achieve and different economic factors. Peterseim et al. (2014) completed a study which evaluates different hybrid plant designs for Australia. In his design the biomass boiler provides a constant supply of energy, seen as Energy from Boiler (EfB) or Energy from Waste (EfW) in Figure 21. The CSP system provides additional power during daytime, when the electricity demand and prices are higher in Australia.

Different CSP technology can be implemented with the hybridisation, this will have an impact on the solar system efficiency as well as on the economic factors like the IRR. The studies of Peterseim et al. (2014) and Iftekhar Hussain et al. (2017) found that a linear Fresnel system with direct steam generation would yield the best economic results in a hybrid plant compared to parabolic trough, solar tower and other linear Fresnel systems with different heat transfer fluids.

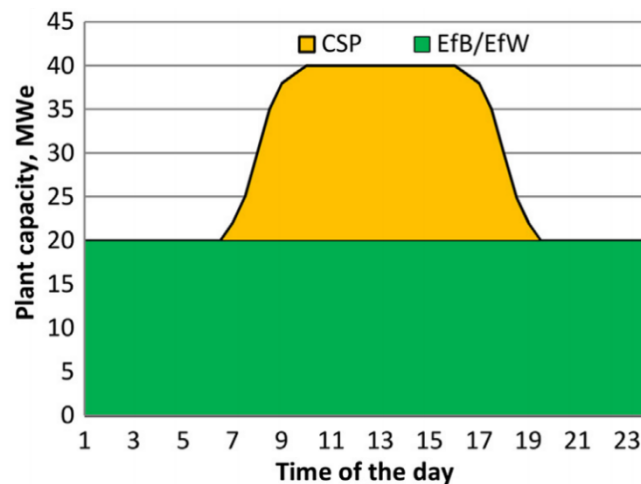


Figure 21: Electricity output of the hybrid concept designed by (Peterseim et al, 2014)

Adding CSP to an existing biomass plant would be cheaper than developing a stand-alone CSP plant, due to the fact that infrastructure can be shared. Most of the savings come from the power block, where most biomass plants and sugar mills already have boilers, turbines, generators and condensers (Bhatt, 2014). Peterseim et al. (2014) reports that the investment costs of a new CSP and biomass hybrid plant is 12 % lower compared to a stand-alone CSP power plant, also mainly due to the fact that infrastructure can be shared. On top of that, a hybrid plant can generate more power annually than a stand-alone CSP plant of the same rated capacity. In order to create a CSP plant to generate the same annual electricity output, the investment costs will have to be 69 % higher than that of the equivalent hybrid plant (Peterseim et al., 2014). A hybrid plant, is however, more expensive than a biomass-only plant, but as biomass prices increase, it can soon be cost competitive with the biomass-only plants (Nixon et al., 2012).

As noted in Section 2, sugar mills (without refineries) usually only operate during the crushing season. The installation of CSP can enable the power cycle in the mills to operate outside of the crushing season as well, increasing the amount of electricity exported per annum. Sugar mills are an important source of electricity in large sugar producing countries. Brazil, for example, has 10.6 GW installed electrical capacity at sugar mills, which represents 7.1 % of the country's total installed capacity. Sugar mills can benefit from CSP integration in the same way as biomass plants. It will allow for biomass to be saved and extra electricity can be generated without having to make capital investments into the power block.

Burin et al. (2016) completed an evaluation of integrating a solar power tower into an existing Brazilian sugarcane cogeneration plant. The study evaluated three different solar integration points, similar to Hess et al. (2016). The integration points were: feed water preheating, saturated steam production and live steam production. The live steam production proved to have the biggest impact, with the other two integration points proving costly in terms of the impact that they could make.

In the live steam production integration point, shown in Figure 22, CSP was used to create live steam during sunny hours, easing the boiler's load. Outside of the crushing season the CSP system can run on a solar only mode during sunny hours, utilising the condensing extraction steam turbines (CEST) installed at the mill to create electricity. The bagasse saved during the crushing season can be used during hours of low solar irradiance. According to Burin et al.'s study this hybridisation mode can increase electricity production by 19.8 %. These results show that a CSP system can still make a considerable impact despite having annual DNI readings lower than 1700 kWh/m^2 as suggested by Peterseim et al. (2013), since the annual DNI reading for the site considered by Burin et al. (2016) is 1502 kWh/m^2 .

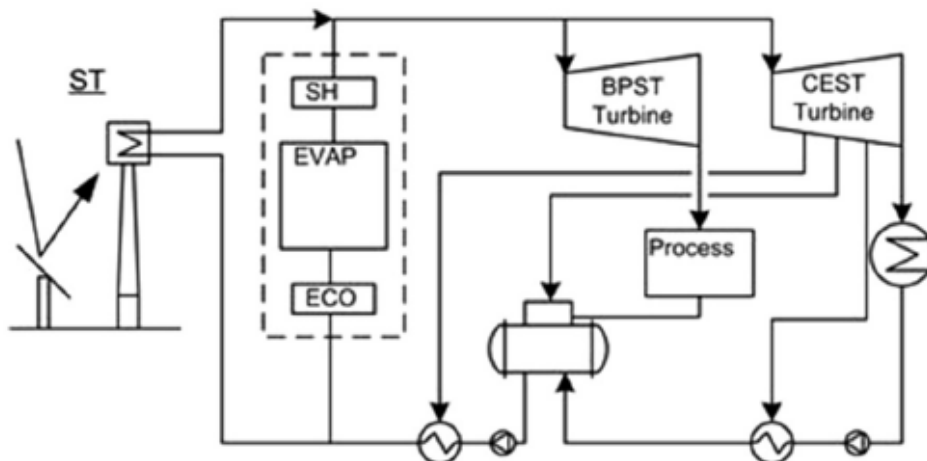


Figure 22: Simplified layout of CSP integration into a Brazilian sugar mill (Burin, et al., 2016)

The bagasse savings fulfils the role thermal storage would normally serve, allowing hybrid plants to save on investment costs (Servert et al., 2011). However, storage can increase the percentage of electricity which the CSP system itself delivers annually. The increased electricity production, reduction in biomass usage and extra capital costs almost balances each other out, with CSP systems utilising thermal storage only showing a slight drop in IRR (Peterseim et al., 2014).

Soria et al. (2015) shows that in order for a solar system to deliver 50 % of the needed energy, the ratio of installed thermal capacity of CSP to biomass should be 70:30. The biomass needs less installed thermal capacity since it can run 24 hours a day, whilst the CSP system can only run during sunny hours. The solar multiple can also be increased to allow for a higher annual CSP capacity factor. The solar multiple is defined as the ratio between the thermal power which the solar field could deliver at design conditions and the amount of thermal power needed at nominal conditions (Montes et al., 2009). So higher solar multiples allows for more thermal energy, but during times of high irradiance it will be too much, forcing parts of the solar field to defocus. Defocussing lowers the solar field's efficiency, due to the fact that it does not use the energy available.

Burin et al. (2016) found that a solar multiple of 1.4 is ideal for the designed CSP system in their study, resulting in the lowest levelised cost of energy (LCOE) of 220 US\$/MWh as can be seen in Figure 23. The LCOE is the average price per unit of energy generated by the system (Hess et al., 2016). It is a common way to assess the feasibility of a project and is frequently used to compare renewable energy projects to one another.

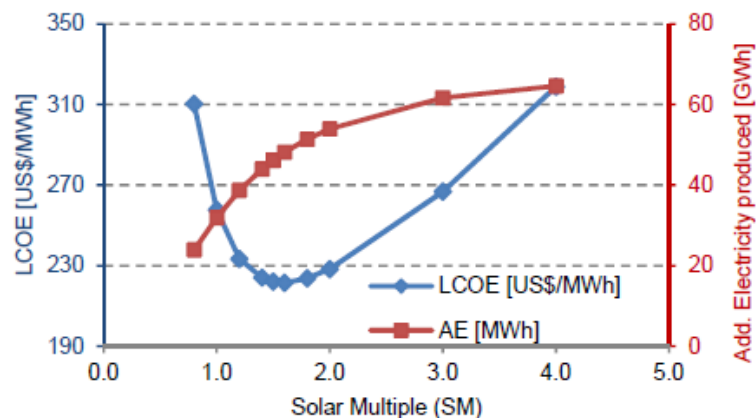


Figure 23: LCOE and additional electricity produced for different solar multiples (Burin, et al., 2016)

The LCOE of 220 US\$/MWh is in the same range as older commercial CSP plants, whose LCOEs ranges from 200-400 US\$/MWh (Burin, et al., 2016). This is quite a good result considering the low annual DNI mentioned previously.

However, CSP plant have reached record low prices in 2017, with SolarReserve reaching a price of 61 US\$/MWh with its Aurora project in Australia (Kraemer, 2017). Servert et al. (2011) calculated the LCOE of a hybrid plant to be 153 €/MWh or roughly 183 US\$/MWh.

The differences in LCOE can be due to a number of factors since the LCOE is subject to change depending on technology and location. In Servert et al.'s (2011) study the annual DNI was 2000 kWh/m², but the factor that probably had the biggest impact is that Burin et al.'s (2015) study is based on sugar mill technology, while Servert et al. (2011) and the Aurora project focuses on power generation technology. Sugar mills focus on co-generation, so a large fraction of the thermal energy and electricity is used for the milling process, which in most cases is the first priority, the extra thermal energy can then be used for power generation and electricity export.

Despite the Borges Termosolar plant running for 5 years, the hybridisation of solar and biomass is still seen as relatively new and unproven technology (Iftexhar Hussain et al., 2017). The uncertainty surrounding the technology due to its novel status means that there are various economic and technological hurdles it still has to overcome before being widely accepted.

Technical hurdles that need to be overcome are the balancing out the different fluctuations in each of the solar field and biomass boilers, as well as avoiding situations where thermal energy needs to be dumped (Iftexhar Hussain et al., 2017). Some of the economic hurdles are similar to what stand-alone CSP plants face, like obtaining the necessary funding for the high initial capital costs. Milling companies are focussed on maximising their profits and prefer to invest in projects with short payback periods, something solar thermal integration cannot always offer due to the high capital investment (Backen et al., 2017). An issue which can arise in South African, is finalising a power purchase agreement with Eskom, the national power provider, an issue which has proven to be a massive obstacle for many independent power producers (SAIPPA, 2017).

However, hybrid plants can become a lucrative option in the future due to the predicted increases of fossil fuels, the expected decrease in CSP installation costs (IRENA, 2016) and countries' willingness to decrease carbon emissions. Biomass prices are also expected to increase (Nixon et al. 2012) and can be used to generate extra income through the production of bio-ethanol or selling it for other applications.

4 Solar Bagasse Drying

This section will explain how the proposed bagasse drying system will work with solar heated air. The section will go on to explain how the drying system's characteristics and thermal requirements were determined using Simprosys; how the solar system was modelled using a Matlab code and Aircow; and finally how the solar field was simulated using Solgain, in order to see how the system would perform during the crushing season.

4.1 Integration Point

The primary focus of introducing bagasse drying at a sugar mill will be to reduce bagasse usage. However, dryer bagasse also presents various advantages in the boiler, as discussed in the literature review. As mentioned in Section 3.2, most of the studies done on bagasse drying uses pneumatic dryers (Sosa-Arnoa et al., 2006). The flue gas temperatures in South American sugar mills (where most of these studies were done) tend to be considerably higher compared to South African sugar mills, this is due to the fact that the whole mill operates at higher steam temperatures and pressures. Therefore, the high temperatures needed to quickly and effectively dry bagasse in a flash dryer might not be achievable in South African sugar mills.

Another issue with using flue gas to dry bagasse in South Africa is the risk of flue gas condensation, which can cause corrosion due to the acid that can form. In South Africa flue gas temperatures are typically 160 °C and its dew point temperature ranges from 90 °C - 152°C, depending on the amount of sulphur in the gas (Laubscher, 2017; Kotze, 2016). The higher the sulphur content, the higher the dew point and the larger the risk of condensation, and in South Africa it is possible to get high amounts of sulphur in the flue gas due to the use of coal. The risk of using flue gas opens the door for low – medium temperature solar thermal integration and for the drying system a co-current rotary dryer was chosen to dry the bagasse. This technology was chosen due its robustness, ability to handle various sizes of particles and ability to handle large amounts of bagasse at a time.

A co-current system was chosen over a counter-current system, because of the risk of small particles of bagasse being transported into the wrong direction with the counter-current air stream. With a co-current system a cyclone can be placed at the end of the dryer to collect the smaller bagasse particles which were carried away with the air stream. The fan is placed at the beginning of the system and not after the dryer systems, as seen in Figure 24, so that it does not have to endure the relatively high heat. This will also make place for the cyclone and any other dust and particle collectors that may be put in place if necessary. Furthermore, the fan would use slightly less power if installed at the front, as all the evaporated moisture does not have to pass through it

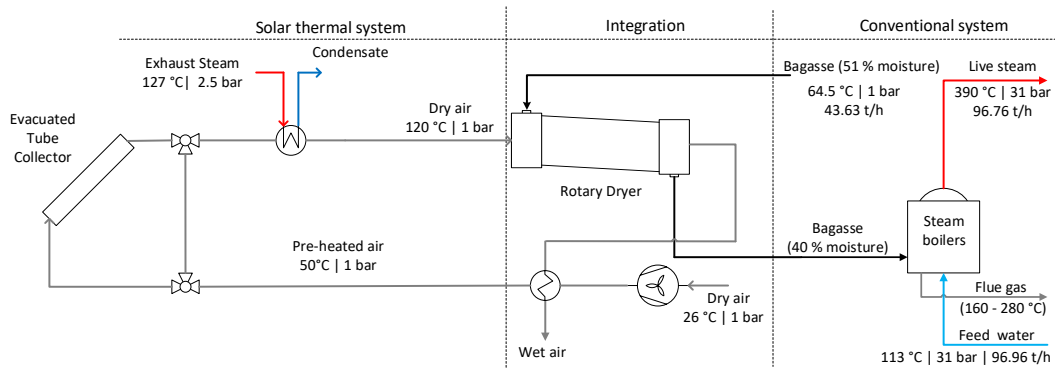


Figure 24: Basic schematic of solar bagasse drying integration point.

The system starts by sucking in ambient air through the fan mentioned above. The air is pre-heated by the air exiting the rotary dryer. The air is then pre-heated even further by a field of evacuated tube air collectors. Evacuated tube air collectors are used for this integration point, because they are uncomplicated and its temperature range falls perfectly in the safe temperature for bagasse drying. Exhaust steam also falls in this temperature range and is already used as heating medium in the sugar drying operations installed in various South African sugar mills. The collector field can heat the air up to any temperature between 50 °C and 120 °C and the exhaust steam air heater will ensure that the final air temperature is constantly 120 °C.

The exhaust steam in typical South African sugar mills can range from 117 to 127 °C (Foxon, 2017). The exhaust steam at each factory also does not have to stay at a certain temperature, as most mills vary between the above mentioned temperatures between cleaning cycles, using hotter exhaust steam when scaling reduces the heat transfer capacity in some of the processes. Therefore, although the BRTEM model lists the exhaust steam temperature as 121 °C, it can easily be adjusted to 127 °C, which should ensure a high enough temperature difference between the exhaust steam and the air that needs to be heated.

The exhaust steam will allow for a constant drying rate for the bagasse through day and night. The solar system will reduce the thermal load of the exhaust steam air heater, saving exhaust steam and, therefore, bagasse. During night time the solar loop can be bypassed and the pre-heated air can go directly to the exhaust steam heater as seen in Figure 24.

It would be of great benefit to the mill if the bagasse was dried to the same moisture content all the time, since this would greatly simplify boiler operation and control. If the exhaust steam is not used in the air heating system and the air is just heated by the solar system, the drying air temperature would change constantly as the solar irradiance varies throughout the day. This will lead to bagasse with varying moistures and the plant operators will have their hands full ensuring the boiler is run correctly. One option to eliminate the fluctuations of the

thermal energy produced by the solar field is to implement a thermal storage system. The solar field's solar multiple can be increased, with the extra energy going to the storage system so that the drying system can use it again during transient conditions.

However, the thermal storage can only supply heat for transient conditions and for a few extra hours after sunset. It is uncommon for storage systems to be able to supply the full load thermal energy during night time as well, because this would require a storage system of considerable size. Therefore, there will always be a need for the exhaust steam air heater. A storage system will be able to assist the collector field to offset exhaust steam, but at an extra cost. This study will therefore not look at thermal storage systems as the energy consumption of the processes surpasses the capability of the solar thermal systems significantly.

Correct boiler operation is a major source of concern for the sugar milling industry. This is the reason why the bagasse is only dried to 40 % moisture content. If the bagasse is dried to below this point the bagasse can respond differently to suspension burning and most of the South African sugar mills' boilers are not designed to handle bagasse with very low moisture content. Another problem arising from bagasse that is too dry is that it can be very hard to handle, since it tends to fly around, becoming a hazard for people who work with it (Foxon, 2017). It was due to all the above reasons that it was agreed with the SMRI to design a bagasse dryer that would dry the bagasse to only 40 % moisture content.

4.2 Drying Model

4.2.1 Simprosys

Bagasse drying and drying systems in general are very complex. Since it is not the goal of this study to create a detailed drying simulation, therefore, a simple drying program was used to model the bagasse drying process. The software package used is called Simprosys (Simprotek, 2006); it is a Windows based program which can solve heat and mass balances of drying processes and is based on the work of Masters (1985), Mujumdar (1995) and Perry (1997). The program can also do scoping design calculations, which is based on the work of Kemp and David (2002). Simprosys was designed to help engineers quickly obtain the drying process parameters and dryer size by calculating the necessary air flow to the dryer and the heating duty of the air heater.

The program calculates all the necessary psychrometric properties of the air-vapour mixtures in the drying system for the user. The program then goes on to use Equation 4.1 and 4.2 from Gong and Mujumdar (2008) as heat and mass balances respectively. Here \dot{m}_a is the air mass flow and \dot{m}_b is the bagasse mass flow. In Equation 4.1, I represents the enthalpy of the air and bagasse streams,

while Q_c , Q_l , Q_t and Q_m represent the indirectly supplied heat to the dryer, the heat losses, the heat carried in by the transport device and the mechanical energy input. In Equation 4.2, Y and X represent the moisture content in the air and bagasse, respectively, and M_{ev} is the amount of moisture evaporated.

$$\dot{m}_a(I_{a,1} - I_{a,2}) + Q_c = \dot{m}_b(I_{b,2} - I_{b,1}) + Q_l + Q_t + Q_m \quad (4.1)$$

$$\dot{m}_a(Y_2 - Y_1) = M_{ev} = \dot{m}_b(X_1 - X_2) \quad (4.2)$$

The program allows the user to define a generic drying material by entering the specific heat of the bone dry material. The specific heat is used in Equations 4.3 and 4.4 from Mujumdar (1995). Where c_{am} and c_{bd} represents the specific heat capacities of the moisture in the air and dry air respectively. The subscripts bm and bd refer to the specific heat capacities of the moisture in the bagasse and the bone dry material. The terms Δh_A and Δh_B are latent heat of vaporization and heat of sorption.

$$I_a = (c_{am} Y + c_{ad})T + \Delta h_a Y \quad (4.3)$$

$$I_a = (c_{bm} Y + c_{bd})T - \Delta h_b X \quad (4.4)$$

The above equations form part of Simprosys's path to determine the temperature rise of the dried material for a given air flow, or a certain exit temperature can be assumed for the dried material and from there an air flow can be calculated. When these equations are balanced, Simprosys can go on to give an estimate of the dryer's size.

The program uses Equation 4.5 to determine the cross sectional area (A) of the dryer. The equation does not differentiate between different dryers; the only way to do this is to use different gas velocities (v_g) as this parameter is different for each dryer technology. Kemp and David (2002) suggest that 20 m/s be used for flash dryers, 0.5 m/s for fluidised bed dryers and 3 m/s for co-current rotary dryers. The length of the dryer depends on the length/diameter ratio, which can be specified by the user.

$$A = \frac{M_A}{\rho_A v_g} \quad (4.5)$$

The program does not take the bagasse's specific drying kinetics or the particle residence time into account, meaning that it can be over optimistic in some of its drying results. However, the cross sectional area of the needed dryer can be estimated surprisingly accurately (Kemp and David, 2002). According to the program developers, Simprosys is the first step towards a comprehensive drying suite. It is affordable and user friendly, allowing people from the drying industry and academia to make accurate estimations and get approximate dryer dimensions (Gong and Mujumdar, 2008).

4.2.2 Drying simulation setup with Simprosys

The main reason for using Simprosys was to calculate the necessary air flow to dry the bagasse coming from the dewatering mills. Figure 25 shows the layout of the whole drying system as it was displayed in Simprosys. It represents the most important elements of Figure 24 as well as a few smaller elements, like an air filter and cyclone. The heater (H in Figure 25) represents the solar field and exhaust steam heating system.

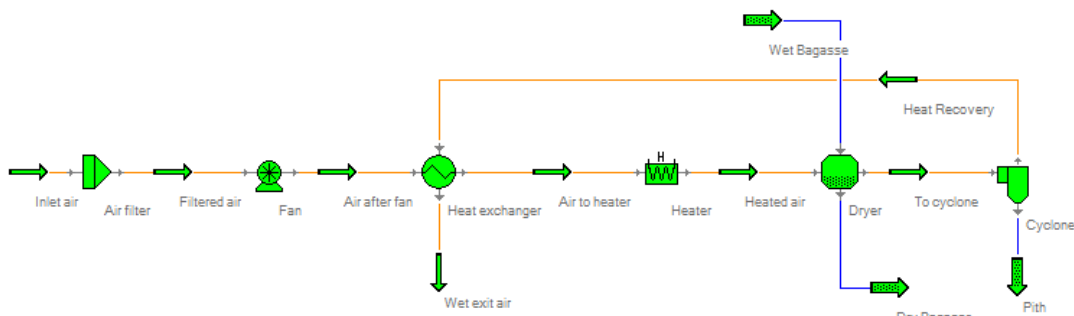


Figure 25: Simprosys model layout.

For this study the bagasse flow rate and moisture content was known, along with the desired bagasse moisture content at the end of the dryer. Furthermore, the air and bagasse inlet temperatures are known and outlet temperatures are assumed to be the same, as suggested by Sosa-Arno and Nebra (2009). Although the study of Sosa-Arno and Nebra (2009) uses a flash dryer, the outlet temperatures for bagasse and air in this study is also assumed to be the same, this is not too an unrealistic assumption, because of the longer residence time of the bagasse in a rotary dryer. Another assumption that was made was that the air pre-heater would be able to heat the air to 50 °C. Table 4 shows the input values which the program had to use to calculate the necessary air flow.

As mentioned in the previous section, the program takes various heat losses and inputs into account for the dryer. For this simulation it was assumed that there is no heat input to the dryer except for the drying air. Furthermore, there is no transport device for the bagasse inside the dryer, so there is not heat loss by the transport device and it was assumed that the mechanical work done by the dryer is only to improve the air-bagasse contact surface and that it did not have an influence on the energy balance of Equation 4.1. Zabaniotou (2000) gives the heat loss from a rotary dryer as 10 – 12 % of the total heat transferred, based on the work of Keey (1994). So for this simulation it was assumed to be only 10 % of the transferred heat, because of the relatively low temperatures compared to other drying systems.

Table 4: Input values for Simprosys simulation.

Stream	Temperature [°C]	Flow rate [ton/h]	Absolute humidity/moisture content [kg/kg]
Inlet air	25	-	0.016
Air to heater	50	-	0.016
Heated air	120	-	0.016
Wet bagasse	64.5	43.63	0.51
Dry Bagasse	75	-	0.4
Air to cyclone	75	-	-

4.2.3 Simulation results

Using all this information the program calculated that 9.49 MW is needed to heat the air from the pre-heated 50 °C to the 120 °C for the dryer inlet. This is the heating load that the solar system and exhaust steam heating system will have to provide. The calculated flow rates are presented in Table 5. As mentioned in the previous section, it is assumed that the ambient air can be pre-heated to 50 °C, this should be possible as the air from the cyclone, which is used to heat it, enters the pre-heater at 75 °C and calculated to exit the pre-heater at 56.67 °C.

After the heat and mass balances were solved, the program's scoping function was used to determine the size of the dryer needed. A gas velocity of 3 m/s was chosen, as recommended by Kemp and David (2002), and the length/diameter ratio was set to 5, which is in the range of effective ratios for rotary dryer design. Simprosys recommends a dryer with a diameter of 7.8 m and a length of 39 m, which is extremely large. This extreme size is due to the very high mass flow rate of bagasse. In order to create a realistically sized drying system it was decided to divide the bagasse flow into four equal streams, so that each dryer dries 10.9 ton/h of bagasse. If the heat loss is adjusted accordingly, then all the flow rates listed in Table 5 would be a quarter of what they were. Each rotary dryer will now have a diameter of 3.9 m and a length of 19.5 m. The heat load for each dryer is now 2.37 MW.

Table 5: Simprosys outputs

Stream	Temperature [°C]	Flow rate [ton/h]	Absolute humidity/moisture content [kg/kg]
Heated air	120	479.169	0.016
Dry Bagasse	75	34.947	0.4
Air to cyclone	75	487.139	0.033
Wet exit air	56.67	487.139	0.033

One advantage of having four dryers is that the boilers can still receive dry bagasse if one of the rotary dryers fail or needs maintenance. The bagasse which would normally go to the out-of-order dryer just needs to be mixed with the dried bagasse before it enters the boiler as noted in the literature review. Furthermore, by dividing the air stream into four, the necessary fans required can also be of a more convenient size, more will be said about this in the results of pressure drop calculations in Section 4.3.4.

4.3 Solar Field Modelling and Simulation

As mentioned previously, it was decided to use evacuated tube air collectors for the solar system. Unfortunately, none of the well-established drying simulation programs (like Polysun, T*Sol or SAM) allow for air collectors. However, there is a program developed by Fraunhofer ISE, called Aircow(Welz, 2017), which transforms the thermohydraulic collector parameters of an air collector into coefficients of an equivalent liquid heating solar thermal collector. For Aircow to do this it needs measured or simulated operational parameters and to find these a model of an evacuated tube air collector was created in Matlab. This section will discuss the Matlab model and the use of Aircow to determine the thermohydraulic collector parameters which can then be used for the simulation of the solar field in Solgain (Ilchmann et al., 2016).

4.3.1 Modelling of an evacuated tube air collector

It was decided to model a collector very similar to the Airwasol collector seen in Figure 26, a brochure of the collector containing more technical specifications can be found in Appendix A. This design was chosen because of its simplicity. To model a collector it was decided to start with just one tube, see Figure 26.b, because the heat transfer in each tube would be more or less the same.

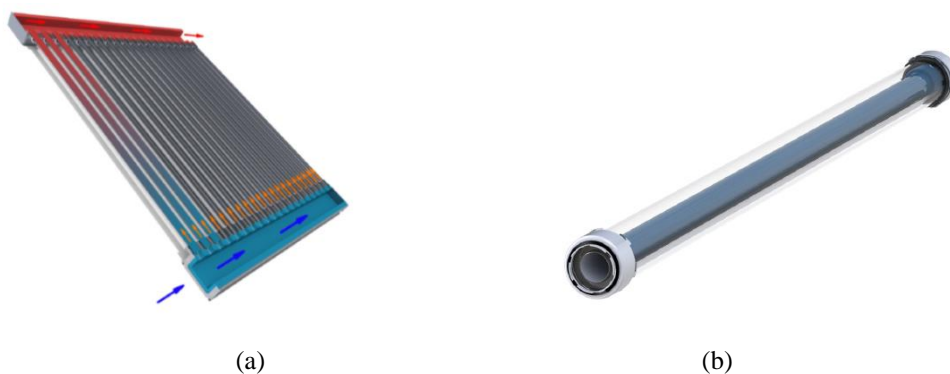


Figure 26: (a) Airwasol air collector. (b) One of the evacuated tubes in the Airwasol air collector (Siems, 2017).

To model the evacuated tube it was divided into little segments of 1 cm and it was assumed that the glass and absorber temperatures are constant over these little segments in order to accurately calculate the thermal physical properties of air. For each one these segments the heat transfer to the air inside and outside the tube was determined. This was done through various calculations, using thermal resistances as set out in Figure 27.

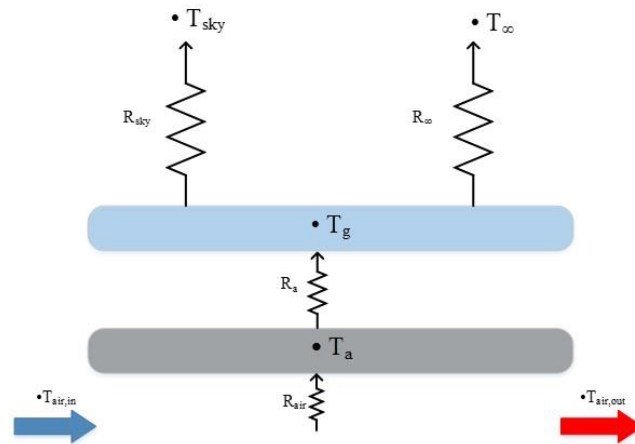


Figure 27: Schematic of heat transfer resistances in an evacuated tube.

Table 6 gives the characteristic of the evacuated tube as specified by Airwasol. They also specified that the glass tube is made of Borosilicate 3.3 and that the absorber tube is made from stainless steel. Appendix B shows how the transmissivity of the Borosilicate was determined by taking the wavelengths of the radiation into account following the method specified by Kalogirou (2009).

Table 6: Airwasol evacuated tube characteristics

Characteristic	Unit	Value
Length	m	2
Glass outer diameter	m	0.09
Glass inner diameter	m	0.085
Absorber tube outer diameter	m	0.0505
Absorber tube inner diameter	m	0.0501
Absorber absorptance	-	0.95

To calculate the glass temperature (T_g) the heat loss through natural convection and radiation losses to ambient conditions were taken into account. For the natural convection between the air and the glass an empirical correlation for the average Nusselt number (Nu) over a horizontal cylinder was used, shown in Equation 4.6 as set out in Çengel and Ghajar (2015), who references Churchill and Chu's 1975 paper. The work of Çengel and Ghajar (2015) is used for all the heat transfer

calculations of this section, unless stated otherwise. Appendix B gives all the formula's used to determine the necessary thermal physical properties of air.

$$Nu = \left(0.6 + \frac{0.387Ra_D^{1/6}}{[1+(0.559/Pr)^{9/16}]^{8/27}} \right)^2 \quad (4.6)$$

Where the Raleigh number (Ra) was calculated as defined in Equation 4.7 and must be smaller than 10^{12} :

$$Ra_D = \frac{9.81\beta(T_g - T_\infty)D_g^3}{\nu^2} Pr \quad (4.7)$$

Once Nu is calculated, the heat transfer coefficient is determined as well as the thermal resistance of natural convection between the glass and the ambient air. The thermal radiation resistance between the glass and sky must also be calculated by first determining the heat transfer coefficient for thermal radiation between the glass and sky, see Equation 4.8. σ represents the Stefan-Boltzmann constant ($5.67 \times 10^{-8} \text{ W}/(\text{m}^2\text{K}^4)$).

$$h_{rad} = \varepsilon_g \sigma (T_g^2 + T_{sky}^2)(T_g + T_{sky}) \quad (4.8)$$

A perfect vacuum was assumed between the glass tube and the steel absorber, resulting in no convection losses between them. Therefore, it is only necessary to calculate the thermal radiation resistance between the two. Equation 4.9 was adapted from Çengel&Ghajar (2015), see Appendix B, in order to calculate the thermal resistance (R_{ag}) between the two tubes. Here ε_a and ε_g represent the emissivity of the absorber and the glass, respectively.

$$R_{ag} = \frac{\frac{1}{\varepsilon_a} + \frac{1-\varepsilon_g}{\varepsilon_g} \left(\frac{r_a}{r_g} \right)}{\sigma A_a (T_a^2 + T_g^2)(T_a + T_g)} \quad (4.9)$$

Once all the thermal resistances were calculated the temperature of the glass cover could be determined. This was done by using Equation 4.10 (see Appendix B for derivation) where the radiation absorbed by the glass ($Q_{rad,a}$) along with the convection and radiation losses were taken into account to calculate the glass temperature. As is evident in Equations 4.6 – 4.9, a glass temperature needs to be guessed to determine some of the values needed for Equation 4.10. Therefore, to accurately determine the glass temperature the guessed glass temperature needs to be compared to the calculated glass temperature. If the error between the two is not very small, the calculations need to be iterated until the difference is negligible. For this study an error of 0.001 was deemed small enough.

$$T_g = \frac{Q_{rad,a} + \frac{T_a}{R_{ag}} + \frac{T_\infty}{R_{g\infty}} + \frac{T_{sky}}{R_{gsky}}}{\frac{1}{R_{ag}} + \frac{1}{R_{g\infty}} + \frac{1}{R_{gsky}}} \quad (4.10)$$

The temperature of the absorber was calculated in a very similar way. The radiation onto the absorber was calculated using the area of the absorber which faces the sun and the amount of radiation that passes through the glass. The Nusselt number for the forced internal convection between the absorber and the air flowing inside of it was determined using Gnielinski's equation, see Equation 4.11. Gnielinski's equation was used because of the expected high mass flows and turbulent flow through the pipe due to the high air demand of the rotary dryers. It was assumed that the turbulent flow in the tube is fully developed over the entire length of the tube as the length/diameter ratio is larger than 10. Another reason for the use of Gnielinski's equation is its accuracy; an error of less than 10 % can be expected when using this formula according to Çengel&Ghajar (2015).

$$Nu = \frac{(f/8)(Re-1000)Pr}{1+12.7(f/8)^{0.5}(Pr^{2/3}-1)} \left(\begin{array}{l} 0.5 \leq Pr \leq 2000 \\ 3 \times 10^3 < Re < 5 \times 10^6 \end{array} \right) \quad (4.11)$$

Where the friction factor (f) is calculated using the first Petukhov equation (Equation 4.12) as recommended by Çengel&Ghajar (2015).

$$f = (0.790 \ln(Re) - 1.64)^{-2} \quad (4.12)$$

The Nusselt number was again used to determine the heat transfer coefficient and this was in turn used to calculate the thermal resistance to the internal forced convection (R_{air}). The thermal resistance for radiation heat transfer between the absorber and glass was already calculated to determine the glass temperature so now the absorber temperature can be calculated as shown in Equation 4.13 (see Appendix B for derivation). As with the calculation of the glass temperature, an absorber temperature had to be assumed before the actual temperature could be determined and the two temperatures needs to have an error smaller than 0.001.

$$T_a = \frac{Q_{rad} + \frac{T_g}{R_{ag}} + \frac{T_{air}}{R_{air}}}{\frac{1}{R_{ag}} + \frac{1}{R_{air}}} \quad (4.13)$$

The air temperature can be calculated using the absorber temperature and the thermal resistance to the internal forced convection. The derivation of Equation 4.14 can be found in Appendix B. For this calculation the inlet air temperature ($T_{air,i}$) does not have to be guessed, because the air into the first segment is pre-heated to a constant temperature and for the segments that follow, the inlet temperature will be that of the previous segments' output.

$$T_{air,i+1} = T_{air,i} + \frac{T_a - T_{air}}{R_{air} \dot{m} c_{p,air}} \quad (4.14)$$

4.3.2 Matlab simulation results

For this simulation the ambient air temperature was set to 25 °C, with a sky temperature of 20 °C. The solar irradiance onto the tube was set to 1000 W/m² and the air mass flow was 0.0108 kg/s. Figure 28 shows the simulation's calculated temperature rise across the evacuated tube for the glass, absorber and air.

Unfortunately an experimental study could not be done to validate the simulation's results. There is, however, a study on evacuated tube air collectors done in Canada by Paradis et al. (2015) where a similar model was created and then validated with experimental results. In order to see how the current study's model holds up against the model of Paradis et al. (2015) their experimental conditions were fed into this study's Matlab model and the evacuated tubes were set to the same size. By comparing the model like this, it ensures that the heat transfer modelling was at least done correctly. Appendix C shows a further comparison of the two models' outlet air temperature and efficiency.

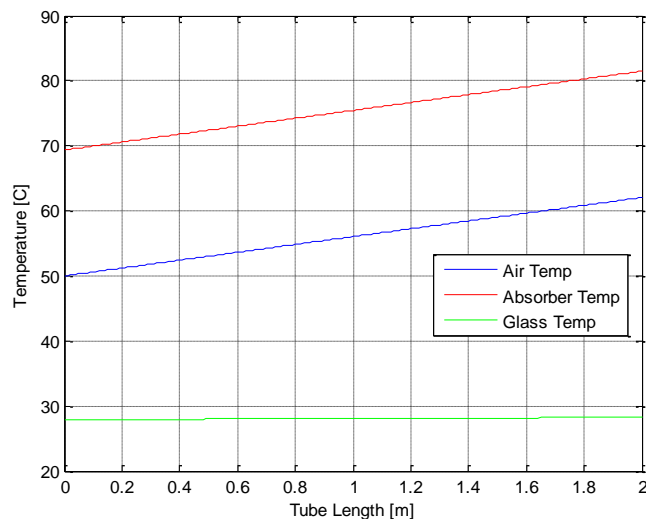


Figure 28: Matlab simulation results for the evacuated tube

For their experiment, they tried to reach a steady state operating condition by providing constant volume flow. During the experiment most of the other parameters like the ambient air and solar irradiance also stayed relatively constant. As can be seen in Figure 29, the tube outlet temperature tends to 278 K when the volume flow rate is at 28 m³/h. If the same flow rate and ambient air conditions are fed into the current study's model the outlet air temperature is calculated to be 277.87 K, which is only 0.05 % less than the value measured by Paradis et al. (2015), showing that the model can be reliable. The size of the segments were varied as well, to ensure that the model output does not rely on segment size; if

the segment sizes are set to 20 cm instead of 1 cm, the change in the output air temperature is only 0.4 %.

Paradis et al. (2015) also incorporated wind speed into their model and experimental results, but showed that it had little effect on the evacuated tube. This was not a factor this model took into account, but it was not deemed necessary due to the Paradis et al.'s (2015) results and because the Matlab model showed that the collector was quite insensitive to changes in the glass temperature. This can be explained by looking at Equation 4.13, here the thermal resistance for radiation heat transfer between the absorber and glass is quite high, minimizing the effect of the glass tube temperature.

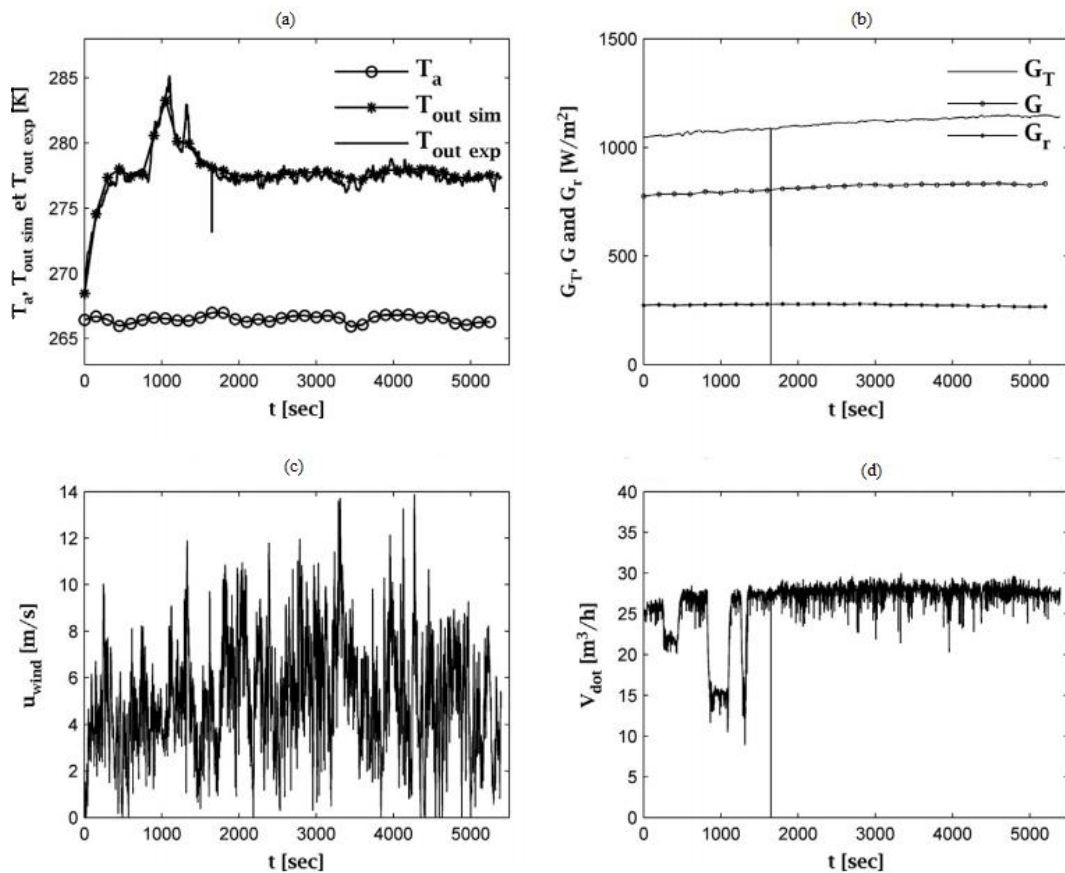


Figure 29: Extract of Paradis et al. (2015) experimental results. (a) Ambient air temperature, simulation output temperature and experimental output temperature as a function of time. (b) Tilted irradiance, horizontal irradiance and reflected irradiance. (c) Wind speed during testing. (d) Volume flow rate through evacuated tube.

4.3.3 System planning using Aircow

Simulated results from the Matlab model described above are given as an input for Aircow. Aircow uses these inputs to calculate the air collector model coefficients in order to optimise the system design. The coefficients can also be converted into equivalent liquid heating collector coefficients of efficiency so that it can be simulated using a conventional simulation tool. All of the information regarding the program comes from the Aircow manual (Fraunhofer ISE, 2017).

The program's optimisation function helps to determine the ideal mass flow, field length and field width. The system planning function also calculates the solar field's total pressure drop and necessary fan power. One important thing to note is that Aircow has only been validated for flat plate collectors with under-flown absorbers and not evacuated tube collectors. This may lead to small errors, however, looking at the program's operations, it does not seem if it would make a difference if a flat plate collector or evacuated tube collector is used.

Aircow considers the air collector's efficiency as a map instead of a line as is common with liquid heating collectors. This is because it uses both the reduced temperature difference and the air mass flow rate as input values. Equation 4.15 shows the thermal efficiency model Aircow uses to determine the collector's conversion factor (η_0), its linear heat loss coefficient (C_1), its quadratic heat loss coefficient (C_2) and the mass flow dependent heat loss coefficient (C_m). The collector efficiency (η), input-output temperature difference (ΔT), solar irradiance (G_t) and mass flow rate (\dot{m}) are all user inputs and in this study is determined using the Matlab model described in the previous section.

$$\eta\left(\frac{\Delta T}{G_t}, \dot{m}\right) = (1 - e^{-C_m \dot{m}})(\eta_0 - C_1 T' - C_2 G_t T'^2) \quad (4.15)$$

Where T' is calculated by:

$$T' = \frac{\left(\frac{T_{in} + T_{out}}{2}\right) - T_{\infty}}{G_t} \quad (4.16)$$

Aircow specifies that the simulated results, which were given as inputs, must represent turbulent flow. Furthermore, it is important to give results from different flow rates in order for the model to determine the various coefficients and construct the efficiency map.

The program uses the calculated conversion factor and heat loss coefficients along with the user defined solar radiation and collector tilt to determine the size of the solar field that is needed to supply the needed amount of thermal power specified. This is done by determining the energy the solar field can produce per m^2 and then dividing the design power output by this amount. The number of collectors in a row is determined using the needed temperature rise and the mass flow rate of

the air through the row. The program can then use the calculated solar field area and number of collectors per row to determine the amount of rows in the solar field.

As mentioned before, Aircow can also determine the field's pressure drop. In order to do this it has a specific model which determines a linear (R_1) and quadratic (R_2) pressure drop coefficients, as can be seen in Equation 4.17. It also determines these coefficients from user input data regarding simulation results of the pressure loss in one collector for a given mass flow.

$$\Delta p_{coll}(\dot{m}) = R_1 \dot{m} + R_2 \dot{m}^2 \quad (4.17)$$

In order to determine the collector's pressure drop, it can be seen as a manifold with parallel flow (refer back to Figure 26.a) and the equation for the pressure drop in a manifold was calculated as specified by Bajura & Jones (1976). For this study Equation 4.18 was used to determine the pressure loss over the evacuated tube.

$$\frac{p_1 - p_2}{\rho_a} = \frac{v_{31}^2}{2} \left(\frac{A_{31}}{A_{32}} \right)^2 + \frac{v_{31}^2}{2} \left[C_{TD} + \left(\frac{fL}{D} \right) + C_{TC} \left(\frac{A_{31}}{A_{32}} \right) \right] \quad (4.18)$$

The various parameters of Equation 4.18 are displayed in Figure 30.a. The equation makes allowance for a change of area in the lateral, but for this study the area is constant, therefore the ratio $A_{31}/A_{32} = 1$. The term's C_{TD} and C_{TC} represent the minor losses as the flow enters the lateral from the distribution header and then exits the lateral into the combining header. The term fL/D accounts for the frictional losses in the lateral, the frictional losses in the headers are deemed negligible. This is because, when the collectors are placed in a row, the evacuated tube exit of one collector would directly attach to the entrance of the following tube, as shown in Figure 30.b, at the joining of the tubes there is just a small support. This means that the total header length in the system is considerably shorter than the total evacuated tube length in the system, therefore, the total pressure loss in the headers are much smaller than the total pressure loss in the tubes. The fact that the headers are larger than the tubes with the air flowing through them at a lower speed also significantly reduces the pressure losses.

Aircow then goes on to determine the pressure drop over the entire system ($\Delta p_{sys, before, after}$) for a given volume flow (\dot{V}). The pressure drop due to the equipment in the system, before and after the solar field, are taken into account and allows the program to determine the fan power (P_{fan}) needed for the given air flow as shown in Equation 4.20. The pressure drop before and after the solar field can be determined by using user specified flow resistances (R), see Equation 4.19. The flow resistances of the field can be determined by calculating the estimated pressure drop over the field for a given volume flow; basically just rearranging Equation 4.19 so that R is on the left hand side.

The model also takes dynamic pressure ($p_{sys,dyn}$) into account, for when the air flow velocity reduces due to flowing into a large volume, but for this study it was not considered, since the air does not flow into a large volume, only the rotary dryer. The pressure loss over the rotary dryer is accounted for in the pressure drop after the solar field. Another function which will not be used is Aircow's air leakage model, this is because the Airwasol collector which this study tries to model, does not have any leakage losses (Siems, 2017).

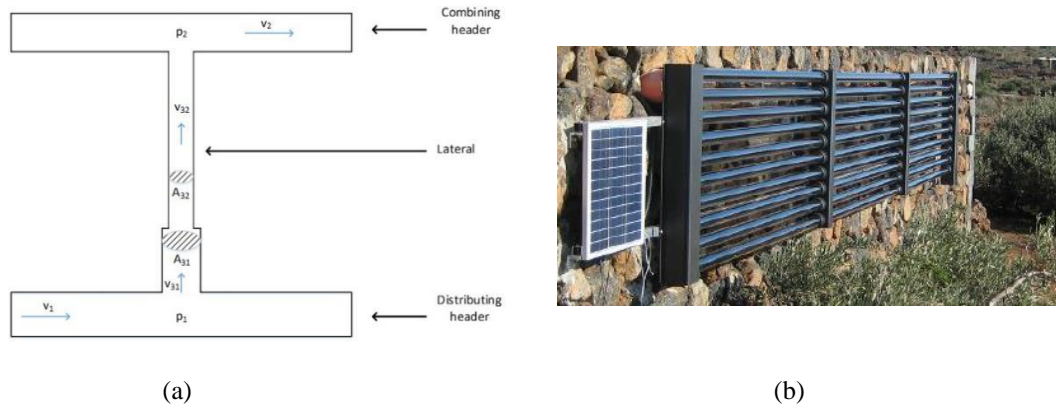


Figure 30: (a) Flow in a manifold's lateral from Bajura& Jones (1976). (b) Airwasol collectors connected in a row, with headers on the far left and far right and supports in between (Siems, 2017).

$$\Delta p_{sys_{before,after}} = R_{sys_{before,after}} \dot{V}^2 \quad (4.19)$$

$$P_{fan} = \frac{(\Delta p_{sys_{before}} + \Delta p_{sys_{after}} + p_{sys_{dyn}} + \Delta p_{coll}) \dot{V}}{\eta_{fan}} \quad (4.20)$$

The main goal of using Aircow is to convert the collector coefficients so that it can be used in a simulation program for liquid heating collectors. Aircow specifically mentions ScenoCalc as a simulation program that can be used, but the converted coefficients are not limited to this software. To determine the coefficients for a liquid heating collector, one operating mass flow is considered for Equations 4.21-4.23. Appendix D shows how the mass flow can be optimized using Aircow. Only one operating point is necessary for a collector without leakages, if the collector experiences any air leakages, three operation points need to be considered. The converted coefficients can now be used in Equation 4.24, as is common for liquid heating collectors.

$$\eta_0 = \eta_{0_{max}} (1 - e^{-c_m \dot{m}_{row}}) \quad (4.21)$$

$$C_1 = C_{1_{max}} (1 - e^{-c_m \dot{m}_{row}}) \quad (4.22)$$

$$C_2 = C_{2_{max}}(1 - e^{-c_m \dot{m}_{row}}) \quad (4.23)$$

$$\eta \left(\frac{\Delta T}{G_t} \right) = \eta_0 - C_1 T' - C_2 T'^2 \quad (4.24)$$

4.3.4 Aircow results

Simulation results from the Matlab model described previously was used as data points for Aircow in order to determine the various heat loss coefficients and the efficiency map. The mass flow, irradiance and inlet temperature for the Matlab model was varied in order to give Aircow a wide range of data. Table 7 shows the 7 data points entered for Aircow. The mass flow through the collector was determined by multiplying the mass flow through one tube, as specified in the Matlab model, by 17, which is the amount of tubes in one Airwasol collector.

Table 7: Data points for Aircow input

Irradiance [W/m ²]	Mass flow [kg/h]	Inlet Temp [°C]	Outlet Temp [°C]	Collector Efficiency [%]
700	593.64	50	58.87	43.76
1100	593.64	50	64.08	44.20
700	1242.36	70	74.15	42.93
1100	1242.36	70	76.67	43.90
700	2282.76	100	102.13	40.68
1100	2282.76	100	103.51	42.55
1100	4284	25	27.04	46.16

The collector's efficiency increases with an increase in mass flow, but decreases for an increase in temperature as expected from air collectors. The last data point does not follow the same pattern as the ones before it, this point was used to try and simulate a very efficient point. However, the collector's efficiency does appear to be quite low. The main reason for this is the large glass tube diameter compared to the absorber diameter. The efficiency was determined with Equation 4.25. By looking at the equation, it is possible to see that the area of the collector plays a very important role. If the absorber area was used instead of the glass tube outside area the efficiency would be in the range of 0.7 – 0.8.

$$\eta_{coll} = \frac{\dot{m} c_p \Delta T}{G_t \left(\frac{A_g}{2} \right)} \quad (4.25)$$

Aircow determined the efficiency map and with that it also calculated the various coefficients given in Table 8. To determine the pressure drop over the collector Equation 4.18 was used, with the same mass flows as listed in Table 7. In

Equation 4.18, C_{TD} as well as C_{TC} was set to 2 to account for the minor losses in the threaded T-junctions where the evacuated tubes join the distributor and collection headers (Çengel & Cimbala, 2010). Aircow gives R_1 and R_2 of Equation 4.17 as -0.0263 Pa/kg/h and $0.000224 \text{ Pa/(kg/h)}^2$, respectively.

Table 8: Evacuated tube quadratic model coefficients as determined by Aircow.

Quadratic model inputs	Units	Calculated values
Conversion factor (η_0)	-	0.4613
Linear heat loss coefficient ($C_{1,\max}$)	W/(m ² K)	0.440
Quadratic heat loss coefficient ($C_{2,\max}$)	W/(m ² K)	0.00859
Mass flow dependent heat loss coefficient (C_m)	h/kg	0.007598

To optimise the mass flow and to determine the equivalent liquid heating collector coefficients, a design point has to be set. The peak operation point was chosen for these inputs. Therefore, the irradiance was taken as 1060 W/m^2 , which was the highest global tilted irradiance measured during the crushing season, it was measured on 31 October. The ambient temperature was set to $25 \text{ }^\circ\text{C}$. The collector tilt was set to 29 ° , which is Durban's latitude and the needed temperature rise over the solar field needs to be $70 \text{ }^\circ\text{C}$, with an inlet temperature of $50 \text{ }^\circ\text{C}$. The thermal power transferred to the air at the field outlet needs to be 9.49 MW , the total amount needed to dry all of the bagasse. Using the above information Aircow determined that there should be 5.88 collectors in a row and the solar field should consist of 755.39 rows, which equates to a solar field size of $22\,165.83 \text{ m}^2$.

The flow resistances before and after the field, as mentioned in Equation 4.19, was found to be:

$$R_{before} = 6.33 \times 10^{-9} \frac{\text{Pa}}{\left(\frac{\text{m}^3}{\text{h}}\right)^2}$$

$$R_{after} = 1.656 \times 10^{-8} \frac{\text{Pa}}{\left(\frac{\text{m}^3}{\text{h}}\right)^2}$$

For this study the flow optimisation for the net system power savings and for cost savings was compared, that is options 2 and 4 set out in Appendix D. The price per unit electrical auxiliary energy is given as 0.50 ZAR/kWh (Hess et al., 2016) and the price of the energy replaced is 0.168 cent/kWh (see Appendix D for calculation). For the cost optimisation Aircow suggests a mass flow rate of 510.9 kg/h per row and for the system savings optimisation a mass flow of 639.8 kg/h per row is suggested. The lowest flow rate that should be allowed in the evacuated tubes is 550 kg/h , because this is the lowest flow rate where the internal flow's Reynolds number is still above $10\,000$. The Matlab model and

Aircow both need turbulent flow values, therefore the system power savings optimisation flow rate will be used.

In reality there cannot be a decimal amount of collectors in a row. By following the steps set out in Appendix D, the system is recalculated with 6 collectors in a row, but with 749 rows, so that the power at the field outlet will still be the same. However, the outlet temperature will be 121.3 °C. This temperature is not dangerous for the drying system, because it is not high enough to cause a fire in the system. Furthermore, the temperature of the air which reaches the drying system will be lower than the air temperature directly at the field outlet, due to heat losses in the piping system. The instantaneous efficiency of this point according to Aircow is 40.3 %, which is quite low. This is most probably due to the high temperatures and low flow rate in the solar field, with both factors negatively impacting the efficiency.

For the optimised system, Aircow calculates that the pressure drop over the solar field will be 449.2 Pa and 6 105.5 Pa over the rest of the system. The pressure drop is quite high due to the rotary dryer, which accounts for half of the drop. So in total the system has a pressure drop of 6 554.7 Pa with a volume flow rate of 444 438.9 m³/h. If a fan with an electric to hydraulic efficiency of 57.2 % (an Aircow default value) is used, the fan will require 1.41 MW_{el}. This could result in a very large fan being used, therefore it is suggested that, like the drying system, the solar system is also split into four sections. Each solar section will provide the necessary heated air to the rotary dryer it is connected to and a smaller fan of a more convenient size can then be installed into each section.

The flow rate in each collector row will stay the same, as well as the number of collectors in each row, since the same temperature lift is still needed. The number of rows for each section will just be a quarter of the rows specified above. The volume flow rate for each section will also be a quarter of what is specified above. It is important that the mass flow rate through the solar system is the same mass flow rate that is needed in the drying system, because it would lead to efficiency losses if extra air had to be sucked in from the ambient or if excess air had to be released. The pressure drop across each section is assumed to be the same, therefore, the fans' will still have to produce the necessary pressure lift, but because the volume flow rate in each system is a quarter of what was mentioned above, each fan can be much smaller.

Now that a specific operation point has been identified, Aircow can calculate the coefficients that can be used in a liquid collector simulation, as shown in Table 9.

Table 9: Converted coefficients for liquid collector simulation.

Coefficients	Units	Converted values
Conversion factor (η_0)	-	0.4577
Linear heat loss coefficient (C_1)	W/(m ² K)	0.437
Quadratic heat loss coefficient (C_2)	W/(m ² K)	0.008524
Mass flow per row per row gross area	kg/(sm ²)	0.006
Mass flow per row per collector gross area	kg/(sm ²)	0.036

4.4 Solar Field Simulation

For this study Solgain (Ilchmann et al., 2016) was chosen as simulation program for the evacuated tube collector system rather than ScenoCalc. This was done, because ScenoCalc does not take the whole solar field into account, only the power per m². Furthermore, it does not allow the user to specify temperatures above 100 °C, something which is necessary for this study. Solgain is an open source tool which can be used to simulate the entire solar system and it can be edited to function with temperatures above 100 °C. Solgain was created to accurately and quickly determine the solar gains of a system without too much effort from the user (Ilchmann et al., 2016).

4.4.1 Simulation setup with Solgain

In order to simulate a solar thermal system the user should give inputs regarding the climate, location and process. For the climate data, hourly GHI values, DNI values and the ambient air temperature should be given as inputs. For the location input, the latitude and hemisphere of the system must be given. The climate and location data is used to determine the GTI (named G_t in Solgain), which is the total irradiance that falls on the collector's surface and was calculated using Equation 4.25.

$$G_t = G_{bt} + G_{st} + G_{rt} \quad (4.25)$$

G_{bt} represents the direct irradiance on the tilted collector aperture, G_{st} is the diffuse irradiance on the tilted collector aperture and G_{rt} is the reflected irradiance onto the tilted collector aperture. These terms were calculated using Equation 4.26- 4.28.

$$G_{bt} = G_{bn} \times \cos\theta \quad (4.26)$$

Where θ is the incidence angle, calculated for each hour and G_{bn} is the DNI.

$$G_{rt} = G \left(\frac{\rho_{\text{grd}}}{2} \right) (1 - \cos\beta_c) \quad (4.27)$$

Where G is the GHI, ρ_{grd} is the ground reflectivity and β_c is the collector tilt.

$$G_{st} = G_d \times \frac{1 + \cos\beta_c}{2} \quad (4.28)$$

Where G_d is the diffuse horizontal irradiance, which can be calculated by subtracting the direct horizontal irradiance (G_b) from the GHI. G_b can be calculated as specified in Equation 4.29, where θ_s represents the zenith angle of the sun.

$$G_b = G_{bn} \times \cos\theta_s \quad (4.29)$$

After the program calculated the various irradiances that falls on the collector's aperture it can determine the specific collector gains (Q_{gain}). This is done by using the coefficients which were originally specified in Equation 4.24 and given in Table 9. The incidence angle modifiers for direct (K_b) and diffuse (K_d) irradiance are also used to determine the collector gain, as can be seen in Equation 4.30. Solgain already has specific collector coefficients for a flat plate collector and for an evacuated tube collector, so for this study, the coding was changed so that it uses the coefficients in Table 9.

$$Q_{gain} = \eta_0 [K_b G_{bt} + K_d G_{st} + K_d G_{rt}] - C_1(T_f - T_a) + C_2(T_f - T_a)^2 \quad (4.30)$$

Solgain goes on to use the specific collector gains to calculate the field outlet temperature. For this calculation Equation 4.31 is used. Solgain does not allow the user to specify that more than one collector in a row is needed, it only calculates the temperature rise over one collector and then assumes that this is the needed outlet temperature of the field. So in order to simulate a field where there are multiple collectors in a row, the coding needed to be changed. A loop was used which took the first calculated outlet temperature and then used it as the inlet temperature for the next collector. The outlet temperature was then again calculated using Equation 4.31. The loop runs for the amount of collectors there are in each row.

$$T_{out} = \frac{\dot{m} c_{p,c} T_{in} - \frac{c_{eff}}{2\Delta t} T_{in} + Q_{gain} + \frac{c_{eff}}{\Delta t} T_f(t - \Delta t)}{\dot{m} c_{p,c} + \frac{c_{eff}}{2\Delta t}} \quad (4.31)$$

In this equation the $c_{p,c}$ represents the average heat capacity, while c_{eff} represents the effective collector heat capacity (kJ/m²K). For the average heat capacity value, the heat capacity of air between 50 °C and 120 °C was embedded into the program, while the effective collector heat capacity was kept the same, because it is related to the aperture, rather than the heat transfer fluid. Δt represents the width of the time steps Solgain work with, which is one hour, since hourly data is used as input. For Equation 4.31, \dot{m} represents the specific mass flow through the collector field. T_f is the mean collector temperature and is dependent on the outlet

temperature, therefore, Equations 4.30 and 4.31 along with T_f will have to be iterated, where the error between outlet temperatures should be smaller than the user defined value. When the outlet temperature is finally determined, the total thermal energy delivered by the solar field can be determined using Equation 4.32.

$$Q_{coll} = \dot{m}_c c_{p_c} (T_{out} - T_{in}) \quad (4.32)$$

Solgain assumes that there is a heat exchanger between the solar field and the process to which it delivers the thermal energy, as can be seen in Figure 31. The integration point for this study does not include a heat exchanger and to effectively remove the heat exchanger its efficiency was just set to 100 %, so that the heat delivered by the solar field equals the heat that goes to the process. Solgain also allows the user to define the distance between the solar field and the process. The program then calculates the amount of heat loss across this distance to and from the process.

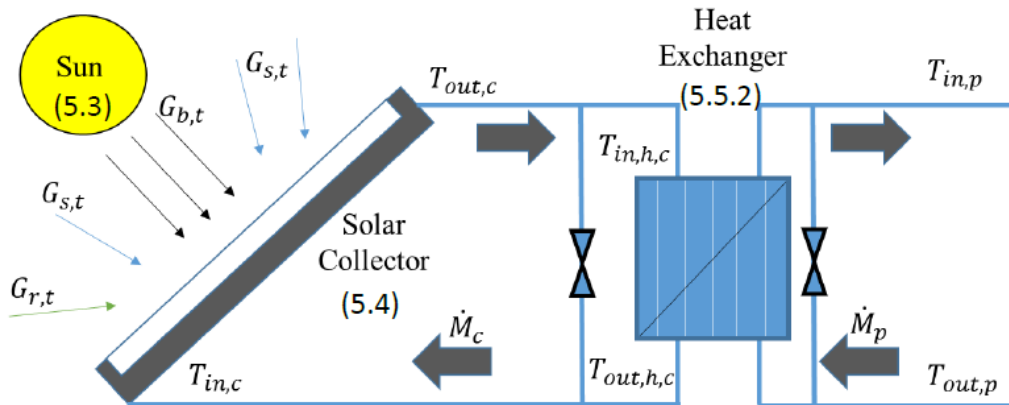


Figure 31: Solgain system layout (Ilchmann et al., 2016).

In order to determine how the system performs, Solgain completes three calculations to describe the system's characteristics. These calculations are that of the solar fraction (F), degree of utilization (η_u) and the annual system efficiency (η_s). The solar fraction is the percentage of thermal energy needed by the process (Q_{need}) which the solar system can provide throughout the year (Q_p). The degree of utilization is the percentage of the energy provided by the solar field (Q_{coll}) which the process can actually use. The annual system efficiency shows how much of the sun's energy (Q_{sun}) the solar field could use and send to the thermal process. The equations for the three characteristics are shown in Equations 4.33 - 4.35.

$$F = \frac{Q_p}{Q_{need}} \quad (4.33)$$

$$\eta_u = \frac{Q_p}{Q_{coll}} \quad (4.34)$$

$$\eta_s = \frac{Q_p}{Q_{sun}} \quad (4.35)$$

4.4.2 Simulation results

The same solar resource data from Solargis[®], referred to in the literature study, is used for this simulation. As mentioned before, Solgain only needs the hourly DNI, GHI and ambient temperature. Most of the other inputs are summarised in Table 10.

Table 10: Inputs for Solgain

Input	Unit	Value/decision
Heat demand type	-	Pre-heating
Process feed temperature	°C	120
Process Return Temperature	°C	50
Heat capacity of process medium	kJ/(kgK)	1.009
Energy consumption of the process	kW	9492.251
Collector tilt	°	29
Collector orientation	-	North
Collector area	m ²	22 425.06

The ground reflection was set to 0.2, the default value in Solgain. The maximum difference for the output temperature iteration is set to 0.01, again the default value in Solgain. The distance between the collector and process is set as 20 m, this is to ensure there is enough space for the exhaust steam heater, rotary dryer drive system and the bagasse feeding system. The maximum collector power output is set to 427.31 W/m², this value is determined by dividing the maximum power output from the solar field with the collector area calculated by Aircow.

For this study the crushing season is taken from 1 April to 20 November, so the heat demand profile in Solgain was set that the system only operates between weeks 14 – 47 in the year. It was assumed that the drying system will have the same overall time efficiency as the rest of the sugar mill, therefore the load was set to 80.83 %.

Table 11 gives the results of the system characteristics as it was calculated by Solgain. Two types of results are given, one for the actual system, which would only operate during the crushing season and one for a system which would operate throughout the whole year. The solar fraction initially seems to be quite low, but one has to remember that the drying system runs day and night and the solar system is only able to produce thermal energy throughout the day. On top of this, the solar field only comes near to producing the total needed amount of

thermal energy for drying close to solar noon for about 2-3 hours each day, as it is essentially a pre-heating system. The solar fraction for the annual system is a bit higher than for the crushing season, this is because the sun can provide more power during the summer months, which is outside of the crushing season.

Table 11: Simulation characteristics as calculated by Solgain

Characteristic	Crushing Season [%]	Annually [%]
Solar fraction	15.93	16.61
Degree of utilization	70.44	95.49
Annual system efficiency	12.88	19.46

The degree of utilization during the crushing season is quite low, this is because the drying system cannot use the thermal energy produced by the solar field outside of the crushing season. The degree of utilization for the annual system in turn is quite high, the reason why it is not 100 %, is because of the piping losses from the solar field to the process.

Figure 32 shows the relationship of the solar radiation available and the thermal energy that the field can deliver at design conditions. This is a representation of the system's efficiency, since it compares the radiation flux onto the solar field with the energy delivered to the drying system. The annual system efficiency in both cases are quite low, usually it is in the range of 40 – 60 % (Ilchmann et al., 2016). This is due to the low collector efficiency, especially the fact that the glass tubes are considerably bigger than the absorber tubes. This results in an aperture area which is much larger than the area that could actually use the irradiation. Therefore, by looking at Equation 4.35, the term Q_{sun} is calculated using the aperture area, while Q_p depends on the absorber area.

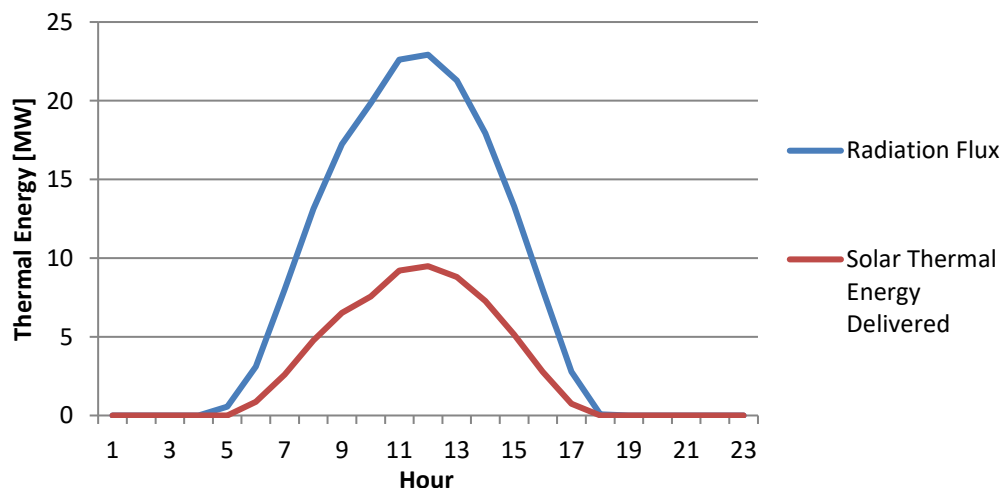


Figure 32: Comparison of available solar radiation and thermal energy delivered to process.

Figure 33 shows the thermal energy delivered to the drying system during the crushing season. The drying system needs 9.49 MW when running at full load, the highest amount of thermal energy the solar system can deliver is 9.48 MW, just below the maximum needed energy. This is due to the fact that the peak conditions were used to size the field, as the solar system only serves as a type of pre-heater, it would be unnecessary and wasteful if the air is heated up too much and producing excess thermal energy. Now none of the solar thermal energy gained will go to waste, everything can be used by the drying system. An excess of solar thermal energy can lead to lower system efficiencies, because some of the energy will have to be dumped before it heads to the drying system.

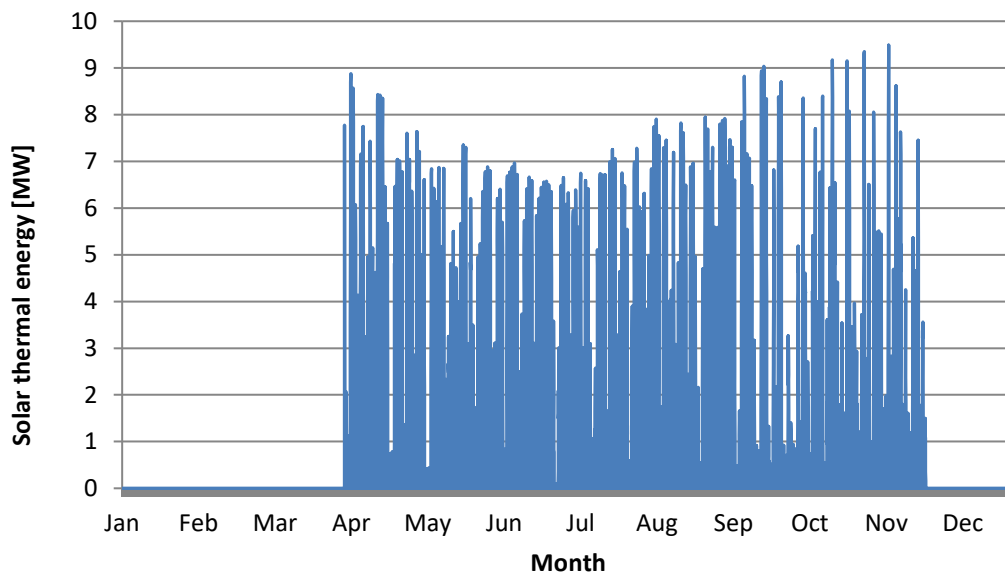


Figure 33: Simulated solar thermal energy delivered to the drying system.

4.5 Effect on Sugar Mill

By using the results from the drying model and Solgain simulation, the amount of bagasse that is saved or the reduction in coal usage can be determined. Equation 4.36 can be used to determine the amount of dry bagasse (\dot{m}_{bag}) that needs to be used to produce the same amount of live steam (\dot{m}_{ls}) than the wet bagasse.

$$\dot{m}_{bag} = \frac{(\dot{m}_{ls}h_{ls}) - (\dot{m}_{bfw}h_{bfw})}{\eta_{NCV} NCV} \quad (4.36)$$

The boiler's efficiency (η_{NCV}) based on the NCV of bagasse was calculated to be 87.48 % when the boiler operates with wet bagasse. This is very close to the value simulated by Laubscher (2017) when looking at Figure 15. His simulation roughly shows a 2.45 % increase in boiler efficiency with the use of 40 % moisture

content bagasse. Assuming that the generic boiler will respond in the same way and by using Equation 4.36 it was calculated that only 32.64 ton/h of the dried bagasse is needed to produce the necessary live steam. It is, however, important to keep in mind that the 40 % moisture content bagasse is lighter than the wet bagasse, due to the reduction in moisture. Therefore, when looking at the actual amount fibres used, 21.38 ton/h is needed of the wet bagasse and 19.58 ton/h is needed of the dry bagasse.

The amount of exhaust steam (\dot{m}_{exhs}) required to deliver all of the needed thermal energy ($Q_{th,dry}$) to the drying system can be calculated using Equation 4.37. Where h_{exhs} and h_{cond} represent the enthalpy of the exhaust steam and condensate respectively. According to Rein (2007) one ton of live steam can be let-down to 1.2 tons of exhaust steam, by taking this into account and using Equation 4.36 and 4.37, it can be calculated that an extra 0.72 ton/h of the dry fibres are needed to generate the needed exhaust steam. Therefore, the total amount of dry fibres needed when using 40 % moisture content bagasse is 20.3 ton/h.

$$\dot{m}_{exhs} = \frac{Q_{th,dry}}{h_{exhs} - h_{cond}} \quad (4.37)$$

The solar field can help to save more bagasse, since it decreases the amount of exhaust steam needed for the drying system. The previous section mentions that the solar system can deliver 15.93 % of the necessary heat for the drying system. This relates to 6 833.16 MWh_{th} energy delivered. By multiplying this value with 3600 to get the energy delivered over the given period and plugging this value into Equation 4.37, the amount of exhaust steam it saved can be determined. By using this method it is calculated that the solar system saves 11 164.94 ton of exhaust steam throughout the crushing season, this relates to 3 140.62 ton of dry bagasse or 1884.37 ton dry fibre. This leads to a further 2.05 % reduction in bagasse usage, therefore by integrating the bagasse dryer with the solar system the bagasse usage can be reduced with 7.05 %.

To give a better idea of the value added by the solar system the amount of bagasse saved can be expressed in tons of coal. This is done, because bagasse does not have a specific monetary value, while coal does. The amount of coal saved can be determined by comparing the calorific values of the two fuels. According to Smith et al. (2016), 1 ton of coal is equal to 4 tons of bagasse. Based on NCV, 1 ton the dried bagasse is equal to 1.3 tons of the 51 % moisture content bagasse. Therefore 1 ton of coal is equal to 3.08 tons of dried bagasse and it can be calculated that the solar system will save 1020.38 tons of coal.

5 Solar Live Steam Generation

This section will explain how the proposed live steam generation system will work using CSP collector technology. It will briefly discuss how the boiler and solar system will work together, as well as how more electricity can be generated in South African sugar mills. The section goes on to explain how the solar system was simulated and the simulated results will be presented and discussed.

5.1 Integration Point

The integration of solar live steam into the generic system shown in Figure 3 in Section 2.2 will help to ease the boilers' load, saving bagasse and/or coal. This study assumes that the generic sugar mill has three boilers which run at part load to supply the necessary steam to the mill. They are sized similar to what is described in the study of Reid and Rein (1983) where two boilers running at 110 % load would be able to supply the necessary steam (Reid and Rein, 1983). Furthermore, each individual boiler can only be turned down to 50 % of its nominal load capacity, resulting that the boiler house as a whole can only turn down to 68 % of its load if all three boilers are running. This configuration severely limits the size of the solar system and the impact it can make on the sugar mill.

Although a solar thermal system would make it possible to shut down one or more of the boilers during daytime, the boiler would have to be started again during night time or hours of low DNI. Sugar mills refrain from shutting down boilers and starting it up again on a regular bases as this may cause various problems in the boiler (Foxon, 2017). An extremely large solar thermal storage system would be needed if it was to supply energy to the mill throughout the whole night.

The proposed solar system would consist of parabolic trough collectors using thermal oil. This technology was chosen since it is the most mature solar CSP technology on the market (Calamateo and Zhou, 2015) and South Africa has various operational parabolic trough plants like Bokpoort CSP and KaXu Solar One.

The fact that there are large parabolic trough plants in South Africa means that the necessary practical knowledge to implement and operate such a system is available within the country. Although central receiver systems are becoming more popular around the world, there is no need for its high operational temperature which is one of its key advantages. Furthermore, the high humidity in the sugar milling region would significantly reduce the efficiency of a central receiver system (Cardemil et al., 2013). Linear Fresnel systems were deemed too immature, considering that there is only one small system installed in South Africa. Immature technology can make it difficult to secure funding as financiers want to have certainty over technology capabilities (Peterseim et al., 2013).

Figure 34 shows how a parabolic trough solar system could be integrated into a conventional sugar mill. One problem with using thermal oil is that it has a maximum operating temperature of 393 °C (Heller, 2013). The oil will have to pass through a heat exchanger to create steam, so the maximum temperature which could be delivered to the sugar mills is 385 °C (Peterseim et al., 2014), while the steam used in the mill is 390 °C. However, according to the SMRI this will not be a problem, the temperature difference should just not be more than 10 °C (Foxon, 2017). The steam pressure is a more important parameter that needs to be adhered to. This is the reason for the pressure valve in the integration setup in Figure 34.

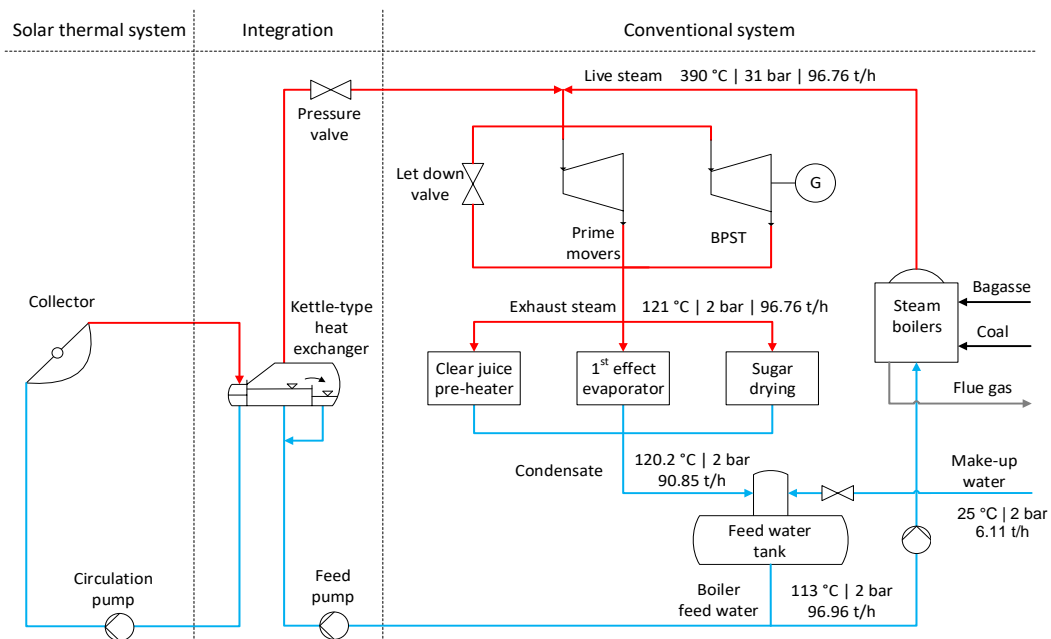


Figure 34: Solar live steam integration into a generic sugar mill, adapted from Hess et al. (2017).

The required steam temperature is another reason why thermal storage was not considered. As mentioned in Section 3.1, molten salt is usually used as storage medium, therefore, a heat exchanger is needed between the oil and molten salt. This would result in a temperature drop when the tank is being charged and another temperature drop when the tank is being discharged, creating steam at a temperature closer to 370 °C. Oil can also be used as storage medium, but this would result in rather large storage facilities and high costs (Liu, et al., 2016). As mentioned before, conventional sugar mills do not operate outside of the crushing season. Therefore, the solar system will also not be able to function outside of the crushing season. This is because there are no operations that can use

the live steam generated by the solar system. If extra electricity was to be generated, then there are no processes that can use and condense the exhaust steam from the BPST. The configuration above, from here on referred to as Configuration 1, will also not allow for extra electricity production during the crushing season, because there are no processes that can use the extra exhaust steam from the BPST.

For a sugar mill with a back-end refinery the solar field will unfortunately still not be able to operate outside of the crushing season, because the steam consumption of the refinery is so small compared to the mill, that only one boiler running at its minimum load would be able to supply the necessary steam. The solar live steam could also not be used generate extra electricity since there are no extra processes that can use and condense the extra exhaust steam.

The fact that the solar system is out of use during large parts of the year will lead to low annual efficiencies and a relatively expensive system. An option that would allow the solar system to function outside of the crushing season as well will be discussed in the following section.

5.2 Increasing Electricity Production

The previous section identified that the BPST indirectly stands in the way of extra electricity production and whole year operation of the solar system. Therefore, one option is to replace the BPST with a CEST and a condenser. Figure 35 shows such a configuration, which would from here on be referred to as Configuration 2.

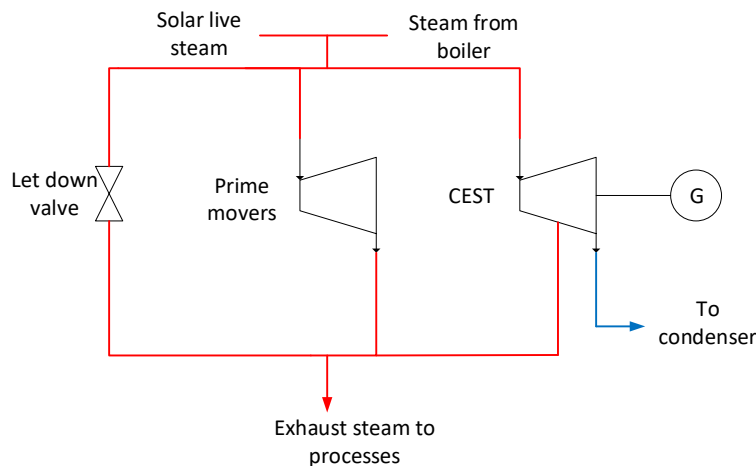


Figure 35: Schematic of Configuration 2

During the crushing season the steam passing through the CEST would be extracted at the right conditions to supply the necessary exhaust steam. This configuration will also eliminate the need for a let-down valve. This is because the

new CEST can be designed to handle additional live steam and therefore additional exhaust steam can be extracted as well. The steam which would have normally been let-down can now go to the CEST, creating extra electricity.

The amount of steam that passes through the new CEST is thus the amount of steam that would have gone through the old BPST plus the steam that would have gone through the let-down valve. Newer CEST technology is more efficient than the old BPST used in South African sugar mills (Ensinas et al., 2007; Foxon, 2017) which will lead to a large increase in electricity generated.

The solar system would ease the boilers load during the crushing season and would now be able to function on its own outside of the crushing season. This is because the CEST would allow for the steam to be exhausted to below atmospheric pressure before it heads to the condenser. This configuration can, therefore, save bagasse or coal during the crushing season and create extra electricity throughout the whole year.

Another option that will allow the solar system to be in use outside of the crushing season is to implement the setup shown in Figure 36, hereon referred to as Configuration 3. In this configuration a CEST is placed in parallel with the existing BPST. This configuration would also need a condenser as well as a new turbo alternator, making it more expensive than the previous configurations. It is a similar configuration to what is used in various international sugar mills (Bhatt, 2014; Burin, et al., 2016).

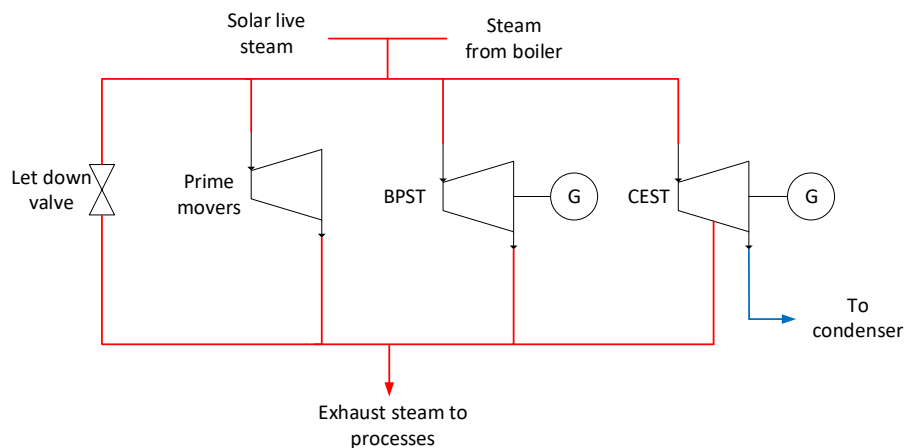


Figure 36: Schematic of Configuration 3

For this configuration all the steam that is produced by the solar system throughout the year can pass through the CEST, generating extra electricity. This configuration would also allow the steam that would normally pass through the let-down valve to go to the CEST, creating even more electricity during the crushing season as is the case with Configuration 2. The BPST and boiler would

just go on to function as they did and the let-down valve could stay in place in case of extra exhaust steam shortages or any other irregularities.

Sugar mills with back-end refineries will also be able to benefit from Configurations 2 and 3. They will function the same way as the normal mills described above during the crushing season. Outside of the crushing season, the refinery part of the mill will still be operating, as mentioned before, one boiler running at its minimum load would be able to supply the necessary steam. Unfortunately the solar system cannot help to ease the boilers load, since it cannot be turned down any further and the sugar mills want to avoid shutting down the boiler and starting it up again on a regular basis. The solar system can, however, provide extra steam to increase the power generation outside of the crushing season for the mill with the refinery as well.

5.3 System Advisor Model Simulation Setup

The System Advisor Model (SAM) (National Renewable Energy Laboratory, 2017) is a simulation program developed for the renewable energy industry. It is used in this study to make performance predictions of the proposed parabolic trough system. SAM's *Process heat parabolic trough* performance model was used to simulate the solar fields, one for a sugar mill without a refinery and one for a mill with a refinery

The *Process heat parabolic trough* performance model is very similar to the more commonly used *CSP parabolic trough (physical)* model which is used for power generation systems. The process heat model, however, does not take the power block into account nor solar thermal storage. The design point is also determined slightly differently with the process heat model, as it has a *System Design* setup. Here the user can define the design point DNI, the target solar multiple, the heat transfer fluid operating temperatures and the thermal power it needs to deliver. This is basically a combination of the usual parabolic trough model's *Solar Field* and *Power Cycle* setups.

SAM calculates the aperture area of the solar field using the information from the *System Design* setup, the loop optical efficiency and total loop conversion efficiency which SAM determines using characteristics of the solar collector. The model does not give the user the option to define the field aperture as with the usual model. For the simulations done for this study, solar noon on the vernal equinox (20 September) was chosen as the design point, resulting in a design point DNI of 790 W/m² being used.

Therminol VP-1 was chosen as heat transfer fluid and it is set to operate with a loop inlet temperature of 290 °C and a loop outlet temperature of 393 °C. There are four solar collector assemblies in each loop of the solar field which will ensure that the heat transfer fluid is heated up to the required maximum temperature.

FE GmbH (formerly Flabeg GmbH) Ultimate Trough collectors along with Schott PTR 70 receivers were used for the simulations. Both the collector and receiver are available in SAM's library, along with their default efficiency values, which is what was used during this study. This is very similar to the solar collector assemblies which were used at Bokpoort CSP near Groblershoop in South Africa (National Renewable Energy Laboratory, 2017).

The main difference being that the Bokpoort CSP collectors are not as wide as the Ultimate Trough collectors. This means that there will be less loops in the simulated solar field compared to when the collectors of Bokpoort CSP would be used, however, the impact in performance should be minimal as the optical efficiencies stay the same. The decision to use the above mentioned collector technology was based on the success Bokpoort CSP has had and the fact that this means that there is an assembly plant operational in South Africa.

Equation 5.1 was used to determine the maximum flow rate of the heat transfer fluid in each loop, to ensure that the solar system does not provide too much thermal energy to the sugar mill. In the equation \dot{m}_{HTF} is the maximum loop flow rate, Q_{PT} is the maximum thermal power the solar field needs to deliver, N_L is the number of loops in the solar field, $c_{p,HTF}$ is the specific heat of the heat transfer fluid and ΔT is the temperature difference of the heat transfer fluid at the inlet and outlet of the solar field.

$$\dot{m}_{HTF} = \frac{Q_{PT}}{N_L c_{p,HTF} \Delta T} \quad (5.1)$$

The row spacing is set to 3 times the width of the collector as suggested by Gunther et al. (2013), this should minimize shading without allowing the solar field to become too large. The solar field was set so that it has a tracking axis in the north-south direction. The length of the piping between the solar field and the process was set to 100 m, quite a large distance, but as it is still uncertain how the solar field would be situated in relation to the mill, it was decided to rather be conservative and give a large value. This is conservative as SAM uses this distance to model heat losses between the solar field and processes, therefore, the longer the distance, the higher the heat loss.

Table 12 shows more of the solar field parameters used for the simulations. The solar field size, actual solar multiple and number of loops are all automatically calculated by SAM.

Table 12: Solar field parameters for the two SAM simulations.

Parameter	Unit	Sugar Mill	Sugar Mill with Refinery
Maximum Solar Heat Production	MW	22.93	30.23
Solar Field Size	m ²	41 280	55 040
Actual Solar Multiple	-	1.08	1.09
Number of Loops	-	6	8
Maximum Flow per Loop	kg/s	15.22	15.05
Row Spacing	m	24	24

5.4 System Advisor Model Simulation Results

Table 13 gives a summary of the simulation results as well as some key performance factors for the solar system. The simulations show that the capacity factors of the two systems are quite low. The capacity factor is the percentage of energy the solar field creates compared to the energy the installation can create if it was to run continuously. In most CSP systems without storage the capacity factors range from 20-25 % (IRENA, 2012). The reason the systems' capacity factors are so low is because of the low annual DNI received, most CSP plants receive almost double the DNI per year.

Table 13: SAM simulation results

System	Energy Generated by Solar Field [MWh/a]	Capacity Factor		Average Solar Field Efficiency [%]
		Crushing Season [%]	Outside of Crushing Season [%]	
Sugar Mill	27 549	13.0	14.8	49.4
Sugar Mill with Refinery	36 525	13.1	14.9	49.1

The solar fields' efficiencies compare well to what was found in literature (Giostri et al., 2012) and incorporates the optical, thermal and piping efficiencies. The effect of the piping length from the solar field to the heat exchanger does not seem to make a major influence, the annual solar gains increases or decreases with less than 1 % if the length is reduced or increased by 100 m.

The solar system designed for the normal sugar mill has higher annual solar field efficiency, but a lower capacity factor compared to the solar system designed for the mill with the refinery. This is due to its lower solar multiple. The solar multiples are not exactly 1 due to the sizes of the collectors, they do not exactly fit the theoretical solar field size, and therefore, the actual solar multiple is a bit more than what is needed.

Figure 37 shows the solar field's annual output for the normal sugar mill simulation. From this image one can clearly see that there are quite a lot of days with very low DNI, resulting in low to almost no thermal power being produced by the system. The low DNI are due to cloudy and rainy days, September – November especially have many of these days due to the rainy season. Despite this, the capacity factor outside of the crushing season is still higher than during the crushing season. This is due to the fact that on the days that the sun actually shines, the system can run at full capacity for almost the entire day.

The system performs worse during the winter months. The lower performance is due to a combination of cosine losses and the incidence angle modifier. The fact that the solar field does not perform very well during the winter does not bode well for Configuration 1, as winter covers most of the crushing season and it is the only time when it will operate.

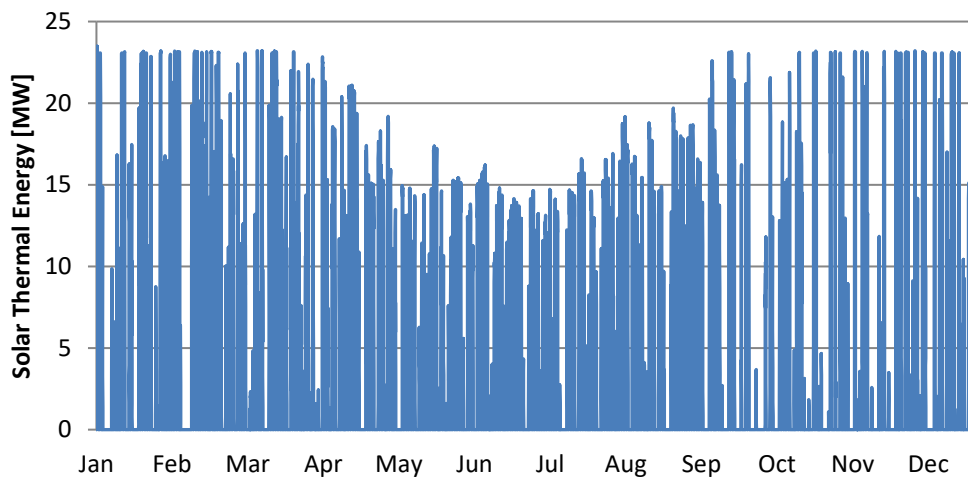


Figure 37: Simulated annual solar field output

In order to counter the negative effects of the cosine losses and incidence angle modifier during the winter months, it was decided to simulate a solar field with an east-west tracking axis. As mentioned in Section 3.1.1, this can reduce the difference in energy yield between the summer and winter months. This tracking option also needs less power to track the sun, as it does not follow the sun on its east-west path each day, but rather its north-south path as it changes throughout the year.

However, the annual energy yield is expected to be lower than for the north-south tracking axis system, because the east-west tracking axis's performance during the day is quite uneven due to large incidence angles close to sunrise and sunset. Appendix E shows the output of the two different tracking systems for specific days of the year to illustrate this.

The simulated results of Figure 38 shows that the system can reach the maximum thermal output during the winter, seemingly performing better than the north-south tracking axis system. However, when looking at Table 14, one can see that the systems perform better during the crushing season, but considerably worse outside of the crushing season. This is because there are so many cloudy and rainy days outside of the crushing season, and unlike the north-south tracking system, the east-west tracking system does not operate at full load for long periods of the day, therefore, it cannot take advantage of the higher solar resource during the summer months as it can only reach its maximum for a short period during solar noon.

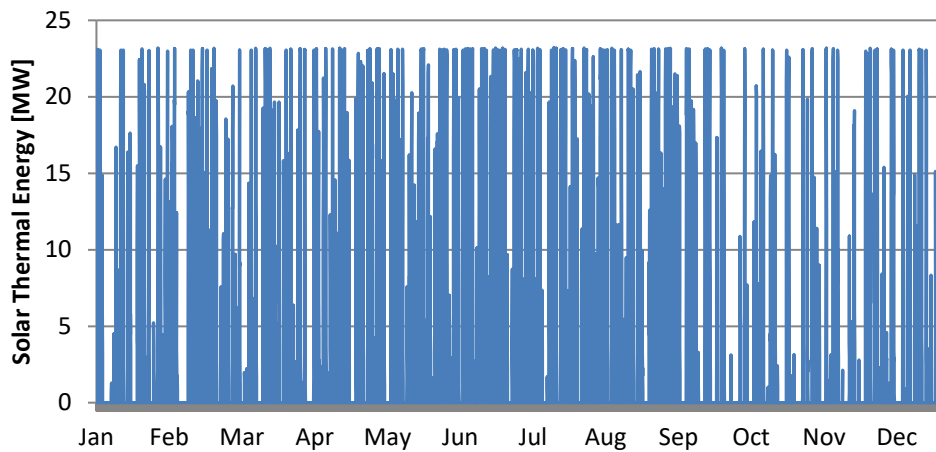


Figure 38: Simulated annual solar field output for an east-west tracking axis system

The thermal output during the crushing season is calculated to be 5.2 % higher for the east-west tracking system compared to the north-south tracking system. If the performance of the whole year is considered, the east-west tracking system produces 7 % less thermal power than the north-south tracking system. It would, therefore, make sense to use the north-south tracking axis system for Configuration 2 and 3, and then use the east-west tracking axis system for Configuration 1.

Table 14: SAM simulation results for an east-west tracking system.

System	Energy Generated by Solar Field [MWh/a]	Capacity Factor		Average Solar Field Efficiency [%]
		Crushing Season [%]	Outside of Crushing Season [%]	
Sugar Mill	25 635	13.7	11.0	46
Sugar Mill with Refinery	33 943.5	13.8	11.1	45.6

5.5 Effect on Sugar Mill

This subsection will discuss the effect the integration point will have on the sugar mill and how each of the different configurations is expected to perform. There is an emphasis on electricity export, as this will give an indication of how the sugar mills can expand their additional income stream.

As mentioned previously, the live steam temperature generated for the sugar mill should not be below 380 °C. Therefore, it was assumed that only solar field outlet temperatures above 385 °C will be able to generate steam of the necessary quality for the mill. This resulted in no steam being generated by the solar field just after sunrise and before sunset, as the solar field could not reach the necessary temperature during these times of the day. The thermal energy created by the solar field just after sunrise can, however, be used to start heating the kettle-type heat exchanger.

Equation 5.2 was used to determine the amount of live steam the solar field can create. Where Q_{PT} is the heat produced by the solar system, h_{ls} is the enthalpy of the live steam and h_{bfw} is the enthalpy of the feed water.

$$\dot{m}_{ls} = \frac{Q_{PT}}{h_{ls} - h_{bfw}} \quad (5.2)$$

If the solar field can only operate during the crushing season, as with Configuration 1, then 21 820.04 ton live steam can be generated for the normal sugar mill and 28 817.4 ton for the mill with the refinery, using the east-west tracking system. For Configuration 1 the solar generated live steam cannot be used to generate extra electricity, only to ease the boiler's load, which will save bagasse or coal. For the generic sugar mill, the ratio of bagasse to live steam is 0.45:1 (Starzak and Davis, 2016). Using this, the amount of bagasse that can possibly be saved was determined, as shown in Table 15. The amount of coal saved is determined by using the 1:4 coal to bagasse ratio as specified by Smith et al. (2016). As in Section 4, this is to better show the added value of the solar system.

Table 15: Impact of solar live steam generation.

Setup	Bagasse savings		Coal savings		Extra electricity generated	
	Normal mill [ton]	Mill with refinery [ton]	Normal mill [ton]	Mill with refinery [ton]	Normal mill [MWh _{el}]	Mill with refinery [MWh _{el}]
Configuration 1	9 838.7	12 993.8	2 459.7	3 248.45	-	-
Configuration 2	8 964.32	12 290.55	2 241.08	3 072.64	2034.6	2 682.3
Configuration 3	-	-	-	-	5 170.8	6 825.2

As mentioned previously, Configuration 2 will allow the solar system to save bagasse and generate extra electricity. The amount of bagasse which can be saved is calculated using the same method as for Configuration 1. Table 15 shows that the amount of bagasse or coal saved is a bit lower than for Configuration 1, this is because the north-south tracking system is used for Configuration 2. Configuration 3 can generate the most electricity, because the solar field is used exclusively for this throughout the whole year, not saving any bagasse.

Table 15 just shows the impact the solar system can make, however, the use of the different configurations also have an impact on the electricity generation. As mentioned before, extra electricity can be generated because of the more efficient CEST, the fact that the let-down steam can now pass through the turbine and the fact that it can function outside of the crushing season. Equation 5.3 was used to determine the amount of electricity (W) produced by the turbines and Table 16 shows the values used for these calculations. This was also used to determine the amount of electricity produced by the solar system as reported in Table 15.

$$W = \eta_{OTE} \times \eta_{el} \times \eta_{is} \times m_{is} (h_{is} - h_{tur,out}) \quad (5.3)$$

Table 16: Values used to determine electricity generation.

Parameter	Symbol	Value	Reference
Overall time efficiency	η_{OTE}	80.83 %	Smith et al. 2016
Electrical efficiency	η_{el}	97 %	Giostri et al. 2012
BPST isentropic efficiency	η_{is}	75 %	Foxon 2017
CEST isentropic efficiency	η_{is}	80 %	Ensinas et al. 2007
CEST steam outlet enthalpy	$h_{tur,out}$	2 332.9 kJ/kg*	Petchers 2012

* The CEST outlet steam temperature and pressure is taken as 40 °C and 7.34 kPa.

Sugar mills usually do not use all of the electricity it produces, exporting the extra electricity. If the exported electricity can be sold to the national grid it can become a major source of additional income as in Brazil (Burin, et al., 2016). Sugar mills use 22 kWh_{el} per ton of cane crushed (Rein, 2007) and the refinery uses 65 – 70 kWh_{el} per ton of raw sugar refined (Foxon, 2017). The SAM simulations show that the two solar systems use 275 MWh_{el} and 361 MWh_{el} throughout the year due to the parasitic loads of the tracking systems and heat transfer pumps. Therefore, to calculate the amount of electricity that can be exported, the electricity usage of the mill and solar field is subtracted from the amount of electricity generated as calculated using Equation 5.3.

Figure 39 shows the possible electricity exports for the various configurations. Configuration 1 exports the same amount of electricity the mill would have, since no extra electricity is generated through this setup. Configuration 2 shows a 257 % increase in electricity export for the normal mill and a 102 % increase for

the mill with the refinery. Configuration 3 shows a 297 % increase in electricity export for a normal mill, while the mill with the refinery shows a 111 % increase.

The normal mill sees a higher increase in electricity exports compared to the mill with the refinery. This is due to the fact that the mill with the refinery was already exporting a bit of electricity outside of the crushing season, due to the refinery which still operates then. Therefore, the extra electricity produced and exported outside of the crushing season due to the CEST and solar field, does not have such a big impact as with the normal mill.

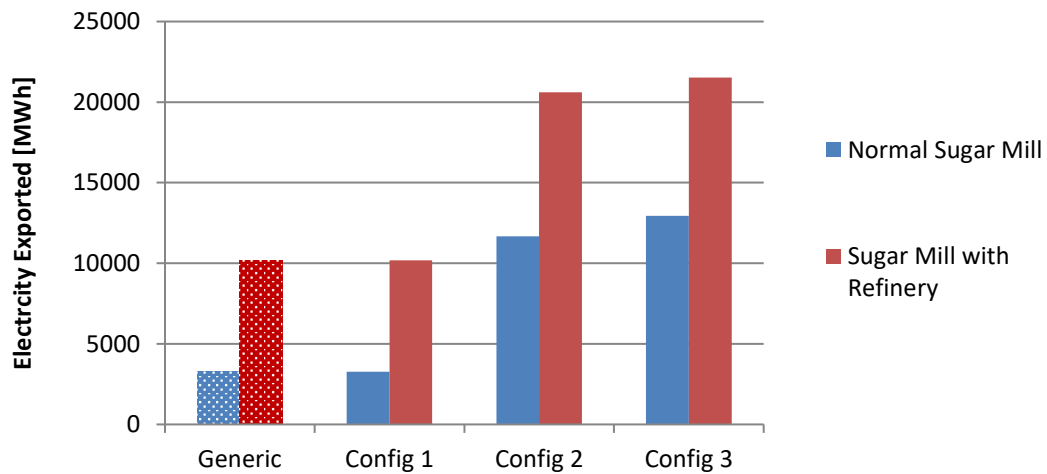


Figure 39: Possible electricity exports.

6 Economic Assessment

This section will discuss various economic factors that need to be considered for solar thermal integration. It will discuss the levelised cost of heat (LCOH) and internal rate of return (IRR) for both integration options and how these indicators can help determine if the integration points are indeed feasible or not. This study uses Euro for the financial calculations because it is a much more stable currency than the South African Rand. This will allow for price comparisons in the future, without worrying too much about the effect of the exchange rate.

6.1 Investment Costs

6.1.1 Specific investment costs of the bagasse drying solar field

In order to obtain reference values for the solar bagasse drying integration point, the plant database for solar heat for industrial processes (AEE Intec, 2017) was assessed. By October 2017 the database lists 253 solar systems, unfortunately only a few of the listings supply any economic information. The Blackdot database (Blackdot Energy, 2017) unfortunately does not give any economic information about the listed projects.

The database lists 20 solar systems using air collectors. For this study only systems larger than 200 m² were considered, because the suggested solar system is quite large and smaller plants tend to be more expensive due to the economics of scale. A larger value was not chosen due to the very limited amount of large scale systems listed on the database. Of the 10 listed air collectors only two give any economic information. The specific investment costs differ considerably with one system costing 73.54 €/m² and the other 291.67 €/m², resulting in an average system cost of 183€/m², but with major deviation.

This large deviation does not seem uncommon, Wang et al. (2015) mentions that solar heating costs can vary considerably due to factors such as weather conditions, system complexity and application. Joubert et al. (2016) also mentions that the solar system costs in South Africa vary considerably due to the factors listed above and a low level of market maturity.

The two systems mentioned above both use flat plate collectors, so to get a better idea of the cost of an evacuated tube air collector, the evacuated tube collector solar systems in the database were also analysed. The database was filtered for systems larger than 1000 m². This could be done, because there are much more registered evacuated tube collector systems than air collector systems in the database. This should also give a better estimate of the specific investment cost, as the smaller systems in the database are much more expensive. Of the 7 systems listed in the database, four of them give economic information. The specific investment cost vary from 129 €/m² to 200 €/m², resulting in an average of

168.78 €/m². It was decided to rather use this value for this study's financial calculations as it seems more representative of the simulated solar system and the fact that the values which have been averaged do not vary as much as with the air collectors.

6.1.2 Specific investment costs of the live steam generation solar field

Kurup and Turchi (2015) set out a report on parabolic trough collector costs, specifically focusing on some of the collectors available in SAM. As mentioned in Section 5.3, FE GmbH Ultimate Trough collectors were used for the simulation, Kurup and Turchi (2015) calculated that the overall installed cost for the collector should be 178 \$/m². This is however, for a collector which would use molten salt as heat transfer fluid, therefore, the collector's receiver would be more expensive than for a collector using thermal oil. The cost of a receiver for oil is 3 \$/m² lower than the receiver for molten salts according to one of the other cost analysis in the report. Therefore, it can be estimated that the installation cost of the collectors for this study is 175 \$/m².

The heat transfer fluid system is estimated to cost 70 \$/m², this is the cost for the oil, piping and hardware costs (Kurup and Turchi, 2015). The site improvements necessary to install the parabolic troughs are estimated to cost 30 \$/m². Therefore, the total specific investment cost for the solar field will be 275 \$/m² or 236.5 €/m².¹

The steam generation system is estimated to cost 4.77 €/kW_{th} (Montes et al., 2009). By multiplying this number with the thermal energy the simulated field in SAM can produce and then dividing the answer by the solar field size, it is possible to represent the steam generation value as 2.65 €/m². Therefore, the total specific investment costs for the parabolic trough system is 239.15 €/m².

6.2 Levelised Cost of Heat

The LCOH is a common measure to assess and compare the costs of renewable energy projects. It represents the average price per unit of thermal energy generated throughout the lifetime of the solar system and it is independent of the value of the energy it replaces. The LCOH compares the project's annual costs over its financial life time to the annual yield.

Equation 6.1 (Hess et al., 2016) shows how the LCOH can be calculated. The annual costs (C_n) include the capital investment costs as well as the operation and maintenance costs. The annual yield (Q_n) refers to the amount of thermal energy produced by the solar system each year (n).

¹The Dollar to Euro exchange rate was taken on 1 November 2017 as \$ 1 to € 0.86.

$$LCOH = \frac{\sum_{n=0}^N \frac{C_n}{(1+d)^n}}{\sum_{n=0}^N \frac{Q_n}{(1+d)^n}} \quad (6.1)$$

The project's financial life span (N) was taken as 20 years, even though the solar systems can well exceed this. The nominal discount rate (d) was taken as 10 % for this study as suggested by Beukes et al. (2015) and Hess et al. (2016). This value is based on the expected weighted average cost of capital of the South African sugar industry, for 30 % equity and 70 % debt. The equity has an expected return of 14 % and the debt an interest rate of 8 % with a loan period of 10 years.

For the evacuated tube collector system it was assumed that the annual maintenance costs will be 1 % of the capital expenditure and the annual operational cost will be 2 % of the yearly energy yield (Verein Detuscher Ingenieure, 2004). For the parabolic trough system the annual maintenance and auxiliary energy costs were assumed at 2 % of the capital costs, as is common for CSP systems (Hernandez Moro and Martinez-Duart, 2012). These costs are set to go up by 6 % per annum along with the consumer price index of South Africa, for both of the systems. The auxiliary electricity tariff imported from the grid is assumed to be constant at a price of 0.5 ZAR/kWh_{el} (3.05 Euro-ct/kW_{el})² (Hess et al. 2016).

The financial calculations in this study only take the cost of the solar systems into account, and not the cost of the drying system or the cost of CEST's for Configuration 2 and 3. This study assumes that the sugar mills are planning to implement the suggested systems or configurations in anyway, as it will benefit the sugar mills. The solar system is only seen as an alternative to using bagasse or coal.

Hess et al. (2016) calculated the LCOH of coal for the STEP-Bio project. It was assumed that an existing boiler can burn the necessary amount of South African coal without having to undergo any alterations or additional costs. Thus, only the cost of the coal is compared to the cost of the solar system. It was calculated that coal has a LCOH of 4.03 Euro-ct/kWh, taking into account that the current value of coal is 1.2 Euro-ct/kWh and will increase with 12.3 % per year. This increase is based on the coal prices paid by sugar mills after delivery (Hess et al., 2016).

Table 17 shows the calculated LCOH values for the two integration options. The LCOH of the integration points are significantly lower if they can run throughout the whole year, as shown in the *Annual* column. This is simply due to the fact that by operating the whole year, the system can produce more energy, while the capital investment stays the same. The LCOH of the mill with the refinery is also slightly higher than the normal mill. This is because of its marginally higher solar multiple and subsequent lower system efficiency.

²The Rand to Euro exchange rate was taken on 1 November 2017 as R 1 to € 0.061

Table 17: LCOH of the solar thermal integration options.

Integration point	Size of solar field [m ²]	Capital Investment [Euro]	LCOH [Euro-ct/kWh]	
			Crushing season	Annual
Solar bagasse drying	22 425	3 784 902	6.77	4.18
Live Steam for normal mill	41 280	9 872 112	8.05	5.17
Live steam for mill with refinery	55 040	13 162 816	8.12	5.22

Despite the annual LCOH values being quite low, they are still higher than the LCOH of coal, meaning that coal would be a cheaper option to produce the thermal heat for the processes. However, if the specific investment costs of the solar systems can be reduced, the LCOH values would be very competitive. As mentioned in Section 6.1.1, the cheapest air collector system cost 73.54 €/m², if this value is used in the calculations, the LCOH for the evacuated tube solar field would be 1.87 Euro-ct/kWh. Even if the system only functions during the crushing season, the LCOH would be lower than that of coal, at 3.0 Euro-ct/kWh.

The International Renewable Energy Agency (2016) predicts that the cost of parabolic trough solar fields will decrease by 23 % by 2025. Therefore the specific investment cost would be 184 €/m², resulting in an LCOH of 3.98 Euro-ct/kWh for the normal mill and 4.02 Euro-ct/kWh for the mill with the refinery if they were to operate throughout the whole year. Unfortunately, a parabolic trough system only operating during the crushing season would still not reach a LCOH close to that of coal.

The proposed carbon tax in South Africa can also have a large influence in the feasibility of using coal as boiler fuel. A maximum of R 120 per ton of CO₂ emitted will have to be payed as carbon tax (Deloitte, 2015); if this is incorporated into the LCOH calculations of coal, the value would increase to 5.12 Euro-ct/kWh. Solar thermal integration is much more competitive if this is taken into account, especially considering the potential future cost reductions of solar thermal collector technology.

The levelised cost of electricity (LCOE) for the live steam generation integration point can be calculated in a very similar manner to the LCOH calculations. Instead of using the annual thermal energy yield, the annual electricity yield is used. By implementing the annual electricity yield in Equation 6.1, it was calculated the LCOE for the normal mill would be 25.7 Euro-ct/kWh and 25.9 Euro-ct/kWh for the mill with the refinery. This figure compares relatively well with the findings of Burin et al. (2016), who calculated that the LCOE of solar thermal integration into a Brazilian sugar mill would be 22 Euro-ct/kWh. It is, however, important, to take into account that the annual DNI is higher at the location considered by Burin et al. (2016) and the central receiver system

simulated by the study is considered to cost less than the parabolic trough system simulated for this study.

6.3 Internal Rate of Return

The IRR estimates the discount rate (d) that would have a zero net present value (NPV) as a result. Unlike the LCOH, the IRR takes the value of the fuel the solar system replaces into account. The IRR of each integration point was determined using Equation 6.2 (Hess et al., 2016), to see if it exceeds the sugar milling industry's hurdle rate of 10 - 15 % for projects or investments.

$$NPV = \sum_{n=0}^N \frac{C_n}{(1+d)^n} \quad (6.2)$$

The value of the coal used by South African sugar mills is taken as R 1 100 per ton (Hess et al., 2016). In order to calculate the value of the thermal energy produced by the solar systems, Equation 6.3 was used. The amount of coal saved and thermal energy delivered to the systems are shown in Table 18 along with the calculated value of the solar thermal energy and the IRR.

$$\text{Value of solar thermal energy} = \frac{\text{Total value of coal displaced}}{\text{Total thermal energy delivered}} \quad (6.3)$$

Table 18: IRR for the integration options.

Integration	Energy delivered [kWh _{th}]	Coal displaced [ton]	Value [Euro-ct/kWh]	IRR [%]	
				CS	A
Bagasse Drying	6 833 160	1 020.38	1.00	-0.4	4.2
Live steam for normal mill	15 602 360	2 459.7	1.06	-3.9	2.0
Live steam for mill with refinery	20 651 280	3 248.45	1.06	-4.0	1.9

From Table 18 it is possible to see that it is imperative that the solar systems run throughout the whole year, as this makes a considerable difference in the financial feasibility of the systems. However, the annual figures are still not high enough for the sugar industry to consider investment, as it falls well below their hurdle rate.

The solar bagasse drying rate can reach an IRR of 12.9 % if the specific investment cost is set to the minimum of 73.54 €/m² and it operates throughout the whole year. Rotary dryers are quite robust and can be used to dry various types of materials, this is one of the reasons it was chosen. The drying system can therefore be used to dry other biomass, like wood chips for example, which is sometimes used as an auxiliary boiler fuel in sugar mills. The chips can be dried outside of the crushing season and then stored until it is needed.

Unfortunately the solar live steam generation integration systems still cannot reach the required IRR even when the potential future cost reductions are taken into account. For this integration option a financial help or subsidies of at least 35 % of the capital cost is needed to reach an IRR above 10 %.

The proposed carbon tax can increase the IRR's of the integration options, because the coal it replaces is more expensive. However, it does not make a big enough difference for any of the integration points to reach the industry's hurdle rate. For the solar bagasse drying integration point, the IRR can increase with 2.4 percentage points and the solar live steam integration points can both increase with 2.6 percentage points.

The electricity generated by the solar energy in the sugar mills can be exported to the national grid under South Africa's Renewable Energy Independent Power Producer Procurement Program (REIPPPP), creating a new income stream for the sugar mills. To reach an IRR of 15 % the sugar mills would have to receive a feed-in tariff of 36 Euro-ct/kWh. This is a very high tariff and would most probably not be accepted by REIPPPP. If the cost reduction measures are taken into account the feed-in tariff can be lowered to 17.5 Euro-ct/kWh, but this would still be almost double compared to what South African CSP plants received for the previous bidding round, Window 3 (Eberhard et al. 2014).

The necessary feed-in tariff is quite high due to two main factors. One is the low annual DNI of Durban. As mentioned before, the annual sum of DNI at Durban is 1350 kWh/m², while for normal CSP plants it is significantly higher. Upington, the centre of South Africa's CSP developments, receives almost 3000 kWh/m² of DNI per year (GeoSUN, 2013), making CSP power plants very feasible there. The other reason for the high feed-in tariff is the relatively low thermal to electricity ratio of the sugar mill's power block, despite considering the CEST. The ratio of the thermal energy delivered to the sugar mill and the possible electricity it can generate was calculated to be 20 %. In commercial CSP plants the power block efficiency can be expected to be above 35 % (Montes et al., 2009).

7 Conclusion

The conclusion gives a short summary of the results and highlights the best integration option in terms of results and economic feasibility. It will also mention assumptions that were made which influenced the outcome of the study. The implications of the findings in this study on the sugar milling industry are discussed and finally recommendations for further work are given.

7.1 Summary of Findings

This study looked at the potential integration of solar thermal energy into South African sugar mills. The two options researched for this integration is solar live steam generation and solar bagasse drying. Both of the integration points were developed further from previous STEP-Bio studies done by Beukes et al. (2015) and Hess et al. (2016). Detailed simulations of the solar fields were created in order to determine the impact they could make on a generic sugar mill. The simulation results were also used to complete an economic assessment to determine the financial feasibility of the two integration points.

The simulations show that the solar systems can make a relatively sizeable impact despite the sugar mill's energy consumption significantly surpassing their capabilities. However, the simulation results did point out a few concerns. For the bagasse drying integration point, the relatively low efficiency of the air collectors hampered the solar system's performance and for the live steam generation point the low annual DNI of Durban greatly limits the performance of the solar system.

The bagasse drying system would allow the mill to reduce its bagasse usage by 5 %. By integrating the solar thermal energy system the decrease in bagasse usage can be lowered to 7.05 %, making a significant contribution compared to when only exhaust steam is used. The solar live steam generation integration point will allow for bagasse/coal saving and extra electricity generation. Configuration 1 can save the most coal, 2 459.7 ton for a normal mill and 3 248.4 ton for a mill with a refinery. Configuration 3 can generate the most electricity and would enable to increase the electricity exported by 297 % for a normal mill and by 111 % for a mill with a refinery. It is, however, Configuration 2 that can make the largest impact, as it can save almost as much coal and produce as much electricity as Configuration 1 and 3, respectively.

The economic assessment shows that under current conditions the bagasse drying integration point offers the lowest LCOH and highest IRR. However, even for this integration point, the solar system would still be more expensive than using coal as fuel to produce thermal energy. The IRR is also lower than the hurdle rate set by the sugar milling industry. The economic assessment underlines the importance of the solar systems operating throughout the whole year, showing

that there would be no return on investment if the systems were only to operate during the crushing season.

There is some uncertainty regarding the economic calculations due to varying reported investment costs, potential reductions in parabolic trough collector costs and the increase of coal costs due to planned carbon taxation in South Africa. If the carbon tax is taken into account the solar systems would be very competitive, as the LCOH of coal would be quite close to that of the solar systems'. If the lowest prices for solar integration are taken into account the LCOH of both integration options will be significantly lower than that of coal. However, despite the low LCOH values that can be reached, the IRR values still stay relatively low compared to the hurdle rate set by the sugar industry. Only the bagasse drying integration point will be able to achieve an IRR higher than 10 % if the lower investment costs are taken into account.

If the sugar mills can export the extra electricity that can be generated to the national grid, a feed-in tariff of 36 Euro-ct/kWh is needed to achieve an IRR of 15 %. This is an extremely high price if it is compared to what current CSP power projects receive as feed-in tariff. If the reduced collector prices are considered the tariff can be lowered to 17.5 Euro-ct/kWh, which is close to what CSP plants received in the REIPPPP bidding Window 1, but almost double what they received in bidding Window 3. The high needed feed-in tariffs can be attributed to the low annual DNI of Durban and the low thermal to electricity efficiency of the sugar mills compared to commercial power plants.

7.2 Concluding Remarks

Solar thermal integration into South African sugar mills is technically possible, allowing the mills to save bagasse/coal and generate extra electricity. It is, however, not yet financially feasible, with coal being able to provide thermal energy at a lower cost.

The economic assessment shows that the solar bagasse drying integration point would be the best option to pursue due to its lower LCOH and higher IRR. It would also require less capital investment due to a smaller solar field being needed. The evacuated tube collectors are also better suited for Durban's solar resource as it uses GTI, which is higher than the DNI in Durban. The collectors also require less maintenance and are considerably less complicated to operate compared to parabolic trough collectors.

The success of the solar live steam generation point will depend on the feed-in tariff that can be negotiated between the sugar milling industry and Eskom. The chances of the needed feed-in tariff being paid seems to be rather slim due to how high it is in comparison with the latest CSP power plants and Eskom's reluctance to sign IPP agreements.

The future of the solar thermal integration, however, looks bright as collector costs are set to decrease and the price of using coal increases due to carbon taxation. If both of these factors come into play solar integration can become very feasible and should always be considered as a potential thermal energy source.

7.3 Recommendations for Further Work

This study was based on the generic sugar mill described in the BRTEM model. In order to fully realise the potential impact solar thermal integration can make, an actual sugar mill will have to be analysed. Some of the existing sugar mills are located in areas with a higher solar resource and may be better suited for solar thermal integration due to alternative boiler house configurations which can allow for a higher boiler turn down ratio.

Some mills have lower steam parameters, which opens the door for thermal storage systems. A new silicon based heat transfer fluid, developed by HELISOL®, has recently been introduced and can operate at temperatures up to 425 °C (Zoschke et al., 2017). This will also allow the integration system to incorporate solar thermal storage. Therefore, the impact a small – medium sized thermal storage system can make should also be researched. It would help the solar system deal with transient conditions and allow the solar system to provide thermal energy after dark. This can make up for the days with very low to no DNI when the solar system cannot produce any useful thermal energy.

To reach lower LCOH's and IRR's for the solar live steam generation integration point alternative collector technologies must be researched. Linear Fresnel systems and direct steam generation offer the lowest investment cost and according to Peterseim (2014) is the best option for hybridisation and cogeneration. However, the uncertainty of this technology's performance will also have to be taken into account and how potential financiers would react to it.

In order to get a more accurate value of the thermal requirements of the bagasse drying system further research will have to be done on the drying kinetics of bagasse in a rotary dryer. A more detailed drying simulation will have to be done which takes all the aspects of a rotary dryer into consideration, like the speed of rotation, number of flights and tilt of the dryer. This will give a clearer picture of how effective a rotary dryer will be in drying bagasse and if exhaust steam and solar thermal energy can indeed deliver the needed thermal energy. Furthermore, the precise effect of the dry bagasse on the boiler efficiency will have to be calculated using boiler design calculations. This will allow for more accurate estimations on the effect of bagasse drying on the sugar mill.

Appendix A: Airwasol Brochure



easy + safe + efficient
vacuum tubes - solar air collector TSTair

Technical specifications



TSTair - S + M + L

TSTair - Versions

- Header sizes: **S, M und L**
- TST - tube lengths 50 cm, 100 cm, 150 cm, 175 cm und **200 cm (Standard)**
- TST - header lengths:
 - Length = 58 cm with 5 TST-tubes
 - Length = 115 cm with 10 TST-tubes
 - Length = 150 cm with 13 TST-tubes
 - **Length = 195 cm with 17 TST-tubes (Standard)**

TSTair - Dimension of S, M and L

		Header length in cm									
		100	200	300	400	500	600	700	800	900	1000
TST 200 -row	1	S	S	S	M	M	M	L	L	L	L
	2	S	S	M	M	M	M	L	L	L	L
	3	S	M	M	M	L	L	L	L	L	L
	4	M	M	M	L	L	L	L	L	L	L
	5	M	M	L	L	L	L	L	L	L	L

S	Vp = 80 - 300 m ³ /h
M	Vp = 300 - 950 m ³ /h
L	Vp = 750 - 4000 m ³ /h



TSTair-M - Technical specifications



	TSTair-M	Units
Collector type	Solar air collector	
Header height	200	mm
Header width incl. mounting groove	270	mm
Header length	580 - 1955	mm
Specific volume flow (A_a)	55	m ³ /(h*m ²)
Heat transfer medium	only ambient air	
Material Header	Aluminium	
Material glass tube	Borosilicate 3.3	mm
Outer diameter glass tube	90	mm
Material thickness glass tube	2.5	mm
Material absorber tube	Stainless steel	mm
Outer diameter absorber tube	50.5	mm
Material thickness absorber tube	0.2	mm
Solar absorptance (AM 1.5)	95 ±2	%
Thermal emittance (100 °C)	5 ±2	%
Stagnation temperature	210	°C

TSTair M header length 195 cm x tubes in row TST-200 cm

	Units	1x1	1x2	1x3	1x4	1x5
TST-200 tubes	Pcs	17	34	51	68	85
Total area A_G	m ²	4.99	9.10	13.22	17.34	21.45
Apertur area A_a	m ²	2.74	5.48	8.22	10.96	13.70
Weight	kg	106	189	274	357	441
Length collector field	cm	265	476	686	897	1107

Appendix B: Matlab Model Calculations

The following polynomial equations from Kröger 1998) were used to determine certain thermo-physical properties of air, which was needed to calculate the heat transfer characteristics in the evacuated tube. Note that all the temperatures should be entered in Kelvin.

Kinematic viscosity:

$$\nu = \frac{(2.287973 \times 10^{-6}) + (6.259793T_f \times 10^{-8}) - (3.131956T_f^2 \times 10^{-11}) + (8.15038T_f^3 \times 10^{-15})}{P/(287.08T_f)} \quad (\text{A.1})$$

Where T_f is the film temperature around the glass tube and is seen as the average between the ambient air temperature and the glass temperature. For the thermal conductivity of the film the following equation was used:

$$k = (-4.937787 \times 10^{-4}) + (1.018087T_f \times 10^{-4}) - (4.627937T_f^2 \times 10^{-8}) + (1.250603T_f^3 \times 10^{-11}) \quad (\text{A.2})$$

To determine the thermal conductivity and kinematic viscosity of the air inside the absorber tube, T_f must be replaced with bulk temperature of the air (T_b) inside the absorber tube. The bulk temperature as also used to determine the specific heat capacity of the air inside the absorber tube.

$$c_p = (1.9327T_b^4 \times 10^{-10}) - (7.9999T_b^3 \times 10^{-7}) + (1.1407T_b^2 \times 10^{-3}) - (4.4890T_b \times 10^{-1}) + (1.0575 \times 10^3) \quad (\text{A.3})$$

Equation 4.9 was derived from Cengel&Ghajar (2015) which gives a formula for the radiation heat transfer between two concentric cylinders. The formula from Cengel and Ghajar (2015) is:

$$Q_{ag} = \frac{A_a \sigma (T_a^4 - T_g^4)}{\frac{1}{\varepsilon_a} + \frac{1 - \varepsilon_g}{\varepsilon_g} \left(\frac{r_a}{r_g}\right)} \quad (\text{A.4})$$

For the Matlab model, the above equation needs to be written in the following form:

$$Q_{ag} = \frac{(T_a - T_g)}{R_{ag}} \quad (\text{A.5})$$

Therefore, the thermal radiation resistance (R_{ag}) can be written as:

$$R_{ag} = \frac{\frac{1}{\varepsilon_a} + \frac{1 - \varepsilon_g}{\varepsilon_g} \left(\frac{r_a}{r_g}\right)}{\sigma A_a (T_a^2 + T_g^2)(T_a + T_g)} \quad (\text{A.6})$$

To calculate the glass temperature (Equation 4.10) the following energy balance was set up:

$$Q_{rad,a} + Q_{ag} - Q_{conv} - Q_{radsky} = 0 \quad (A.7)$$

This can be rewritten as:

$$Q_{rad,a} + \frac{T_a - T_g}{R_{ag}} - \frac{T_g - T_\infty}{R_{g\infty}} - \frac{T_g - T_{sky}}{R_{gsky}} = 0 \quad (A.8)$$

Now all that needs to be done to find Equation 4.10 is to isolate the T_g on the right hand side of the equation:

$$T_g = \frac{Q_{rad,a} + \frac{T_a}{R_{ag}} + \frac{T_\infty}{R_{g\infty}} + \frac{T_{sky}}{R_{gsky}}}{\frac{1}{R_{ag}} + \frac{1}{R_{g\infty}} + \frac{1}{R_{gsky}}} \quad (A.9)$$

In the equations above $Q_{rad,a}$ represents the radiation from the sun which the glass absorbs. This can be determined using Equation A.10:

$$Q_{rad,a} = I_s(1 - \tau - \rho_g) \left(\frac{A_g}{2} \right) \quad (A.10)$$

Here τ and ρ_g represent the transmissivity and reflectivity of the glass. The reflectivity was taken as 5 %, while looking at Figure 40, it was decided to be conservative and assume that the glass only lets wave lengths between 0.3 – 2.8 μm through and for this waveband the transmissivity was taken as 92 %. Borofloat 33 is a Borosilicate glass, very similar to what was used for the Airwasol collector.

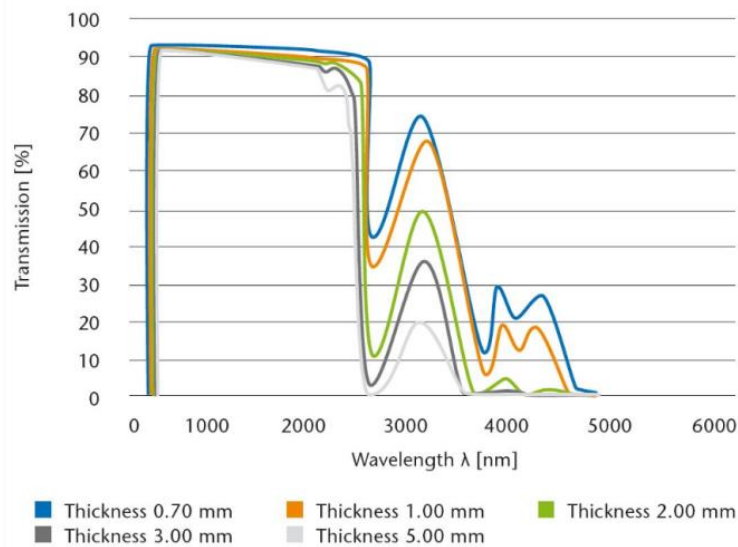


Figure 40: The transmissivity of Borofloat 33 over various wavelengths (Schott, 2017).

The following calculations show how much of the solar energy the glass actually transmits, it was determined using values from Schott (2017) and as set out by Kalogirou (2009). Firstly, the energy that is emitted from the sun for each of the specified wavelengths is calculated and then presented as a fraction of the total emissive power from the sun. Kalogirou (2009), conveniently set up a table where this fraction is specified as a function of the blackbody's temperature (in this case the sun at 5760 K) and the specified wavelengths.

$$\lambda_1 T = 0.3 \times 5760 = 1728 \mu mK$$

$$\lambda_2 T = 2.8 \times 5760 = 16128 \mu mK$$

The following values were read from the table specified above:

$$\frac{E_b(0 \rightarrow \lambda_1 T)}{\sigma T^4} = 3.166 \%$$

$$\frac{E_b(0 \rightarrow \lambda_2 T)}{\sigma T^4} = 97.43 \%$$

Therefore, the fraction of solar energy that can be transmitted in the specified wavelengths is:

$$\frac{E_b(\lambda_1 \rightarrow \lambda_2 T)}{\sigma T^4} = 97.43 - 3.166 = 94.264 \%$$

Now the percent of solar radiation transmitted through the glass can be determined:

$$\tau = 0.92 \times 0.94264 = 86.72 \%$$

The irradiance that finally passes through the glass is then used to heat up the absorber. The following energy balance was set up to eventually derive a method of calculating the absorber temperature (Equation 4.13):

$$Q_{rad} - Q_{ag} - Q_{conv,air} = 0 \quad (A.11)$$

This can then be rewritten as:

$$Q_{rad} - \frac{T_a - T_g}{R_{ag}} - \frac{T_a - T_{air}}{R_{air}} = 0 \quad (A.12)$$

T_a now needs to be isolated on the right hand side of the equation in order to end up with the same equation as Equation 4.13.

$$T_a = \frac{Q_{rad} + \frac{T_g}{R_{ag}} + \frac{T_{air}}{R_{air}}}{\frac{1}{R_{ag}} + \frac{1}{R_{air}}} \quad (\text{A.13})$$

In Equation A.12, Q_{rad} represents the irradiance that falls on the absorber. This can be determined by taking the absorber area exposed to the sun into account along with its absorptance and the irradiance that comes through the glass tube, as can be seen Equation A.14.

$$Q_{rad} = \alpha I_s \left(\frac{A_a}{2} \right) \quad (\text{A.14})$$

The temperature of the air leaving the 1 cm absorber segment under consideration can now finally be determined. Equation 14 was derived from the following energy balance:

$$\dot{m} c_p (T_{air,i+1} - T_{air,i}) = \frac{T_a - T_{air}}{R_{air}} \quad (\text{A.15})$$

This can then be simplified to Equation 14:

$$T_{air,i+1} = T_{air,i} + \frac{T_a - T_{air}}{R_{air} \dot{m} c_{p,air}} \quad (\text{A.16})$$

Appendix C: Matlab Model Comparison

Unfortunately Paradis et al. (2015) et al does not give any results regarding the incremental temperature rise over the tube length during their experiment. They focus on the outlet temperatures of the collector tube and if they can model it correctly as the irradiation, ambient temperature and flow rate changes. They validate their model using the experimental results shown in the thesis.

Their model shows that the flow rate through the collector tube has the largest influence on the outlet air temperature. To show the similarity between their model and the model used for this study, the influence of the flow rate on the outlet air temperature and the collector efficiency is shown for both models in Figure 41 - 44:

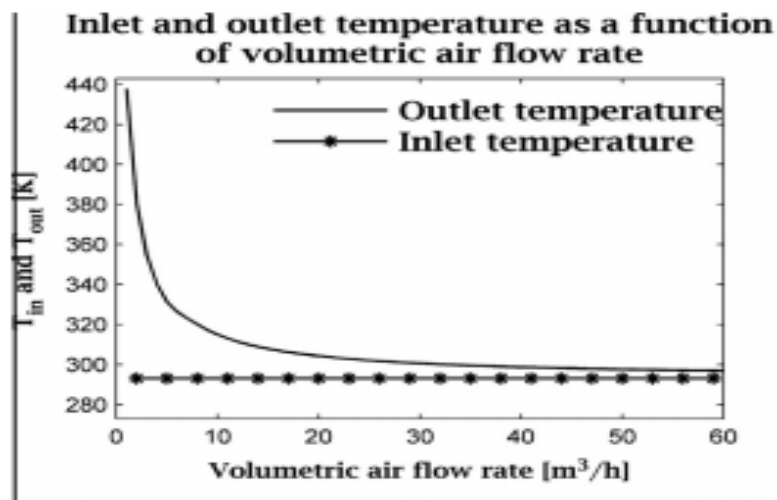


Figure 41: Change in collector outlet temperature as flow rate changes as predicted by model of Paradis et al. (2015)

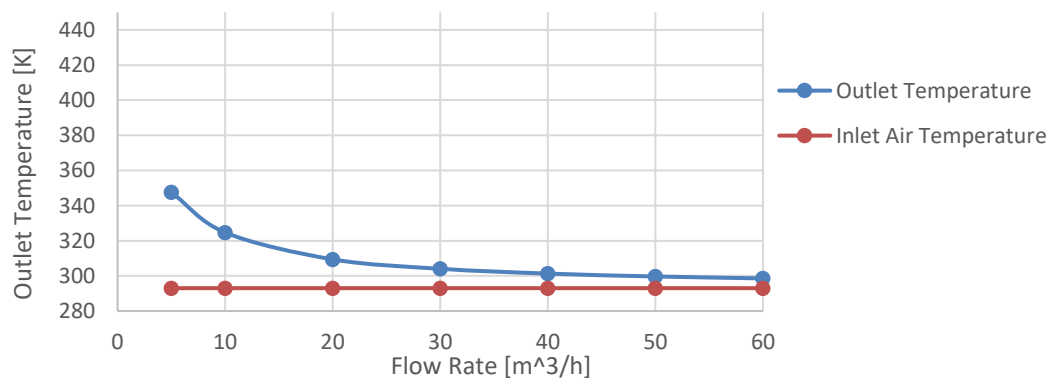


Figure 42: Change in collector outlet temperature as flow rate changes as predicted by model used in thesis.

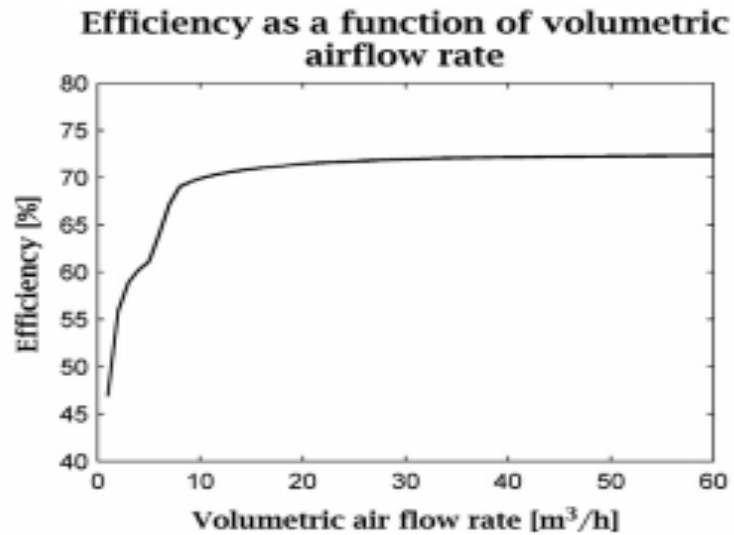


Figure 43: Change in collector efficiency as flow rate changes as predicted by model of Paradis et al. (2015)

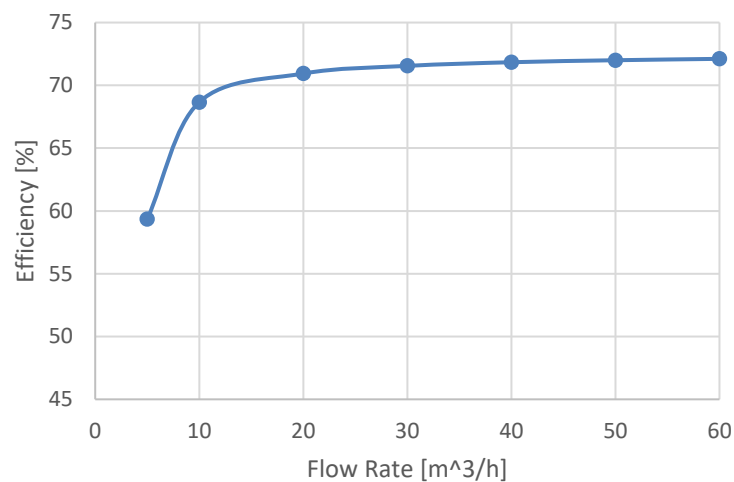


Figure 44: Change in collector efficiency as flow rate changes as predicted by model used in thesis.

The reason the results for the model used in this study does not go below a flow rate of 5 m³/h, is because below this flow rate the Reynold's number is not high enough so that Gnielinski's equation can be used accurately. The comparison of the graphs show that the models' results are very similar and that the heat transfer modelling was, therefore, done correctly.

Appendix D: Aircow Optimisation

Aircow has an optimisation function which determines the optimum air flow through the collector rows in the solar field. The program determines this by considering the system set out in Figure 45.

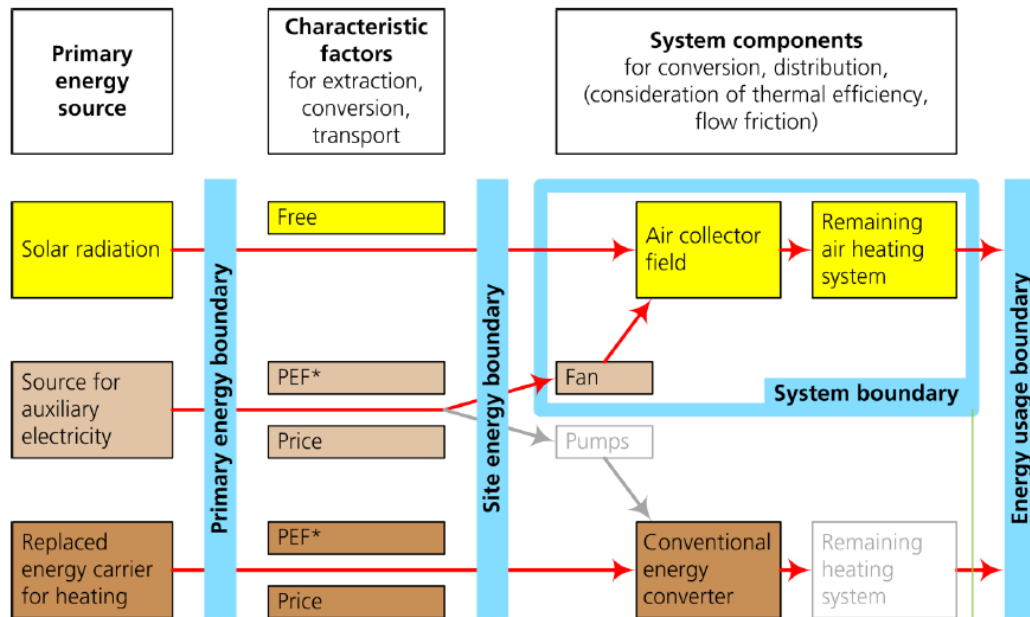


Figure 45: Aircow's Global system considered for mass flow optimisation as shown in the Aircow manual (Fraunhofer ISE, 2017).

The program has four different mass flow optimisation options. The first option is the optimisation of the mass flow for net primary energy savings. The second option is to optimise the mass flow to maximise net monetary savings, which is determined using the value of the auxiliary electricity and the heating medium replaced. The third option is to optimise the flow for maximum net site power savings, while the fourth option maximises the net system power savings. Equations B.1 – B.4 show how the power savings and cost savings were determined for the various options.

$$\text{Option 1: } P_{\text{saved per}} = \dot{Q}_{\text{field}} \left(\frac{f_{p \text{ replaced energy carrier}}}{A_{\text{field}} \times \eta_{\text{system replaced}}} \right) - P_{\text{fan}} \left(\frac{f_{p \text{ auxiliary electricity}}}{A_{\text{field}}} \right)$$

(B.1)

$$\text{Option 2: } \underset{\text{field area}}{\text{Costs}_{\text{saved per}}} = \dot{Q}_{\text{field}} \left(\frac{\text{costs}_{\text{replaced}}}{\text{energy carrier}} \right) - P_{\text{fan}} \left(\frac{\text{cost}_{\text{auxiliary}}}{\text{electricity}} \right) \quad (\text{B.2})$$

$$\text{Option 3: } \underset{\text{field area}}{P_{\text{saved site}}}_{\text{power per}} = \dot{Q}_{\text{field}} \left(\frac{1}{A_{\text{field}} \times \eta_{\text{system replaced}}} \right) - P_{\text{fan}} \left(\frac{1}{A_{\text{field}}} \right) \quad (\text{B.3})$$

$$\text{Option 4: } \underset{\text{field area}}{P_{\text{saved system}}}_{\text{power per}} = \dot{Q}_{\text{field}} \left(\frac{1}{A_{\text{field}}} \right) - P_{\text{fan}} \left(\frac{1}{A_{\text{field}}} \right) \quad (\text{B.4})$$

After the amount of power or cost saved is calculated, Aircow uses an algorithm which considers three different mass flows to determine the maximum of a quadratic curve fitted to the power or cost function. The range of mass flows will be reduced step by step and it will start to focus on the predicted maximum until a high enough precision is reached.

Now that the optimal mass flow rate is known, the amount of collectors in a row can be determined. Aircow can use the efficiency map it created to determine the temperature increase per collector. This is then used along with the user defined solar field exit temperature to determine how much collectors in a row is necessary to gain the necessary temperature lift. The answer Aircow gives almost always has a decimal in it, the problem is that in reality there is no such thing as a fraction of a collector, only an integer amount of collectors can be used.

Therefore, the decimal needs to be rounded up to the nearest integer and the amount of rows in the system needs to be adjusted so that the thermal power at the field outlet is more or less the same or the necessary mass flow rate through the total system is reached. Figure 46 gives a visual representation of this process. The system calculations now need to be repeated with the newly specified collector rows and optimised mass flow rate in order to determine how the “real” system would perform. The amount of collectors calculated initially can also be rounded down, the system performance of the two different collector rows should then be compared to one another as in Figure 46.

To determine the price of the energy replaced the following calculations were made, taking into account that the replaced heating medium is exhaust steam:

$$1 \text{ kWh} = 3600 \text{ kJ}$$

To calculate the amount of steam, the power is divided by the enthalpy difference of the exhaust steam and the condensate that forms after it heats the air.

$$m = \frac{3600}{2707.95 - 504.68} = 1.63 \text{ kg}$$

The ratio between exhaust steam and live steam is 1.2:1. While the ratio between live steam and bagasse is 1:0.45, then lastly the ratio for bagasse to coal is 1:0.25 (Starzak and Zizhou, 2015).

$$1.63 \text{ kg exhaust steam} = 1.36 \text{ kg live steam}$$

$$1.36 \text{ kg live steam} = 0.614 \text{ kg bagasse}$$

$$0.614 \text{ kg bagasse} = 0.153 \text{ kg coal}$$

One ton of coal costs R 1 100 (Hess et al., 2016), therefore:

$$0.153 \text{ kg coal} = R 0.1688 \text{ or } 16.88 \text{ c}$$

Therefore, for each kWh of heat replaced by the solar system, 16.88 c of coal is saved.

	A	B	C	D	E	F
35	Field					
36	Tilt angle (horizontal collector surface = 0°, vertical = 90°, β_{coll})	°		45	45	45
37	Azimuth angle (east = -90°, south = 0°, west = 90°)	γ_{coll}	°	0	0	0
38	Temperature rise	ΔT_{rise}	K	27.0		
39	Field length (number of air collectors per row)	$n_{coll/row}$	coll		5.0	4.0
40	Power (at field outlet or at load)	Q_e	W	14000.0		
41	Field width (number of rows of field)	n_{row}	coll		2.0	3.0
42	Inlet fluid temperature of field	ϑ_i	°C	20.0	20.0	20.0
43	Mean fluid temperature of field	ϑ_m	°C			
44						
45	Air heating system					
58	Global system for mass flow optimization					
66	Mass flow					
67	Manually set outlet mass flow per row (enter or delete)	$\dot{m}_{e,row}$	kg/h		747.2	747.2
68	Autom. optimized outlet mass flow p. row (do not enter)	MMP	kg/h	747.2		
69						
70	Calculation support					
72						
73	Error check					
74						
75	Details					
105	Summary					

106	Summary of error notices			No errors found	No errors found	No errors found
107						
178	Do not insert, delete, or move rows above this row!					
179	Results for system design					
180						
181	Field dimensions					
182	Field length	$n_{coll/row}$	coll	4.35	5.00	4.00
183	Field width	n_{row}	coll	2.48	2.00	3.00
184	Number of air collectors of field	$n_{coll/field}$	coll	10.79	10.00	12.00
185	Thermal performance					
186	Power at field outlet	Q_e	W	14000.0	12698.9	15732.1
187	Instantaneous efficiency at field outlet	η_{use}	%	58.4	57.2	59.0
188	Outlet volume flow of field	V_e	m ³ /h	1703.5	1387.6	2047.4
189	Outlet mass flow of field	\dot{m}_e	kg/h	1854.0	1494.4	2241.6
190	Inlet temperature	ϑ_i	°C	20.0	20.0	20.0
191	Outlet temperature	ϑ_e	°C	47.0	50.4	45.1
192	Temperature rise	ΔT_{rise}	K	27.0	30.4	25.1
193	Mean fluid temperature of field	ϑ_m	°C	33.5	35.2	32.5
194	Fan design					
195	Pressure drop of field	Δp_{field}	Pa	35.2	40.6	32.2
196	Pressure drop of remaining system	Δp_{sys}	Pa	209.2	137.9	302.3
197	Dynamic pressure losses into large load volumes (sum)	$p_{dyn,sum,sys}$	Pa	24.4	16.0	35.4
198	Total pressure rise of total system	$p_{sys,tot}$	Pa	268.7	194.5	369.9
199	Fan volume flow	V_{fan}	m ³ /h	1703.5	1387.6	2047.4
200	Fan mass flow	\dot{m}_{fan}	kg/h	1854.0	1494.4	2241.6

Figure 46: Comparison of different number of collectors in a row with optimised flow as shown in the Aircow manual (Fraunhofer ISE, 2017).

Appendix E: Comparison of Tracking Systems

This appendix shows the difference in the daily outputs of the two different tracking systems. As mentioned in Section 5.4 the output of the east-west tracking system during the day is uneven, while the output of the north-south tracking system varies throughout the year. Figures 47 show the performance of the two systems on the day of the winter solstice. This shows that the north-south tracking system performs rather poor and why it was considered using the east-west tracking system for the crushing season which stretches throughout the winter.

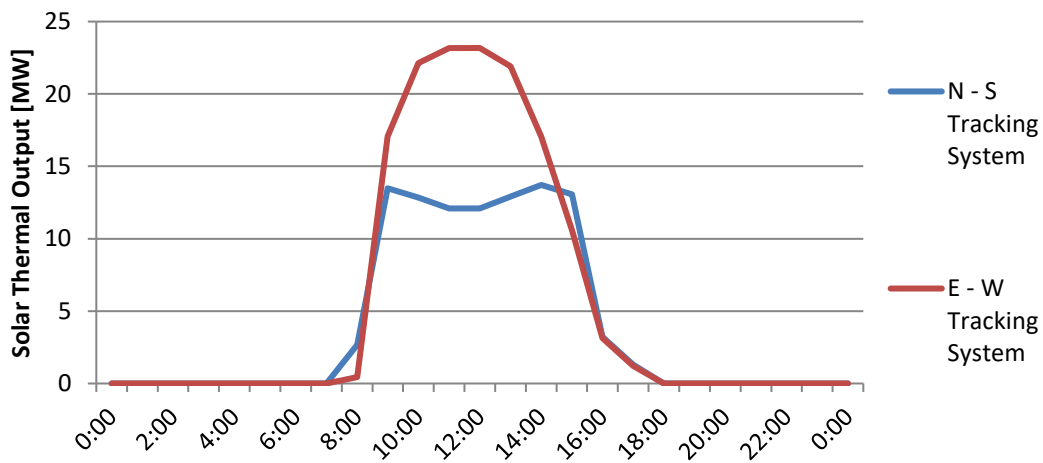


Figure 47: Comparison of the performance of the two tracking systems on 21 June.

Figure 48 shows the two systems on the day of the summer solstice, when the north-south system performs considerably better. The east-west system's performance is much the same as it was on the winter solstice, this is one of the system's advantages, there is little difference in its performance during different seasons.

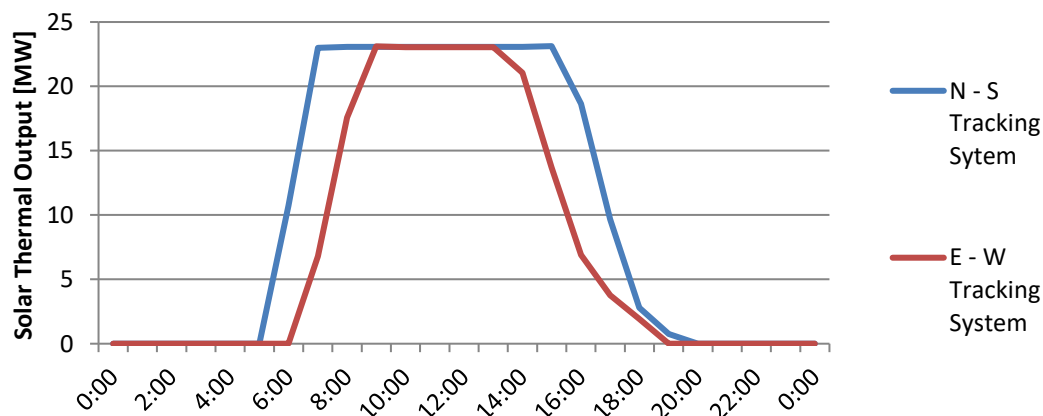


Figure 48: Comparison of the performance of the two tracking systems on 20 December.

References

- Abbas, R., Montes, M. J., Rovira, A., & Martí'nez-Val, J. M. (2016). Parabolic trough collector or linear Fresnel collector? A comparison of optical features including thermal quality based on commercial solutions. *Solar Energy*, 198-215.
- AEE Intec. (2017, 10 14). *Plants Database*. Retrieved from SHIP: <http://ship-plants.info/>
- Amos, W. A. (1998). *Report on Biomass Drying Technology*. National Renewable Energy Laboratory.
- Backen, M., Ferruzza, D., Larsen, L. K., & Haglind, F. (2017). Hybridization of Concentrated Solar Power and Biomass Combustion for Combined Heat and Power Generation in Northern Europe. *SolarPACES*. Santiago .
- Baharoon, D. A., Rahman, H. A., Omar, W. Z., & Fadhl, S. O. (2015). Historical development of concentrating solar power technologies to generate clean electricity efficiently – A review. *Renewable and Sustainable Energy Reviews*, 996-1027.
- Bajura, R. A., & Jones, E. H. (1976). Flow Distribution Manifolds. *Journal of Fluids Engineering* , 654-666.
- Bakshi, A. S., & Singh, R. P. (1980). Drying characteristics of parboiled rice. *International Symposium on Drying* .
- Beukes, H. T., Brent, A. C., & Hess, S. (2015). *Opportunities for Solar Thermal Process Heat Integration in South African Sugar Mills*. Stellenbosch University Faculty of Engineering .
- Bhatt, S. (2014). Concentrating solar power in cane-based sugar cogen plants: a strategic energy option for India. *Electrical and Power Review*, 30-33.
- Biomass Knowledge Portal. (2015). *First Commercial CSP-Biomass Hybrid Plant in Spain*. New Delhi: Ministry of New and Renewable Energy, India.
- Blackdot Energy. (2017, 10 15). *SA's Most Amazing Solar Thermal Projects*. Retrieved from Blackdot Energy: <http://www.blackdotenergy.co.za>
- Bruce, D. M., & Sinclair, M. S. (1996). *Thermal Drying of Wet Fuels: Opportunities and Technology*. Vancouver : H.A. SIMONS LTD.
- Burin, E. K., Vogel, T., Mulhaupt, S., Thelen, A., Oeljeklaus, G., Gorner, K., & Bazzo, E. (2016). Thermodynamic and economic evaluation of a solar aided sugarcane bagasse cogeneration power plant. *Energy* , 416-428.
- Cabrera , F. J., Fernandez-Garcia , A., Silva, R. M., & Perez-Garcia, M. (2013). Use of parabolic trough solar collectors for solar refrigeration and air-

- conditioning applications. *Renewable and Sustainable Energy Reviews*, 103-118.
- Calamateo, D., & Zhou, D. (2015). A Pre-Feasibility Study of a Small-Scale Concentrating Solar Power Plant for an Industrial Application in Sacramento, California. *Proceedings of the 2nd International Conference on Fluid Flow, Heat and Mass Transfer*, (pp. 180-1 - 180-8). Ottawa, Canada.
- Cardemil, J. M., Starke, A. R., Scariot, V. K., Grams, I. L., & Colle, S. (2013). Evaluating solar radiation attenuation models to assess the effects of climate and geographical location on the heliostat field efficiency in Brazil. *SolarPACES*, (pp. 1288-1297). Las Vegas .
- Çengel, Y. A., & Cimbala, J. M. (2010). *Fluid Mechanics: Fundamentals and Applications*. New York: McGraw-Hill.
- Çengel, Y. A., & Ghajar, A. J. (2015). *Heat and Mass Transfer: Fundamentals and Applications - Fifth Edition*. New York: McGraw-Hill Education.
- Cook, E. M. (1991). *Process Drying Practice*. New York : McGraw-Hill.
- CSP World Organisation. (2015). *CSP World Map*. Retrieved October 16, 2017, from CSP World: <http://cspworld.org/cspworldmap/kimberlina-stpp>
- De Oliveira, L. F., Correa, J. L., Tosato, P. G., Borges, S. V., Alves, J. G., & Fonseca, B. E. (2011). Sugarcane Bagasse Drying in a Cyclone: Influence of Device Geometry and Operational Parameters. *Drying Technology*, 29 , 946–952.
- Deloitte. (2015). *Draft Carbon Tax Bill Released*. Retrieved November 3, 2017, from Deloitte : <https://www2.deloitte.com/za/en/footerlinks/pressreleasespage/carbon-tax-bill.html>
- Don, C. E., Mellet, P., Ravno, B. D., & Bodger, R. (1977). Calorific Values of South African Bagasse. *South African Sugar Technologists' Association*, (p. 5). Durban.
- Duffie, J. A., & Beckman, W. A. (2006). *Solar Engineering of Thermal Processes* . New Jersey : John Wiley & Sons .
- Eberhard, A., Kolker, J., & Leigland, J. (2014). *South Africa's Renewable Energy IPP Procurement Program: Success Factors and Lessons*. Washington, DC: Public-Private Infrastructure Advisory Facility.
- Electromagnetic Foundations of Solar Radiation Collection. (2017, July 10). *Solar Energy*. Retrieved October 16, 2017, from Energy Professional Symposium: <http://energyprofessionalsymposium.com/?p=19152>

- Ensinas, A. V., Nebra, S. A., Lozano, M. A., & Serra, L. M. (2007). Analysis of process steam demand reduction and electricity generation in sugar and ethanol production from sugarcane. *Energy Conversion & Management*, 2978-2987.
- Fernandez-Garcia, A., Zarza, E., Valenzuela, L., & PerezM. (2010). Parabolic-trough solar collectors and their applications. *Renewable and Sustainable Energy Reviews*, 1695-1721.
- Foxon, K. (15 May 2017). *Personal communication between Willem Krog (Stellenbosch University) and Katherine Foxon (SMRI) via email.*
- Foxon, K. (22 November 2017). *Personal communication between Willem Krog (Stellenbosch University) and Dr Katherine Foxon (SMRI) via email.*
- Fraunhofer ISE. (2017). *Aircow Version 3.00 Manual*. Freiburg: Fraunhofer ISE.
- Fredrikson, R. W. (1984). Utilisation of Wood Waste as Fuel for Rotary and Flash Tube Wood Dryer Operation. *Biomass Fuel Drying Conference*, (pp. 1-16).
- Freire, F., Figueiredo, A., & Ferrao, P. (2001). Postharvest Technology: Modelling High Temperature, Thin Layer, Drying Kinetics of Olive Bagasse. *Journal of Agricultural Engineering Research*, 397-406.
- GeoSUN. (2012). *KZN Solar Maps & GIS Layers*. Retrieved October 17, 2017, from GeoSUN: <http://geosun.co.za/downloads/kzn-solar-maps-gis-layers-2012/>
- GeoSUN. (2013). *South African GIS Layers*. Retrieved November 3, 2017, from GeoSUN: <http://geosun.co.za/downloads/south-african-gis-layers/>
- Giglio, A., Lanzini, A., Leone, P., García, M. R., & Moya, E. Z. (2017). Direct steam generation in parabolic-trough collectors: A review about the technology and a thermo-economic analysis of a hybrid system. *Renewable and Sustainable Energy Reviews*, 453-473.
- Giostrì, A., Binotti, M., Astolf, M., Silva, P., Macchi, E., & Manzolini, G. (2012). Comparison of different solar plants based on parabolic trough technology. *Solar Energy*, 1208-1221.
- Gong, Z.-X., & Mujumdar, A. S. (2008). Software for Design and Analysis of Drying Systems. *Drying Technology*, 884-894.
- Gunther, M., Joemann, M., & Csambor, S. (2013). Parabolic Trough Technology. In D. Institute of Solar Research, *Advanced CSP Teaching Materials* (p. Chapter 5). enerMENA.

- Hanrieder, N., Wilbert, S., Mancera-Guevara, D., Buck, R., Giuliano, S., & Pitz-Paal, R. (2017). Atmospheric extinction in solar tower plants – A review. *Solar Energy*, 193-207.
- Heller, L. (2013). *Literature Review on Heat Transfer Fluids and Thermal Energy Storage Systems in CSP Plants*. Stellenbosch : Soler Thermal Research Group, Stellenbosch University .
- Hernandez Moro, J., & Martinez-Duart, J. M. (2012). SP electricity cost evolution and grid parities based on the IEA roadmaps. *Energy Policy*, 184-192.
- Hess, S. (11 July 2016). *Personal Communication between Willem Krog and Dr Stefan Hess at Stellenbosch University* .
- Hess, S., Beukes, H., Dinter, F., & Smith, G. (2016). Initial Study on Solar Process Heat for Sout African Sugar Mills. *South African Sugar Technologists' Association Congress*, (pp. 324-349). Durban.
- Ho, C. K. (2017). Advances in central receivers for concentrating solar applications. *Solar Energy*, 38-56.
- Hugot, E. (1972). *Handbook of cane Sugar Engineering* . Elsevier Publishing Company .
- Iftekhhar Hussain, C. M., Norton, B., & Duffy, A. (2017). Technological assessment of different solar-biomass systems for hybrid power generation in Europe. *Renewable and Sustainable Energy Reviews*, 1115-1129.
- Ilchmann, C., Klatt, M., & Hess, S. (2016). *Modeling of Solar Process Heat Systems in an Open Source Simulation Environment*. Cottbus: Brandenburgische Technische Universität.
- IRENA. (2012). *Renewable Energy Technologies: Cost Analysis Series*. International Renewable Energy Agency.
- IRENA. (2016). *The Power to Change: Solar and Wind Cost Reduction Potential to 2025*. International Renewable Energy Agency.
- Joubert, E. C., Hess, S., & Van Niekerk, J. L. (2016). Large-scale solar water heating in South Africa: Status, barriers and recommendations . *Renewable Energy*, 809-822.
- Kalogirou, S. A. (2009). *Solar Energy Engineering: Processes and Systems* . Burlington : Elsevier .
- Keey, R. B. (1994). Progress in Understanding Drying. In R. B. Keey, & V. Rudolph, *Drying '94'* (pp. 75-88). Univeristy of Queensland .
- Kemp, I. C., & David, E. O. (2002). Modelling of Particulate Drying in Theory and Practice . *Drying Technology*, 1699-1750.

- Kotze, C. (2016). Four Ways of Improving Boiler Efficiency . *South African Sugar Technologists Association Congress*, (pp. 498-507). Durban.
- Kraemer, S. (2017, August 25). *SolarReserve Breaks CSP Price Record with 6 Cent Contract*. Retrieved 2 September, 2017, from SolarPACES: <http://www.solarpaces.org/solarreserve-breaks-csp-price-record-6-cent-contract/>
- Kröger, D. G. (1998). *Air-Cooled Heat Exchangers and Cooling Towers* . Stellenbosch: University of Stellenbosch.
- Kurup, P., & Turchi, C. S. (2015). *Parabolic Trough Collector Cost Update for the System Advisor Model (SAM)*. Alexandria, USA: National Renewable Energy Laboratory.
- Laubscher, R. (2017). *Personal communication between Ryno Laubscher and Willem Krog at Stellenbosch University*.
- Liu, M., Tay, N. H., Bell, S., Belusko, M., Jacob, R., Will, G., . . . Bruno, F. (2016). Review on concentrating solar power plants and new developments in high temperature thermal energy storage technologies. *Renewable and Sustainable Energy Reviews*, 1411-1432.
- Madho, S., Davis, S. B., & Bhyrodeyal, L. (2017). Ninety-Second Annual review of the Milling Season in Shouthern Africa (2016/2017). *South African Sugar Technologists' Association Congress*, (pp. 20-50). Durban.
- Magasiner, N. (1987). The Effect of Fuel Moisture Content on the Performance of a Tycpial Bagasse Fired Watertube Boiler. *The South African Sugar Technologists' Association*, (pp. 86-89).
- Magasiner, N., Van Alphen, C., Inkson, M., & Misplon, B. (2001). Characterising Fuels For Biomass – Coal Fired Cogeneration . *South African Sugar Technologists' Association*, (p. 17). Durban .
- Masters, K. (1985). *Spray Drying Handbook*. New York: John Wiley & Sons.
- Meyer, R. (2016). *Solar Resource Assessment/Mapping*. Stellenbosch : STERG/GeoSun.
- Miles, T. R., Miles, T. R., Baxter, L. L., Bryers, R. W., Jenkins, B. M., & Oden, L. L. (1995). *Alkali Deposits Found in Biomass Power Plants*. National Renewable Energy Laboratory .
- Montes, M. J., Abandes, A., Martinez-Val, J. M., & Valdes, M. (2009). Solar multiple optimization for a solar-only thermal power plant, using oil as heat transfer fluid in the parabolic trough collectors. *Solar Energy*, 2165-2176.

- Mujumdar, A. S. (1995). *Handbook of Industrial Drying Second Edition*. New York: Marcel Dekker.
- Mujumdar, A. S., Borde, I., & Levy, A. (2006). *Handbook of Industrial Drying, Third Edition*. CRC Press.
- Munoz-Anton, J., Biencinto, M., Zarza, E., & Diez, L. E. (2014). Theoretical basis and experimental facility for parabolic trough collectors at high temperature using gas as heat transfer fluid. *Applied Energy*, 373-381.
- National Renewable Energy Laboratory . (2017, January 17). *System Advisor Model Version 2017.1.17*. Retrieved April 7, 2017, from National Renewable Energy Laboratory : <https://sam.nrel.gov/download>
- National Renewable Energy Laboratory. (2013). *Concentrating Solar Power Projects: Borges Termosolar*. National Renewable Energy Laboratory of the U.S. Department of Energy.
- National Renewable Energy Laboratory. (n.d.). *Concentrating Solar Power Projects*. Retrieved October 19, 2017, from National Renewable Energy Laboratory: <https://www.nrel.gov/csp/solarpaces/>
- Naude, D. P., McIntyre, P. J., & Field, S. J. (1993). The Design and Operation of Boiler Plant Utilising Furfural Residue as a Fuel . *South African Sugar Technologists' Association*, (p. 5). Durban.
- Nixon, J. D., Dey, P. K., & Davies, P. A. (2012). The feasibility of hybrid solar-biomass power plants in India. *Energy*, 541-554.
- Oliverio, J. L., Avila, A. C., Faber, A. N., & Soares, P. A. (2014). Juice Extraction System: Mills and Diffusers - the Brazilian Experience. *International Sugar Journal*, 190-202.
- Paradis, P.-L., Rouse, D. R., Halle, S., Lamarche, L., & Quesada, G. (2015). Thermal modeling of evacuated tube solar air collectors. *Solar Energy*, 708-721.
- Perry, R. H., Green, D. W., & Maloney, J. O. (1997). *Perry's Chemical Engineer's Handbook*. New York: McGraw-Hill.
- Petchers, N. (2012). *Combined Heating, Cooling & Power Handbook: Technologies & Applications* . Routledge Chapman Hall.
- Peterseim, J. H., Hellwig, U., Tadros, A., & White, S. (2013). Hybridisation optimization of concentrating solar thermal and biomass power generation facilities. *Solar Energy*, 203-214.
- Peterseim, J. H., Herr, A., Miller, S., White, S., & O'Connell, S. A. (2014). Hybridisation optimization of concentrating solar thermal and biomass power generation facilities. *Energy*, 1-14.

- Rayaprolu , K. (2009). *Boiler for Power and Process* . CRC Press.
- Reid, M. J., & Rein, P. W. (1983). Steam Balance for the New Felixton II Mill. *Proceedings of the South African Sugar Technologists' Association*, (pp. 85-91). Durban.
- Rein, P. W. (2007). *Cane Sugar Engineering*. Berlin: Bartens.
- Sabiha, M. A., Saidur, R., Mekhilef, S., & Mahian, O. (2015). Progress and latest developments of evacuated tube solar collectors. *Renewable and Sustainable Energy Reviews*, 1038-1054.
- SAIPPA. (2017). *News*. Retrieved November 6, 2017, from South African Independent Power Producers Association: <http://www.saippa.org.za/News.aspx>
- Schott. (2017). *www.schott.com/borofloat*. Retrieved August 12, 2017, from www.schott.com: <http://www.schott.com/borofloat/english/attribute/optical/index.html>
- Siems, T. (2017). *Airwasol Brochure, e-mail to W. Krog. [16 May 2017]*.
- Simprotek. (2006). *Drying Software, Simprosys 3.0*. <http://www.simprotek.com/Products.aspx>.
- Singels, A., McFarlane , S. A., Nicholson , R., Way, M., & Sithole , P. (2017). *Review of South African Sugarcane Production in the 2016/2017 season: Light at the End of the Tunnel?* . Durban: South African Sugar Technologists' Association Congress .
- Smith, G. T., Davis, S. B., Madho, S., & Achary, M. (2015). Ninetieth Annual Review of the Milling Season in Southern Africa (2014/2015). *South African Sugar Technologists' Association Congress*, (pp. 23-54). Durban.
- Smith, G. T., Davis, S. B., Madho, S., & Achary, M. (2016). Ninety-First Annual Review of the Milling Season in Southern Africa (2015/2016). *Proceedings of the South African Sugar Technologists' Association Congress* , (pp. 21-51). Durban .
- Smithers, J. (2014). Review of sugarcane trash recovery systems for energy cogeneration in South Africa. *Renewable and Sustainable Energy Reviews*, 915-925.
- Solar Advice . (2016, June 22). *Flat-Plate Solar Water Heating Collectors*. Retrieved October 16, 2017, from Solar Advice: <https://solaradvice.co.za/flat-plate-solar-water-heating>
- Solar Reserve. (n.d.). *Photos*. Retrieved October 15, 2017, from Solar Reserve: <http://www.solarreserve.com/en/newsroom/photos/crescent-dunes-solar-energy-plant>

- Solargis. (2017). *Duban Solar Resource Overview* .
- Sosa-Arnoa, J. H., & Nebra, S. A. (2009). Bagasse Dryer Role in the Energy Recovery of Water Tube Boilers. *Drying Technology*, 587-594.
- Sosa-Arnoa, J. H., Correa, J. L., Silva, M. A., & Nebra, S. A. (2006). Sugar Cane Bagasse Drying - a Review. *International Sugar Journal*.
- Starzak , M., & Zizhou, N. (2015). *Biorefinery Techno-Economic Modelling: Sugar Mill and Ethanol Distillery Process Model. Technical Report No. 2210*. Durban: Sugar Milling Research Institute .
- Starzak, M., & Davis, S. B. (2016). MATLAB® modelling of a sugar mill: model development and validation. *South African Sugar Technologists' Association*, (p. 20). Durban.
- Stine, W. B., & Geyer, M. (2001). *Power from the Sun*. John Wiley and Sons: New Jersey.
- Strumillo, C., & Kudra, T. (1986). *Drying: Principles, Applications and Design*. Montreaux, Switzerland: Gordon and Breach Science Publishers.
- Sun & Wind Energy. (n.d.). *News: New parabolic trough collector from 3M and Gossamer*. Retrieved October 16, 2017, from Sun & Wind Energy: The Platform for Renewable Energies : <http://www.sunwindenergy.com/news/new-parabolic-trough-collector-3m-and-gossamer>
- Tawfik, A. A., El Rahman, A. K., Bayoumi, M. R., & Morsy, M. G. (2003). Bagasse Drying: Advantages and Merits. *Arab Region and Africa in the World Sugar Context*. Arwan.
- Verein Detuscher Ingenieure. (2004). *Solar heating for domestic water - General Principles, system technology and use in residential building*. Düsseldorf: Verein Detuscher Ingenieure.
- Vijayaraj, B., Saravanan, R., & Renganarayanan, S. (2007). Studies on thin layer drying of bagasse. *International Journal of Energy Research* , 422-437.
- Wang, Z., Yang, W., Qiu, F., Zhang, X., & Zhao, X. (2015). Solar water heating: From theory, application, marketing and research. *Renewable and Sustainable Energy Reviews*, 68-84.
- Weiss, W., & Rommel, M. (2008). *Process Heat Collectors* . Gleisdorf : AEE Intec .
- Welz, C. (2017, March 9). <https://www.ise.fraunhofer.de/de/servicebereiche/testlab-solar-thermal-systems.html#tabpanel-5>. Retrieved April 3, 2017, from <https://www.ise.fraunhofer.de>: <https://www.ise.fraunhofer.de/en/press->

[media/news/2017/fraunhofer-ise-develops-freeware-aircow-to-calculate-solar-air-heating-collector-fields.html](#)

- Wienese, A. (2001). Boilers, Boiler Fuel and Boiler Efficiency . *South African Sugar Technologists' Association*, (p. 7). Durban .
- Zabaniotou, A. A. (2000). Simulation of Forestry Biomass Drying in a Rotary Dryer. *Drying Technology*, 1415-1431.
- Zoschke, T., Rohani, S., Fluri, T., Hu, Q., & Fang, Q. (2017). Parabolic Trough Plant Performance in China with Focus on Comparison of Heat Transfer Fluids HELISOL®5A and Therminol® VP-1. *SolarPACES*. Santiago .